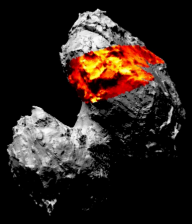

European Space Agency

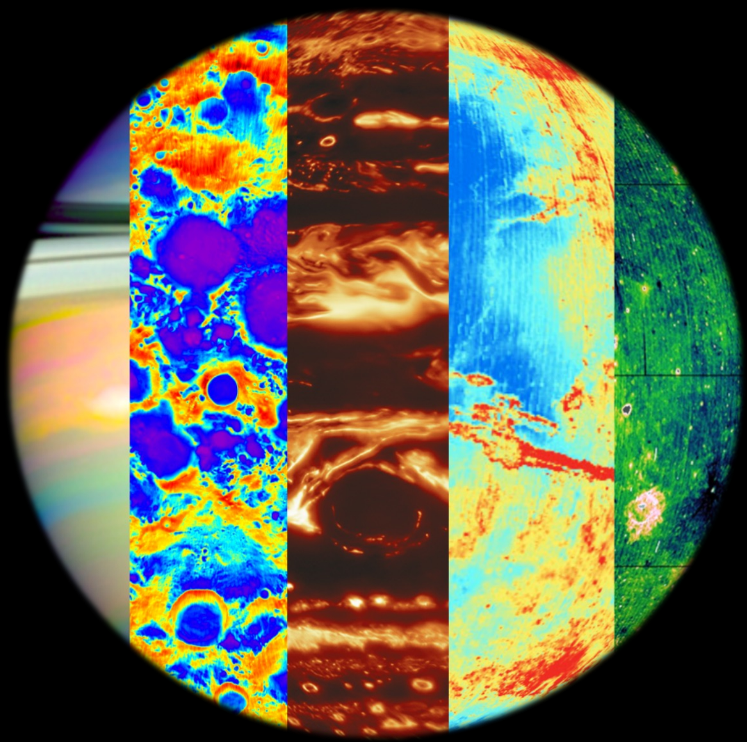

18-20 April 2023

ESA/ESTEC, Noordwijk, The Netherlands

TherMoPS IV
Abstract Book

4th Workshop on Thermal Models for Planetary Science

https://www.cosmos.esa.int/web/thermops4

Science Organising Committee

Jens Biele
Marco Delbo
Paul Hayne
Ozgur Karatekin
Thomas Müller
Tatsuaki Okada
Andrew Ryan
Naoya Sakatani

Local Organising Committee

Johannes Benkhoff
Sebastien Besse
Sarah Boazman
Hannah Goldberg
Philipp Hager
David Heather
Mylène Riemens
Elliot Sefton-Nash
Ines Torres

Table of Contents

Session 1 – Advances in Thermal Modeling: Theory and Computational Approaches.

Talks

Posters

Session 2 – Thermal Modeling of Asteroids and Small Bodies.

Talks

Posters

Session 3 – Thermal Modeling of the Moon and moons of the Solar System.

Talks

Session 6 – Planetesimal Thermal Evolution.

Talks

Session 7 – Laboratory Investigations and Validation of Thermal Models.

Talks

SESSION 1

Advances in Thermal Modeling: Theory and Computational Approaches

RADICALLY NEW MODEL FOR HEAT TRANSFER IN GRANULAR MEDIA WITH WEAKLY INTERACTING PARTICLES

J. Biele[1], B. Persson[2,3], Andrew J. Ryan[4]
[1] German Aerospace Center, DLR RB-MUSC, 51047 Cologne, EU, Germany (jens.biele@dlr.de)
[2] Peter Grünberg Institute (PGI-1), Forschungszentrum Jülich, 52425 Jülich, EU, Germany
[3] Multiscale Consulting, Wolfshovener Str. 2, 52428 Jülich, EU, Germany
[4] Lunar and Planetary Laboratory, University of Arizona, Tucson, AZ, USA.

Introduction: The accuracy and sensitivity of MIR radiometers has now reached a level that (a) the T-dependence of effective thermal conductivity, k_{eff} and specific heat capacity, c_P, cannot be neglected and (b) likely layering forces us to abandon "thermal inertia" but separate the three quantities $k_{eff}(z,T)$, $c_P(z,T)$ and bulk density $\rho(z,T)$. As for the effective thermal conductivity of granular media, all theoretical models in current use need empirical "fudge factors" (fit constants) to agree with experiments, some of these factors are strongly particle-size dependent. This is not satisfactory.

A radically new model for granular "contact" conductivity. We reviewed the conventional, notionally physics-based models of effective thermal conductivity of granular media (e.g., [1, 2] found them not applicable to rough, irregular, polydisperse particles that make up real regolith on planetary bodies, moons and asteroids. We developed, based on significant advances in rough contact mechanics and near-field optics over the last 2 decades (but overlooked by the planetary community) a new model applicable to regolith in vacuum or in a gaseous medium, with or without capillary bridges caused by humidity. There are no free parameters, provided the average roughness power spectra and some material properties of the particles and the porosity of the mixture is known. We find that heat transfer by near-field evanescent waves contributes significantly to contact conductivity, and the weak-contact phononic heat transfer is important, especially due to contact stiffening by adhesion forces, but cannot be described by conventional contact mechanics theories (JKR contact radius → constriction resistance). Constriction resistances are usually negligible. Temperature dependence of k_{eff} can deviate strongly from the customary *ansatz* $A+BT^3$.

Knowledge gaps and way forward

We will present where the main gaps in our understanding are and outline (work in progress) the way forward to get a deeper, physics-based insight into all the important quantities interesting for thermal modeling,

1. <u>Effective k of a granular medium</u> considering recent insights into contact thermal conductance of rough particles led us to a radically new model for weak phononic, capillary bridge, gas and near-field evanescent wave "contact" conductivity [3, 4]. We then add the classical radiative conductivity in the geometrical optics limit as determined by [5, 6] including non-isothermality correction. Practical software routines are in preparation (TU Braunschweig, J. Bürger). Not quite clear how to handle pore sizes < thermal wavelength (The Planck law is not valid at $D<\lambda_T=4107$ µm·K/T) and the transition from geometrical optics as used by A. Ryan. k_{eff} of polydisperse granular media are not clear yet. Geometric pre-factors for polydisperse media not clear yet. Treatment of lithostatic pressure is not clear yet (probably first ~linear, only at high squeezing pressures $\sim p^{1/3}$ dependence).

2. <u>"Matrix" thermal conductivity</u> of typical, conglomerate material (limit of no porosity) with considerable crystalline disorder, strong heterogeneity and a significant amorphous fraction. Work in progress, main issue is the correct composite conduction model, which may have to be applied hierarchically (Will a Generalized effective medium theory work? Not sure)

3. <u>General question: Is the "resistor model" appropriate?</u> The treatment of heat flow through the contact between the grains diverges on two similar paths. In one path, resistance through the contact reduces the effective solid grain conductivity, empirically (e.g., [7] or through a modeling (e.g., [8, 9], and the result combines in parallel with the void (e.g., [10]. In the other path the contact itself operates in parallel with the void (effectively part of the void conduction between grains), which then connect the grains in series (e.g., [11] follow the second path but we the first.

4. <u>Apparent thermal inertia: transition to "bedrock TI" if the particle size exceeds the diurnal skin depth, how?</u>

Note that for very slow rotators, the thermal skin depth L can be really large (~11 m for Mercury!) but if we use even only meter-sized boulders, the classical radiative conductivity ($\approx 2.510^{-7}$ D T^3) becomes larger than the typical "bedrock" thermal conductivity: puzzling! N.B.: if L/D_{pore} or $L/D_p > \approx 10$ and scattering size parameter $x = \pi D_p/\lambda > \approx 5$, may be treated as continuum [12], and an effective thermal conductivity $\boldsymbol{k_{eff}=k_{Phonon}+k_{NFRT}+k_{rad}(+k_{fluid})}$ may be defined.

5 Effective k of a competent, but very porous "rock" (only empirical relations (fig. 1) exist for now, e.g., [13, 14] - most difficult issue, porosity cannot be the only parameter, but the nature of contacts (by sintering / cold or hot pressing) is fundamental, i.e., the formation of the rock.

6. Very low temperatures. Realistic regolith particles (or meteorite samples) are polycrystalline and composed of various pure mineral grains with potentially very different material thermal conductivities and grain-to-grain interfacial thermal resistances. Extremely low temperatures are encountered, e.g., at permanently shadowed areas (PSAs - of high interest for ISRU due to the potential of finding stable ice in the shallow subsurface) on Moon or Mercury, there the surface temperatures can drop to ~30 K [15]. At these cryogenic temperatures, the conventional assumptions on thermophysical properties of the rock matrix for the description of thermal transport break down. Notably specific heat capacity $c_P(T)$ at low temperature, T, is very different from the ~300 K value. The "material conductivity" $k_m(T)$ of the minerals that make up the regolith can change very significantly at low temperature, but for polycrystalline rocks consisting of several minerals (crystalline or amorphous) it is not yet understood how [15]. For example, crystalline grains at low T can have a solid thermal conductivity order of magnitude higher than amorphous (glassy) particles; it is not clear how to combine this in a mix of crystalline/amorphous grains, there may be percolation effects.

7. porosity (which controls bulk density) of a granular medium as a function of granular Bond number (cohesion for rough particles, also a radically new finding, see [16], particle size distribution, grain shape, compaction), see [17]. Final Bond-number dependence TBD (re-analysis of experimental data, fusion with simulations). Grain shape dependence of porosity is still somewhat inaccurate, simulations planned; much higher porosities (in given g) possible if slightly sintered contacts!

8. The other "ingredients" needed for thermal modeling:

Emissivity: depends on material, wavelength region, and is generally not Lambertian for high emission angles. Becomes interesting if various wavelength bands can be measured by radiometers and data solved for spectral features of emissivity [18]

Models for low-T $c_P(T)$ considered done [19-21].

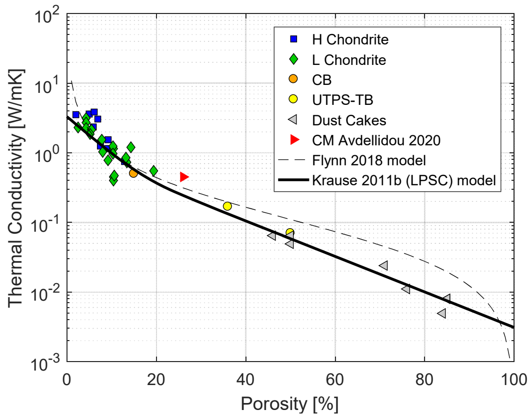

Fig. 1. Empirical dependence of thermal conductivity (at RT) vs. porosity for porous yet competent materials (meteorites, simulants). [Sakatani, 2021 / Grott, pers. comm.]

"Solid" conductivity" → Contact conductivity, Geometric factors

The heat flux is through particles via the particle contacts (or near-contacts) as in Figure 2.

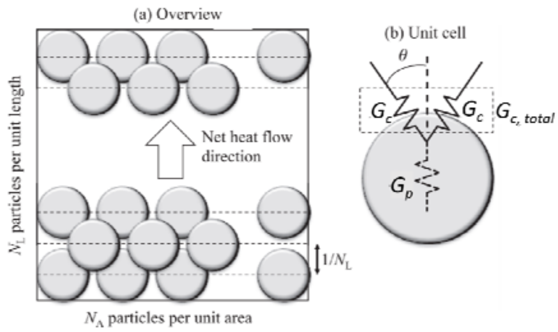

Figure 2. Simplified effective heat transfer model by contacts (or near-contacts) for a granular medium. (modified from [2])

For a general granular medium, we need the precise geometrical factors of order 1 in k_{eff}~G_c/R, which will depend mostly on porosity, and on packing geometry (ordered or random; shape and friction of particles). G_c is temperature- and slightly R-dependent. For now, we use the geometric factors for monodisperse spherical particles found by simulation for all porosities [22]. It is believed that the geometric factor for polydisperse mixtures (e.g. lognormal, power-law size distributions) can similarly be determined by simulation – analytical approximations are not convincing.

Conclusions: We present a new theory of the effective thermal conductivity of granular media consisting of rough, irregular grains, the grains being mechanical polycrystalline or amorphous aggregates of constituent pure minerals. It is computationally intensive, but correlation equations depending on (at least 2) roughness parameters and composition may be derived from numerical calculations. So far, we can estimate the geometric pre-factor of contact conduction (as a function of porosity) only for monodisperse, rather spherical grains, based on previous simulations – we believe that the geometric factors for polydisperse mixtures are best found by simulation experiments as well. The theory is limited to weak confining pressures; extension to higher squeezing pressures will be subject of further investigations. We note that the far-field radiative conductivity ~T^3 and its magnitude is not assured for particles smaller than the thermal wavelength λ_T since the Planck assumption breaks down then. On the other hand, for that small particles the near-field radiative heat transfer may dominate anyhow. Experimental validation is sought and requirements for such experiments are given. We note that it is extremely important to control humidity (water molecules adhering to the surfaces of usually hydrophilic silicate grains), since even a humidity of the order of 1 % can lead to the formation of liquid (or ice-like) capillary bridges at the contact points between grains, increasing the contact thermal conductivity by orders of magnitude.

A credible physics-based solid conduction model for porous "rocks" (or the grains of a granular medium) is not yet available and subject of a current project at DLR. Measurements on meteorite samples give k(T) for various compositions and porosities, though, allowing to extrapolate matrix conductivity to cryogenic temperatures.

As for specific heat, we have recently published a comprehensive review of c_P for all kinds of solar system materials for 1 K <T<1000 K in general, given the bulk composition.

References:

[1] Gundlach, B. and J. Blum, Icarus, 2012. **219**(2): p. 618-629, DOI: http://dx.doi.org/10.1016/j.icarus.2012.03.013.
[2] Sakatani, N., et al., AIP Advances, 2017. **7**(1): p. 015310, DOI: 10.1063/1.4975153.
[3] Persson, B.N.J., EJPB, 2023a(accepted).
[4] Persson, B. and J. Biele, AIP Advances, 2022. **12**(10): p. 105307.
[5] Ryan, A.J., et al., JGR Planets, 2022: p. e2022JE007191.
[6] Ryan, A.J., et al., JGR Planets, 2020: p. e2019JE006100.
[7] Watson, K., *I. The thermal conductivity measurements of selected silicate powders in vacuum from 150°-350° K. II. An interpretation of the Moon's eclipse and lunation cooling as observed through the Earth's atmosphere from 8-14 microns*. 1964, California Institute of Technology.
[8] Sakatani, N., et al., Icarus, 2018. **309**: p. 13-24.
[9] Wood, S.E., Icarus, 2020. **352**: p. 113964, DOI: https://doi.org/10.1016/j.icarus.2020.113964.
[10] Wechsler, A., P. Glaser, and J. Fountain, Prog. Aero. Astron., 1972. **28**.
[11] Mellon, M.T., C.P. McKay, and J.A. Grant, Icarus, 2022. **387**: p. 115211.
[12] Kaviany, M., Mechanical Engineering Series, 2nd edn. Springer.
[13] Grott, M., et al., Nature Astronomy, 2019. **3**(11): p. 971-976, DOI: https://doi.org/10.1038/s41550-019-0832-x.
[14] Sakatani, N., et al., Nature Astronomy, 2021: p. 1-9.
[15] Martinez, A. and M. Siegler, Journal of Geophysical Research: Planets, 2021. **126**(10): p. e2021JE006829.
[16] Persson, B.N.J. and J. Biele, Tribology Letters, 2022. **70**(2): p. 34, DOI: 10.1007/s11249-022-01570-x.
[17] Grott, M. and J. Biele, Preprint on https://essoar.org/ (2020) DOI: 10.1002/essoar.10503201.1, 2020.
[18] Hamm, M., et al., Nature communications, 2022. **13**(1): p. 1-12.
[19] Biele, J. and M. Grott, *Reference Heat Capacity for Asteroid Regolith from 10 to 1000K*, in *49th Lunar and Planetary Science Conference*. 2018, Lunar and Planetary Institute: Houston. p. Abstract #1877.
[20] Biele, J., et al., International Journal of Thermophysics, 2022. **43**(9): p. 144, DOI: 10.1007/s10765-022-03046-5.
[21] Piqueux, S., et al., Journal of Geophysical Research: Planets, 2021. **126**(11): p. e2021JE007003.
[22] Arakawa, S., et al., Icarus, 2019. **324**: p. 8-14.

Acknowledgments: JB acknowledges very fruitful discussions with Matthias Grott and Naoya Sakatani.

AN IMPLICIT THERMAL MODEL FOR 1D MULTI-LAYERED PLANETARY SURFACES

C. Mergny, F. Schmidt[1]
[1]Université Paris-Saclay, GEOPS, UMR 8146, CNRS, France (cyril.mergny@universite-paris-saclay.fr)

Introduction: The thermal evolution of planetary surfaces plays a key role in our understanding of the planet's geophysical process, surface composition and material properties. This study presents an implicit numerical model that simulates and predicts the surface temperature in 1D multi-layered planetary surfaces exposed to solar radiation. Unlike previous thermal models such as THERMPROJRS [1], LMD 1D [2], KRC [3] and [4], this algorithm solves the standard heat equation with a stable implicit scheme for a non-constant depth sampling, accounting for time and depth dependent heat properties.

Methods: Our thermal model [5] calculates the temperature *T*, by solving the heat equation

$$\rho(x,t)c_p(x,t)\frac{\partial T(x,t)}{\partial t} = \frac{\partial}{\partial x}\left(k(x,t)\frac{\partial}{\partial x}T(x,t)\right) + Q(x,t)$$

where ρ is the density, c_p the heat capacity, k the thermal conductivity and Q an optional sink/source term. The surface is subject to boundary conditions, which can be of any type, but for planetary surfaces we assume that the heat flux is zero at the bottom and given by thermal equilibrium at the surface. This equilibrium is calculated using incoming solar flux data from NASA's SPICE Toolkit [6, 7, 8] and considering black body emission to obtain the surface flux condition.

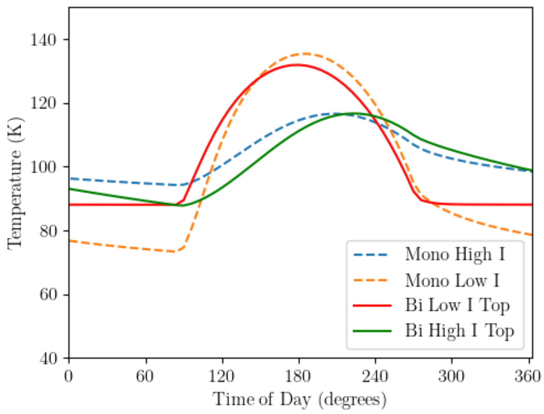

Figure 1: Daily surface temperatures for various material profiles. Dashed lines show homogenous materials and solid lines show bi-layered profiles.

The heat equation is discretized following Euler's scheme, and the resulting system of equations is solved using the implicit solver. The spatial grid can be unequally discretized to make the solver computationally more efficient in areas with higher temperature gradients.

Results: Computation of daily temperature variations for a 100-point space grid over 30 million iterations requires approximately 10 hours on an Intel i7-10750 CPU. The solver is stable regardless of the heat parameters.

Validation of our model for constant heat parameters was achieved using analytic solutions of the heat equation. For more complex, realistic profiles like multilayered surfaces, we compare our method with Spencer's [1] explicit algorithm. Results indicate that our implicit scheme is consistent with Spencer's explicit scheme while providing more flexibility in parameter choice without compromising stability.

Applications: We ran the thermal model on Europa's surface at Lat/Lon (0,0) to study differences in surface temperatures from four ground profiles: two homogeneous profiles of material *High* (thermal inertia of 196 SI) and material *Low* (28 SI), and two bi-layered profiles, one with 5 cm of material *High* on top of *Low* and the other with 1 cm of *Low* on top of *High* both with depth thinner than the thermal skin depth. The results shown in Figure 1 reveal the particular trends of bi-layered profiles. *Low* on top of *High* has a high centered day-side temperature bell shape and almost constant night temperatures while *High* on top of *Low* has a shifted day-side temperature peak and strong cooling at the end of the night. No homogeneous ground profile could match the thermal signature of bilayered ones, indicating that these situations could be identified using surface temperature data alone.

Conclusion: Our model [5] provides a reliable and efficient algorithm for computing the heat transfer and temperature of multi-layered surfaces. It has been validated by comparison with analytical solutions and a reference numerical implementation. Our implicit scheme solver of the heat equation has the advantage of ensuring stability and convergence regardless of the material's properties. It can be used for various planeraty applications, in particular to retrieve surface properties of icy moons in both infrared and radar wavelengths.

References: [1] Spencer et al., Icarus, 83, 1989 [2] Forget et al, JGR, 104, 1999 [3] Kieffer et al., JGR, 118, 2013 [4] Ferrari & Leyrat, A&A, 447, 2006 [5] Mergny et al., Computational Geophysics, 2023 *in prep* [6] Acton, P&SS, 44, 1996 [7] Annex et al., JOSS, 5, 2020 [8] Acton et. al., P&SS, 2017 [9] Rathbun et al., Icarus, 210, 2010

FAST THERMAL MODELS FOR PLANETARY SURFACES

Norbert Schorghofer[1],
[1]Planetary Science Institute, Tucson, Arizona (resident in Honolulu, Hawaii), USA (norbert@psi.edu)

Introduction: Surface and subsurface temperatures can be modeled based on topographic shape models, and are crucial, e.g., for the study of volatiles on the Moon, Mars, and asteroids. Thermal modeling of rough terrain is computationally challenging because of the large number of pixels in available digital shape models and the non-local nature of horizons and terrain irradiance. Here, an overview of implementation of fast algorithms is provided, where "fast" refers to a qualitative improvement in the operation count.

Subsurface Heat Storage: Vertical temperature gradients are nearly always much larger than lateral heat flow, and a set of 1D heat flow models suffices for horizontal scales larger than a few m/pixel. Properly discretized finite-difference solvers conserve the heat flux even across interfaces with drastic changes in soil thermal properties. One implementation [1,2], 21 years old, uses a Crank-Nicolson method with the Stefan-Boltzmann law as nonlinear boundary condition. This method is much faster than simple explicit time step schemes. Recently, a few other semi-implicit solvers with Boltzmann law boundary condition have been published [e.g., 3].

Terrain Shadowing: Terrain shadowing by topography defines local horizons and is important for the surface energy balance. Use of a hierarchy of spatial grids with varying resolutions (multigrid method) dramatically accelerates horizon calculations (Table 1). The hierarchy can be stored as quadtree. Algorithmically fast horizon determinations are available through standard ray-tracing libraries, such as *CGAL* and *Embree*, and are used, e.g., in *IllumNG* [4] and *python-flux* [5]. Others have implemented fast algorithms from scratch [1,6].

	Simple method	Fast algorithm
Incidence angle	$O(1)\cdot N_t$	$O(1)\cdot N_t$
Subsurface heat	$\Delta t < \Delta z^2/(2D)$	$\Delta t <$ const.
	$O(N_z^2)\cdot N_t$	$O(N_z)\cdot N_t$
Terrain shadowing	$O(N)+O(N_t)$	$O(\log N)+O(N_t)$
Terrain irradiance	$O(N)+O(N')\cdot N_t$	$O(\log N)+O(\log N')\cdot N_t$

Table 1: Overview of computational costs (per pixel) of components for surface energy balance models. *N*... number of spatial pixels, N_z... number of vertical subsurface grid points, N_t... number of times steps, *N'*... number of spatial pixels with direct line of sight.

Sky Irradiance can be calculated based on horizon elevations, as long as it is Lambertian [1,7].

Terrain Irradiance: The radiative transfer between pairs of surface facets with a direct line of sight is described by a geometric "view factor". Few algorithmically fast implementations of the terrain irradiance are available so far that are tailored to planetary surfaces [8,9,5]. The model by Paige et al. [8] uses rays that stochastically cover the field of view. Potter et al. [5] implemented a method that uses block-wise SVDs to produce a reduced-rank view factor matrix, which then allows multiplications at a much-reduced computational cost. It also consumes little memory during construction because it operates on blocks.

Conclusions and Discussion: Fast thermal models of planetary surfaces require that each component uses fast algorithms (Table 1). Including direct insolation, subsurface conduction, sky irradiance, and terrain shadowing, but no full-fledged terrain irradiance, digital elevation models (DEMs) with over 10^6 pixels have been modeled for thousands of solar days using a single workstation (Fig. 1) [10]. Time-depended model calculations with terrain irradiance have reached similar pixel dimensions on computer clusters [5,8].

As our thermophysical models grow increasingly complex, it would be beneficial to coordinate efforts for further development.

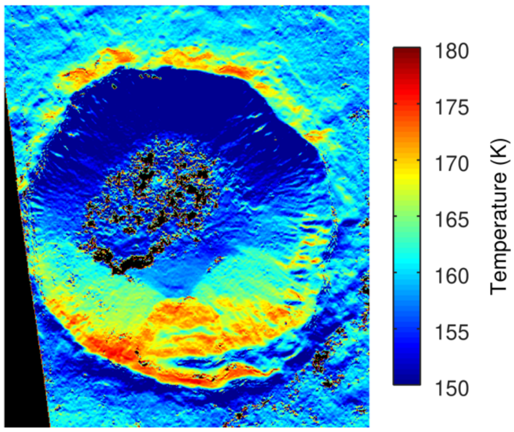

Figure 1: Modelled surface temperatures at Palikir Crater, Mars, before sunrise, based on a DEM with 1.3 million pixels [10].

References:

[1] https://github.com/nschorgh/Planetary-Code-Collection [2] https://github.com/nschorgh/MSIM [3] Young *Icarus 284*, 443 (2017). [4] Mazarico et al. *Adv. Space Res. 62*, 3214 (2018). [5] Potter S.F. et al. *J. Comput. Phys. X*, submitted (2022) doi:10.48550/arXiv.2209.07632. [6] Tong et al. *Icarus 390*, 115302 (2023). [7] Dozier & Frew *IEEE Trans. Geosc. Rem. Sens. 28*, 963 (1990). [8] Paige et al. *Science 330*, 479 (2010). [9] Gläser *A&A 664*, A152 (2022). [10] Schorghofer at al. *JGR 124*, 2852 (2019).

FAST RADIOSITY FOR THERMAL MODELING ON PLANETARY SURFACES

Stefano Bertone[1], Samuel Potter[2], Norbert Schörghofer[3], Erwan Mazarico[4]
[1] CRESST II / SURA / NASA GSFC, USA; INAF, Italy (sberton2@umbc.edu)
[2] Courant Institute of Mathematical Sciences, New York University, NY 10012, USA (sfp@cims.nyu.edu)
[3] Planetary Science Institute, Tucson, AZ 85719, USA (norbert@psi.edu)
[4] NASA Goddard Space Flight Center, Greenbelt, MD 20771, USA (erwan.m.mazarico@nasa.gov)

Abstract: High-fidelity thermal modeling is important to understand the stability and evolution of volatiles, as well as the geophysical history and processes affecting planetary surfaces. Our “Fast Radiosity” method [1] makes large-scale thermal simulations of planetary surfaces possible without the need of High-End-Computing (HEC) resources.

Challenge: Knowing the thermal environment is a critical condition to understanding the stability and evolution of ices and other volatiles in the Solar System. Illumination and temperature on the surfaces of airless bodies are dominated by radiative fluxes, from the Sun or from energy reflected or emitted from nearby topography (see, e.g., [2,3]). The number of element-to-element fluxes to calculate scales quadratically (N^2, with N the number of elements), and time-dependent calculations are often desired for numerous scenarios. Modeling quickly becomes a major computational challenge when leveraging high-resolution topographic maps of planetary surfaces, which are now available for multiple Solar System bodies.

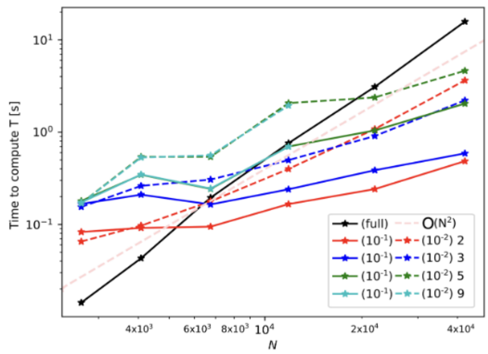

Figure 1: Our compressed view factor requires a similar time and much less memory to assemble [1], and our approach is orders of magnitude faster for each timestep, with no significant accuracy loss.

Approach: We present an algorithm for compressing the radiosity view factor model by recursively partitioning elements, similar to what is done for radiation heat transfer and computer graphics [4]. Our results indicate that the compressed view factor matrix can be assembled (done only once) in quadratic time, which is comparable to the time it takes to assemble the full view matrix itself. Computing light and heat re-radiation (which is repeated at each time step) then scales as $N \times \log(N)$ in our “fast radiosity” method. This yields drastic reductions in memory and execution times, especially for time-dependent problems, thus making highly-resolved (in both space and time) and extensive modelings of thermal conditions on planetary surfaces possible with average machines (see Figure 1).

Applications: As initial validation of our approach, we present numerical experiments with a synthetic spherical cap-shaped crater, where the equilibrium temperature is analytically available. We also present results of our implementation with triangle meshes of rough planetary surfaces derived from digital elevation models recovered by orbiting spacecraft (Figure 2). For a range of compression tolerances, the size of the compressed view factor matrix and the speed of the resulting matrix vector product both scale linearly (as opposed to quadratically for the full matrix), resulting in orders of magnitude savings in processing time and memory space.

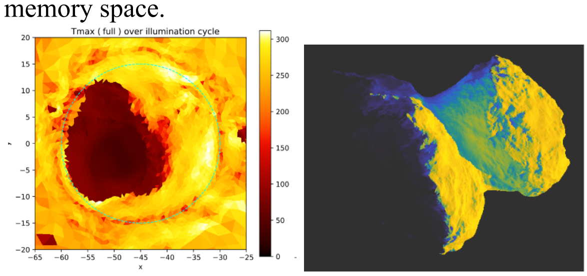

Figure 2: Maximum temperature at the surface of the Haworth crater at the lunar South Pole (left, 20k faces, 0.1 km resolution) and equilibrium temperature at the surface of comet 67P (right, 197k faces).

Conclusion:

Large-scale thermal modeling on the surface of rough airless planetary bodies is a computationally demanding problem. We present an algorithm allowing one to first assemble (e.g., on a cluster) a significantly compressed version of a view factor matrix, and then perform subsequent computations interactively on a laptop or workstation, thereby simplifying the model usability and workflow. Our open-source code is available at https://github.com/sampotter/python-flux .

References:

[1] Potter S.F. et al. *J. Comput. Phys. X*, submitted (2022), doi:10.48550/arXiv.2209.07632 [2] Mazarico et al. *Adv. Space Res.* 62, 3214 (2018) [3] Paige et al. Science 330, 479 (2010) [4] Hanrahan P. et al. *Computer Graphics* 25, 197 (1991)

FAST NEAR-EARTH ASTEROID SURFACE TEMPERATURE EVALUATION FROM DISK-RESOLVED NIR MEASUREMENTS USING A NEURAL NETWORK

Leevi Lind[1*], Antti Penttilä[2], Kimmo A. Riihiaho[1], Eric MacLennan[2], Ilkka Pölönen[1]
[1]University of Jyväskylä, Finland; [2]University of Helsinki, Finland
([*]Corresponding author, email: leevi.j.j.lind@jyu.fi)

Introduction: The cost of asteroid missions could be greatly reduced by using small spacecraft. The ESA Hera mission to near-Earth asteroid (65803) Didymos will include two CubeSats in addition to the main spacecraft to demonstrate this technology [1].

A small spacecraft limits both the instruments and the downlink budget for the mission. If the surface of the target body is warm enough (over 300 K), the temperature distribution over the surface could be evaluated with a spectral instrument working in near-infrared (NIR) wavelengths close to 2.5 µm. In this region the thermal emission co-exists with reflected sunlight, and the two must be separated to analyze them. Constraints on the downlink encourage on-board processing of data, as sending only ready data products can decrease the size of transmissions. Computing on the on-board computer requires efficient methods.

We propose to feed an observed spectral radiance to a convolutional neural network [2] and take as output a prediction for the temperature of the surface element. Neural networks need a lot of computational resources to train them, but producing predictions with a network is relatively cheap and could possibly be done on the spacecraft on-board computer in the future.

Materials and Methods: A 1D convolutional neural network was constructed and trained using Keras. Training data for the network was generated with a rudimentary simulator, where the reflected and and thermally emitted radiances were modeled separately and summed to make one sample. The sum spectrum was fed to the network, and the output of the network was compared to a ground truth temperature value.

Performance of the trained network was tested with synthetic data from our simulator, and with data from (101955) Bennu, produced by the OSIRIS-REx OVIRS instrument [3].

Results and Discussion: Producing temperature predictions with the network was quite fast. For a synthetic dataset of 62 040 samples, the total prediction time was 34.1 s. For one sample this means approximately 0.5 ms.

A plot of predicted temperatures against ground truth temperatures from the Bennu data can be seen in Figure 1. The mean predicted temperature for each ground truth temperature stays close to the ideal result over the temperature range, but many individual results deviate strongly from the mean.

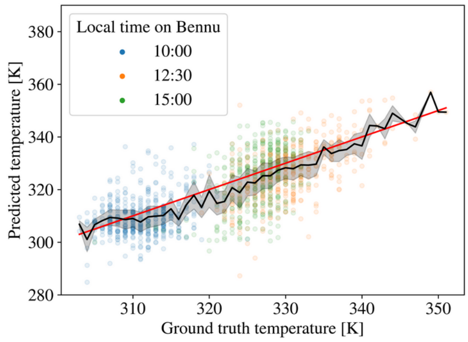

Figure 1: Results of temperature evaluation from OSIRIS-REx OVIRS data of Bennu. The red line corresponds to an ideal result, the black line the mean predicted temperature for each ground truth temperature, and the gray shadow to the standard deviation of predictions.

Bennu is not representative of all asteroids. Therefore, we can not conclusively say that this approach for temperature evaluation will work for any asteroid mission. Suitable test data from other asteroids does not currently exist, but Hera can provide it.

The network performance could be improved with more realistic training data. The simulator used for data generation models reflection with the Lommel-Seeliger law, and thermal emission with Planck's law using an emissivity that is constant over wavelengths.

Conclusion: A convolutional neural network can produce fast and reasonable accurate temperature predictions from NIR radiance spectra. While the approach shows promise for future CubeSat missions, tests with data from other asteroids are yet needed.

References:

[1] P. Michel *et al.*, 'The ESA Hera Mission: Detailed Characterization of the DART Impact Outcome and of the Binary Asteroid (65803) Didymos', *Planet. Sci. J.*, 2022, doi: 10.3847/PSJ/ac6f52.

[2] I. Goodfellow, Y. Bengio, and A. Courville, *Deep Learning*. Cambridge, MA, USA: MIT Press, 2016.

[3] A. A. Simon *et al.*, 'Widespread carbon-bearing materials on near-Earth asteroid (101955) Bennu', *Science*, 2020, doi: 10.1126/science.abc3522.

Acknowledgments: We thank Dr. Amy A. Simon for providing OVIRS data of Bennu. This work was funded by the Academy of Finland (grant 335615).

MOON ROVER THERMAL AND POWER ANALYSIS FOR NIGHT AND PSR SURVIVAL

R. A. Creel[1]

[1] Retired Space and Thermal Systems Engineer and Apollo Lunar Roving Vehicle (LRV) Team Member (roving.ron@gmail.com). RACI, 7228 Statton Dr. S.E., Huntsville, AL 35802.

Previous power needs for extended Moon exploration were studied in 1970 for the ultimately cancelled Apollo 18 mission. This "Dual Mode" operation Apollo LRV would have been provided with a trailer attached to the rear of the 4th LRV so that extensive remotely controlled exploration could be accomplished after that crew left the Moon. This trailer would have included a 70 watt nuclear SNAP-27 Radio-Isotope Thermoelectric Generator (RTG) that was also used for the 5 Apollo Lunar Surface Exploration Packages (ALSEPs) that were left on the Moon and survived and operated for several years until they were shut off in 1977. The author included adverse lunar dust effects on radiator cooldowns in a 19 node Mission Support thermal model and was presented with the Astronaut "Silver Snoopy" award for accurate thermal modeling.

In 2004 this author continued to pursue power solutions for extended Moon exploration, and even presented LRV results in Russia at the Lunokhod remotely controlled Moon rover design and test facility - noting that those 2 rovers survived several lunar night exposures using Radioisotope Heating Units (RHUs). Further studies were conducted to support the 2012 NASA "Nightrover" project for non-nuclear power for Moon exploration. Results, using the LRV test and flight proven thermal model, were that 66 watts of continuous power were required for LRV battery survival alone during the 354 hours (14.75 days) lunar night period with no solar provided energy.

Now, plans are to travel to and survive and operate Artemis systems at low latitude sites near the South Pole of the Moon - which will present even greater challenges for rovers and other systems to survive and operate - including science missions in very cold Permanently Shadowed Regions (PSRs). A recent requirement for new Lunar Terrain Vehicles (LTVs) to survive and operate in very cold PSRs for 150 hours (6.25 Earth days) has been proposed. The Apollo LRV Thermal Model was used again to determine example needed survival power for these Moon science missions. A 110 watt Multi Mission Radio-Isotope Thermoelectric Generator (MMRTG) surface model, supplied by the Jet Propulsion Laboratory (JPL), was included to augment the LRV battery power capabilities.

The special thermal analysis process, for creation of thermal models for extended Lunar Science Missions using CAD surface models for increased accuracy in new studies, is also outlined in this presentation.

APPLYING BAYESIAN OPTIMIZATION TO THERMOPHYSICAL MODELING OF ASTEROIDS

Sean E. Marshall[1], Eric M. MacLennan[2], Christopher Magri[3], Yanga R. Fernandez[4], Ellen S. Howell[5], Kiana D. McFadden[5], Samuel A. Myers[5], Ronald J. Vervack Jr.[6]
[1]Arecibo Observatory & University of Central Florida (sean.marshall@ucf.edu), [2]University of Helsinki, [3]University of Maine at Farmington, [4]University of Central Florida, [5]University of Arizona, [6]Johns Hopkins University / Applied Physics Laboratory

Introduction: We will be working on a software package that applies Bayesian optimization to thermophysical modeling of asteroids, in order to find the thermal parameters of observed asteroids - quickly, in an automated fashion, with minimal human oversight. This presentation is an advertisement to the thermal modeling community, seeking additional collaborators who work with other thermal modeling programs and are interested in having Bayesian optimization scripts that could be run with those programs.

Thermal modeling: Observations of an asteroid at infrared wavelengths provide constraints on its size, albedo, and other properties. One can compare the observations with calculations from various thermal models, to find the model parameters that give the best fits to the data.

Simple thermal models, in which one assumes the target body is a sphere with uniform surface properties, run in seconds on a typical computer. In cases where the asteroid's shape and rotation state are known from other observations, one can get better constraints on its properties by using more complicated thermophysical models [1,2]. However, models that consider complexities such as non-convex shapes or temperature-dependent thermal properties require much more computation time - typically hours or days for each model.

A model's goodness of fit is quantified with a statistic like chi-square, the sum of squared normalized residuals. One can think of chi-square as a function of the model parameters; the goal of thermal modeling is to find the parameters that minimize this function. This involves running numerous models, with a range of thermal parameters - a set of points that span the parameter space. Since each thermophysical model (each evaluation of the chi-square "function") is computationally expensive, the goal is to find near-optimal parameters with as few models as possible.

Bayesian optimization: With a regular grid search, one chooses every test point before starting the search. With Bayesian optimization, the software chooses the next test point "intelligently" based on the previous results [3], trying to choose parameters that are likely to give a lower value of chi-square than whatever was found previously. There is a tradeoff between exploring sparsely sampled regions of parameter space vs. exploiting (looking near) the best (so far) minima; the user can adjust this.

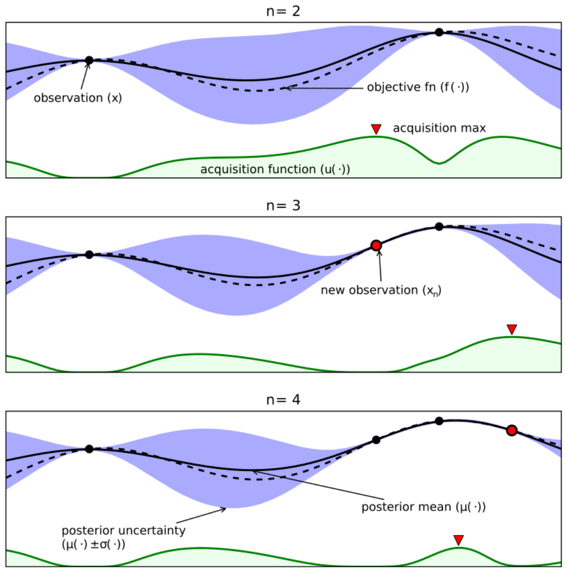

Figure 1: One-dimensional example of Bayesian optimization, searching for the maximum of a function. The true objective function (target) is shown with a dashed black curve, but in practice, it would be unknown. The solid black curve shows the estimated objective function after *n* points (black circles) have been evaluated, and the blue shaded region shows a confidence interval. The uncertainty is greater in regions of parameter space that have not yet been sampled. The green curve is the acquisition function, which balances exploitation with exploration. From Figure 1 of [3].

Tasks: The goal of this project is *not* to write another Bayesian optimization package or another thermal modeling program. The goal is to write scripts that link the two, analyzing the results from previous models (from any thermal modeling program) and then doing the Bayesian optimization calculations to determine which model parameters should be tested next - utilizing existing programs to do the computationally expensive tasks. If you are interested in collaborating on this project, please contact the first author!

References:

[1] Magri et al. (2018), *Icarus* 303, pp. 203-219.
[2] MacLennan & Emery (2019), *Astr. Jour.* 157:2.
[3] Shahriari et al. (2016), *Proceedings of the IEEE* 104:1, pp. 148-175.

Acknowledgment: This work is funded through NASA grant 80NSSC23K0377.

COMPUTATIONAL TECHNIQUES FOR FRACTAL ROUGH THERMAL MODELS

Kay Wohlfarth[1], Christian Wöhler[1]
[1]Image Analysis Group, TU Dortmund University, Otto-Hahn-Str. 4, 44227, Dortmund

Introduction: Fractal surfaces are the most realistic representation of planetary regolith for thermal models of airless planetary bodies. However, the efficient computation of second-order thermal effects such as self-scattering and self-heating remains costly. We introduce three computational techniques that speed up thermal models with rough fractal surfaces such that we can process entire disk-resolved bodies within hours. The three techniques are used in the companion abstracts [1,2] and outlined in the full paper [3].

1. Fixed-point iteration of radiation balance equation: We reformulate the radiation balance as a matrix-vector equation. To this end, we divide the planetary body into N elements, each bearing an individual illumination and viewing vector. For each of these N elements, we compute the temperature of a square fractal rough surface model with K facets. The temperatures of all facets then forms a N x K matrix **T**. Self-scattering and self-heating can be expressed as a symmetric K x K – matrix **F**. The initial illumination is given by another N x K matrix **J**. The problem becomes a fixed-point equation of the temperature matrix **T** raised to the fourth power. We find that a simple Richardson iteration converges after five iterations. (self-scattering is not shown for brevity but considered.)

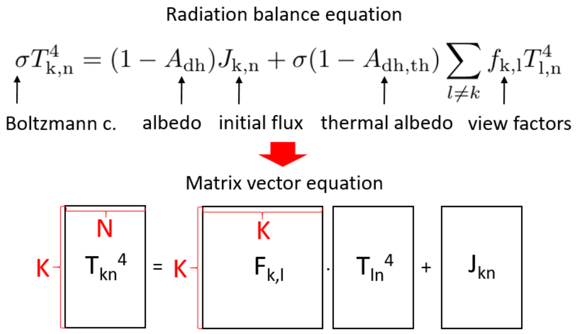

Figure 1. The radiation balance as matrix equation.

2. Subsampling of the geometric feature space: Disk-resolved radiance measurements of airless bodies can easily exceed millions of pixels, each with individual illumination and viewing configurations. A naïve thermal roughness model would require computing a fractal surface with several thousands of surface elements K for each of the N pixels of the planetary body. However, many illumination and viewing angles have similar values, so we can effectively reduce the problem size N. We compute the thermal model only for a small subset of approximately 5,000 geometric configurations of incidence, emission, and azimuth angle. Swift linear interpolation allows for computing the thermal emission for the remaining elements of the planetary body with proper accuracy. This step effectively reduces the matrix dimension N.

3) Periodic fractals: Self-heating and self-scattering collect the power that a facet of a rough fractal surface receives from its neighbors. We can practically limit the neighborhood to a self-heating radius of 100 pixels and still collect more than 95% of the radiation. However, near the edges and the corners, the self-heating radius extends beyond the fractal surface and cannot collect enough radiation. We use the inverse discrete Fourier transform (IDFT) to generate a fractal landscape from regolith statistics [4]. The IDFT ensures that the edges of the fractal are periodically continuous, which means that opposing sides can seamlessly be stitched together. If the self-heating-radius extends beyond one edge, we let it intrude the fractal from the opposing side. Consequently, we can collect enough thermal radiation to fulfill the heat balance equation. If we choose the edge length of the fractal surface to be twice as large as the self-heating radius, we avoid double interactions. This step ensures radiation balance and quadratically reduces the runtime of the self-heating simulation.

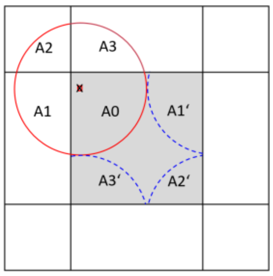

Figure 2. Consider pixel x in the gray center fractal surface. The self-heating radius (red circle) extends beyond the boundary of the gray center. Continuous periodicity means that areas A1, A2 and A3 can be identified with A1', A2' and A3' and used for self-scattering/heating.

Conclusion: These techniques dramatically speed up the thermal model computation. It now takes several minutes on an AMD EPYC 7742 to compute disk-resolved thermal emission for several hundered thousand pixels, considering all second order effects.

References:
[1] Wohlfarth et al. (2023), this conference [2] Tenthoff et al. (2023), this conference. [3] Wohlfarth et al. (2023), A & A, under revision. [4] Helfenstein, P. and Shepard, M. K. (1999) Icarus 141 (1), 107- 31.

UNIQUE NON-CONVEX SHAPE MODELING OF ASTEROIDS FROM THERMAL EMISSION AND REFLECTED LIGHT OBSERVATIONS

Eric M. MacLennan[1], Karri Muinonen[1], Sean Marshall[2], Maxime Devogele[2], and Josef Hanus[3]
[1]Department of Physics, University of Helsinki (eric.maclennan@helsinki.fi) [2]Arecibo Observatory & Unversity of Central Florida, [3]Charles University, Prague, Czech Republic

Introduction: The estimation of shape and spin properties using time-varied observations (lightcurve inversion) is enriched when using data from multiple sources [1]. Inversion using disk-integrated photometry – the most abundant source of data – is theoretically limited to the construction of convex shapes. While these convex shapes are *unique*, real asteroids display various topographical features and concavities that were shaped by various processes.

Motivation: Topographical features on asteroid surfaces result in shadows that are generally not discernible from global shape effects when using visible disk-integrated observations. The exception is when the object is observed at extremely high solar phase angles (> 60°) which is not possible for main-belt asteroids [2]. However, non-convex features produce non-trivial surface temperatures due to both shadowing and self-heating effects [3], and therefore produce a distinct signature in an object's thermal lightcurve (Figure 1). Using a thermophysical model (TPM) and thermal observations, large concave features can be modeled a number of asteroids.

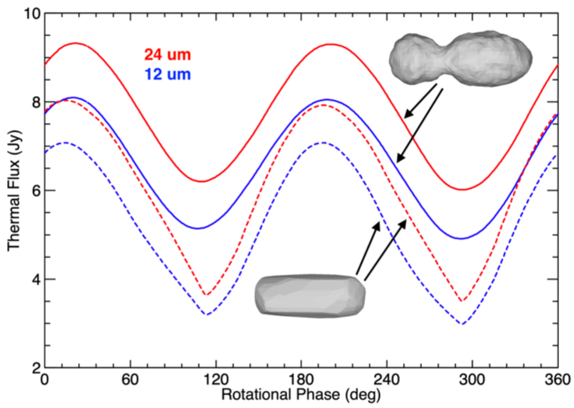

Figure 1: Thermal lightcurve at 12 & 24 μm calculated using a TPM for a convex (dashed) and radar-based (solid) shape model of 1996 HW_1 [4].

Observations: Reflected light detected by the Gaia survey is expected to be very useful for the modeling of spins and convex shapes of asteroids [5]. The WISE mission represents the largest single repository of thermal infrared (TIR; 8-26 μm) observations of asteroids. These data were recently shown to be useful in rotational period determination [6]. The observed flux at near-infrared wavelengths (NIR; 3-5 μm) is often a mixture of reflected solar light and emitted thermal emission. Simultaneous NIR and TIR fluxes that were acquired during nominal WISE mission represent perhaps the only observations of this kind. These observations are thus a unique opportunity to constrain the light scattering and emissivity properties of asteroid surfaces [7]. Multiple NIR sightings of thousands of asteroids have been gathered over several years as part of the reactivated NEOWISE mission.

Approach: The proposed approach can be broken into 4 steps:

Step 1. Period scanning
Step 2. Tri-axial ellipsoid shape estimation
Step 3. Convex shape inversion
Step 4. Non-convex shape inversion

Step 1 is relatively straightforward, but the novelty of using sparse multi-wavelength, long-baseline survey data has unique advantages. Steps 2-3 potentially require large computational resources if surface temperatures are calculated by solving the heat-diffusion equation for every instance [8]. This challenge can be overcome by using temperature lookup tables of a spherical object that can be mapped to any ellipsoid or convex shape [9]. Nonconvex features can be generated by either modifying groups of facets or producing shapes represented by spherical harmonic functions [10].

Expected Results: We will first perform proof-of-concept modeling on ground truth shape models derived from spacecraft and radar observations. We expect that contact binary asteroids will be most easily identified. Sampling of thermal lightcurve at local minima will be crucial for discerning non-convex features (Figure 1).

Future Development: Comments and ideas for collaborative efforts are welcome!

References:

[1] Ďurech, et al. (2015) in Asteroids IV, pp. 183–202. [2] Ďurech & Kaasalainen (2003) A&A 404, 709–714. [3] Rozitis & Green (2013) MNRAS 433, 603–621. [4] Magri, et al. (2011) Icarus 214, 210-227. [5] Muinonen, et al. (2020) A&A 642, A138. [6] Lam, A.L.H., et al. (2022) arXiv:2211.16409v1. [7] Myhrvold, et al. (2022) The Planetary Science Journal, 3:2, id.30. [8] Ďurech, et al. (2017) A&A 604, A27. [9] MacLennan & Emery (2019) The Astronomical Journal, 157:2. [10] Torppa & Muinonen (2005) 2005ESASP.576..321T.

SESSION 2

Thermal Modeling of Asteroids and Small Bodies

Evolution of airless planetary surfaces by thermal cracking: a review

Marco Delbo[1]
[1]Université Côte d'Azur, Observatoire de la Côte d'Azur, CNRS, Laboratoire Lagrange, France (delbo@oca.eu)

Introduction: The surface of airless bodies of our solar system is what we can investigate with remote sensing techniques, sample, and interact with by *in situ* space missions. Thus, it is important to understand how surfaces form and evolve, in order to gain insights into the composition of the whole body and its history throughout the different eras of our solar system.

Several processes that are capable of altering surfaces, their composition, and the properties that can be derived from remote sensing, have been identified and studied into details: these are impacts and crater formation, outgassing from the subsurface, and the waethering due to impacts of micrometeorties and high energy particles from the sun or the galaxy. However, several phenomena whose importance has been largely neglected in the past are those due to effect of temperature and temperarute variations. I will review the most recent developments in the field, with results ranging from asteroids exposed to estereme temperatures at low perhelion distances, to the coldest ones, cometary nuclei, Earth and Moon, and Mars.

Thermal cracking: Temperature variations between day and night can be important on bodies with a thin -- e.g. Mars -- or without an atmosphere, such as aseroids (*1*, *2*). These temperature variations create temperature gradients, which can produce mechanical stresses (*3*–*5*); additional mechanical stresses are generated at microscopic level by the different thermal expansion coefficients of the different materials that form the surface, such as inclusions within rocks or meteorites (*3*, *4*). Despite the resulting stresses can be lower than the material strength, they can still expand cracks, via a process called sub-critical crack growth. Since temperature variations, and the resulting stresses, are cyclic, cracks grow at every cyle, weakening the material. Eventially the material can break, leading, in the long term, to degradation of the object's surface.

Observations of thermal cracking: The evidence for surface weathering due to thermal cracking are growing: On the asteroid 433 Eros it was noted (*6*) that boulders erode in place, forming regolith ponds; On 101955 Bennu, exfoliation layers on boulders (*7*), boulders appearing to break down in place (*8*), and a preferential direction of fractures on boulders (*9*) were interpreted as due to thermal cracking; polygons of thermal contraction fractures have been observed (*10*) all over the nucelus of comet 67P/CG; on the same body the breakdown of cliffs have also been claimed as due to – or assited by – thermal fracturing (*11*); on Mars, rocks have been observed to have fractures preferentially aligned in a qausi N-S direction (*12*); the latter is also observed on Earth (*13*); in addition, experiments have been carried out on martian rock simulants (*14*) and meteorties (*3*), clearly showing that temrepature cycles lead to crack growth and weaking of materials. Other observations that are claimed to be associated with thermal cracking are the spontaneous and violent exfoliation of rock domes on Earth (*15*) and the ejection of materials from asteroids (*16*).

Conclusion: The role of surface evolution by subcrital cracking will be presented and discussed in this work. It is clear that temperature variations play a role more important that previsouly understood in sculpting the surfaces of rocky bodies in our solar system.

References:

1. M. Delbo, et al., "Asteroid Thermophysical Modeling" in *Asteroids IV*, P. Michel, F. E. DeMeo, W. F. Bottke, Eds. (University of Arizona Press, 2015; http://muse.jhu.edu/chapter/1705160).
2. B. Rozitis, et al., Asteroid (101955) Bennu's weak boulders and thermally anomalous equator. *Sci. Adv.* **6**, eabc3699 (2020).
3. M. Delbo, et al., Thermal fatigue as the origin of regolith on small asteroids. *Nature*. **508**, 233–236 (2014).
4. J. Molaro etal., Thermally induced stresses in boulders on airless body surfaces, and implications for rock breakdown. *Icarus*. **294**, 247–261 (2017).
5. B. Ravaji, et al., Unraveling the Mechanics of Thermal Stress Weathering: Rate-Effects, Size-Effects, and Scaling Laws. *Journal of Geophysical Research: Planets*. **124**, 3304–3328 (2019).
6. A. J. Dombard, et al., Boulders and ponds on the Asteroid 433 Eros. *Icarus*. **210**, 713–721 (2010).
7. J. L. Molaro, et al., In situ evidence of thermally induced rock breakdown widespread on Bennu's surface. *Nat Commun*. **11**, 2913 (2020).
8. D. S. Lauretta, et al., The unexpected surface of asteroid (101955) Bennu. *Nature*. **568**, 55–60 (2019).
9. M. Delbo, et al., Alignment of fractures on Bennu's boulders indicative of rapid asteroid surface evolution. *Nat. Geosci.* **15**, 453–457 (2022).
10. N. Attree, et al., Thermal fracturing on comets: Applications to 67P/Churyumov-Gerasimenko. *A&A*. **610**, A76 (2018).
11. M. Pajola, et al., The pristine interior of comet 67P revealed by the combined Aswan outburst and cliff collapse. *Nat Astron*. **1**, 0092 (2017).
12. M.-C. Eppes, et al., Cracks in Martian boulders exhibit preferred orientations that point to solar-induced thermal stress. *Nat Commun*. **6**, 6712 (2015).
13. L. D. McFadden, et al., Physical weathering in arid landscapes due to diurnal variation in the direction of solar heating. *Geol Soc America Bull*. **117**, 161 (2005).
14. H. Viles, et al., *Geophys. Res. Lett.*, in press, doi:10.1029/2010GL043522.
15. B. D. Collins, G. M. Stock, Rockfall triggering by cyclic thermal stressing of exfoliation fractures. *Nature Geosci*. **9**, 395–400 (2016).
16. J. L. Molaro, et al. Thermal Fatigue as a Driving Mechanism for Activity on Asteroid Bennu. *J. Geophys. Res. Planets*. **125** (2020), doi:10.1029/2019JE006325.

PRODUCTION OF FINE REGOLITH ON ASTEROIDS CONTROLLED BY ROCK POROSITY. S. Cambioni[1], M. Delbo[2], G. Poggiali[3], C. Avdellidou[2], A. J. Ryan[4], J. D. P. Deshapriya[5], E. Asphaug[4] , R.-L. Ballouz[6], M. A. Barucci[3], C. A. Bennett[4], W. F. Bottke[7] , J. R. Brucato[8], K. N. Burke[4], E. Cloutis[9], D. N. DellaGiustina[4], J. P. Emery[10], B. Rozitis[11], K. J. Walsh[7] , D. S. Lauretta[4]. [1]MIT, Cambridge, MA, USA (cambioni@mit.edu); [2] Observatoire de la Côte d'Azur, Nice, France; [3]LESIA Observatoire de Paris, Meudon, France; [4] UArizona, Tucson, AZ, USA; [5]INAF Roma, Italy; [6]JHAPL, Laurel, MD, USA; [7]SwRI, Boulder, CO, USA; [8]INAF Florence, Italy [9]U. of Winnipeg, Manitoba, Canada; [10]NAU, Flagstaff, AZ, USA; [11]The Open University, Milton Keynes, UK.

Rocks on airless bodies comminute into regolith via meteoroid bombardment and thermal cracking (Fig. 1, [1, 2]). Early studies proposed that small asteroids could not retain fine-grained ejecta because of their low gravity [3]. However, the JAXA Hayabusa mission observed fine-regolith-covered areas on the 300-m-sized S-type asteroid Itokawa [4], suggesting that fine regolith should be present on small asteroids. But the NASA OSIRIS-REx and JAXA Hayabusa2 missions found a general lack of fine regolith on carbonaceous asteroids Bennu and Ryugu [5, 6], despite signatures of regolith-forming processes [7, 8, 6].

Thermophysical model. To investigate why the surface of Bennu is so rocky, in [1] we analyze thermal infrared data of Bennu's surface collected by the OSIRIS-REx Thermal Emission Spectrometer (OTES) during the detailed survey phase of the mission [9]. Our approach measures the abundance α of fine-regolith particles smaller than the diurnal thermal skin depth (a few cm on Bennu [9]) and the thermal inertia Γ_R of nearby rocks, which is a monotonically decreasing function of rock porosity [10]. To explore the large parameter space of surface properties (including surface roughness) and globally map the surface of Bennu, we use a machine-learning thermophysical model [11] trained to distinguish the thermal signals of fine regolith and rocks of different grain sizes, porosities and relative surface abundances.

Results. On Bennu, we measure [1] a direct correlation between fine regolith α and the thermal inertia of nearby rocks Γ_R with Pearson probability of non-correlation $< 4 \times 10^{-3}$. The correlation is robust and corroborated by spacecraft data independently from OTES [1]. We explain the Γ_R-α correlation as the result of the dependence of regolith-forming processes on rock porosity. Laboratory experiments of meteoroid bombardment [12, 13] show that high-porosity rocks get compacted rather than excavated by impacts. Our model of rock thermal cracking [1] show that more porous rocks take longer to break via thermal fatigue because they suffer weaker thermal stresses [1]. We conclude that where rocks are more porous on Bennu, less rock fragmentation occurs, and thus the production of fine regolith is frustrated (Fig. 1). This explains the general lack of fine regolith on Bennu, where most rocks are highly porous [9].

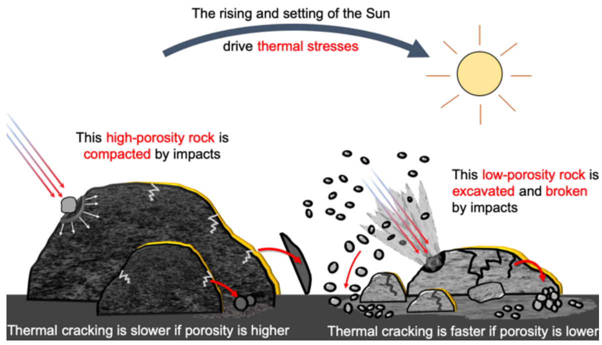

Figure 1. Evolution of two types of rocks on asteroids via regolith-forming processes as proposed in [1].

A general phenomenon of asteroids. A direct correlation between Γ_R and α on Bennu is consistent with the high rock porosity and the lack of fine-regolith ponds on asteroid Ryugu [10, 14, 3], and the low rock porosity and the presence of fine-regolith ponds on asteroid Itokawa [3, 11, 1]. We propose that carbonaceous asteroids like Bennu and Ryugu, which are the most populous type [15], should lack fine-regolith ponds, while S-type asteroids like Itokawa, the second-most populous group [15], should have abundant fine regolith. Future missions like ESA Hera will allow testing this prediction.

References: [1] Cambioni, S. et al. (2021) *Nature* 598, 49-52 ; [2] Delbo, M. et al. (2014) *Nature* 508 233-236; [3] Lebofsky, L.A., et al. (1979), *ApJ* : 885–888;[4] Saito, J. et al. (2006) *Science* 312.5778 : 1341-1344; [5] Lauretta, D. et al. (2019), *Nature* 568 : 55–60; [6] Sugita, S. et al. (2019) *Science* 364 eaaw0422; [7] Ballouz, R.-L. et al. (2020) *Nature* 587, 205-209; [8] Molaro, J.L., et al. (2020) *JGR:planets* 125, e2019JE006325; [9] Rozitis, B. et al. *Sci. Adv.* 6, eabc3699; [10] Grott, M. et al. (2019) *Nat. Astron.* 3, 971-976 ; [11] Cambioni, S. et al. (2019), *Icarus* 325, 16–30; [12] Flynn, G.J. et al. (2015) Planet. Space Sci. 107, 64–76; [13] Housen K.R et al. (2018), *Icarus* 300, 72-96; [14] Okada, T. et al. (2020) *Nature* 579 : 518-522; [15] DeMeo et al. (2015) in *Asteroids IV* : 13-41.

Acknowledgments: This material is based on work supported by NASA under contract NNM10AA11C issued through the New Frontiers Program and CNES. A complete list of acknowledgements is in [1].

The crater-induced YORP effect

Wen-Han Zhou[1], Yun Zhang[2], Xiaoran Yan[1,3], Patrick Michel[1]

[1] Observatoire de la Côte d'Azur, Nice 06304, France (wenhan.zhou@oca.eu)
[2] Tsinghua University, 30 Shuangqing Road, 100190 Beijing, China
[3] University of Maryland, College Park, MD, 20742, USA

Introduction: The Yarkovsky-O'Keefe-Radzievskii-Paddack (YORP) effect, which is a thermal torque produced by surface emission, has a strong influence on the rotational state and evolution of asteroids [1,2]. It can either increase or decrease the spin rate and can also change the spin obliquity of an asteroid on timescales that also depend on physical and dynamical properties of the considered asteroid. However, no investigation has been performed yet regarding how craters with given properties influence this effect. The crater-induced YORP (hereafter CYORP) effect has strong implications on the precise YORP torque calculation, as the YORP effect is known to be sensitive to the surface topology [3,4,5], and on the long-term rotational and orbital evolution of asteroids, as it links the YORP effect with the collision process.

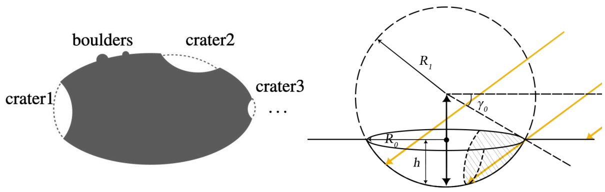

Figure 1: (a) Components on asteroids that contribute to the YORP effect. (b) Shape model of the crater.

Paragraph#1: By using a simple hemispherical shape model of the crater (see Fig. 1), we developed a semi-analytical method to calculate the total YORP torque due to the crater, accounting for self-sheltering and self-sheltering effects. The rapid computation of this semi-analytical method allows us to investigate the CYORP's functional dependence and to perform a MCMC simulation when studying the rotational and orbital evolution of an asteroid family. We define the CYORP torque as the difference between the YORP torques due to the crater and the flat ground without crater:

$$\vec{T}_{\rm CYORP} = \vec{T}_{\rm crater} - \vec{T}_{\rm ground}.$$

Paragraph#2: We also build a numerical model, to make a cross-validation with our analytical model. It turns out that the analytical method behaves well when the thermal conductivity is either low (e.g. < 0.001 W/m/K) or high (e.g. > 1 W/m/K). Considering typical materials on asteroids have thermal conductivities of 0.001, 2.65 and 40 W/m/K for regolith, basalt and metal materials, respectively, our model is prepared for application on real asteroids. The CYORP torque is generally expressed as

$$\vec{T}_{\rm CYORP} = W\frac{\Phi}{c}R^2_{\rm crater}R_{\rm asteroid}.$$

Paragraph#3: Our results show that the CYORP torque produced by a crater one-third of the asteroid size (or equivalently craters covering one-tenth of the asteroid surface) is comparable to the normal YORP torque of the entire asteroid. Figure 3 shows the CYORP coefficient W distribution as a function of the asteroid obliquity and the crater colatitude. As a comparison, YORP coefficient is only ~ 0.001.

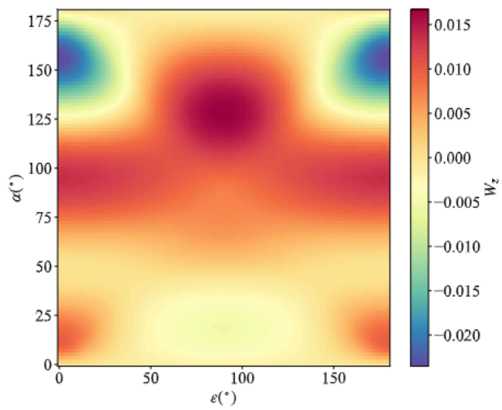

Figure 2: The CYORP coefficient distribution for basalt material as a function of the asteroids obliquity and the crater colatitude.

Conclusion: Craters and roughness on asteroid surfaces, which correspond to concave structures, can influence the YORP torques and therefore the rotational properties and evolution of asteroids. We suggest that the CYORP effect should be considered in the future investigation of the YORP effect on asteroids.

References:

[1] Rubincam, D. P. 2000, Icarus, 148, 2

[2] Vokrouhlick`y, D. & ˇCapek, D. 2002, Icarus, 159, 449

[3] Statler, T. S. 2009, Icarus, 202, 502

[4] Breiter, S., Bartczak, P., Czekaj, M., Oczujda, B., & Vokrouhlicky, D. 2009,Astronomy & Astrophysics, 507, 1073

[5] Golubov, O. & Krugly, Y. N. 2012, The Astrophysical Journal Letters, 752, L11

THE EFFECT OF ORBITAL ROTAION ON THE SURFACE TEMPERATURE DISTRIBUTION OF AN ASTEROD

H. Senshu[1], H. Maximillian[2,3], S. Tanaka[4], N. Sakatani[4], M. Kanamaru[5], Y. Shimaki[4], T. Arai[6], and T. Okada[4]
[1]Planetary Exploration Research Center, Chiba Institute of Technology, Japan (senshu@perc.it-chiba.ac.jp)
[2]Deutsches Zentrum Für Luft- und Raumfahrt (DLR), Germany
[3]Planetology and Remote Sensing, Department of Geoscience, Freie Universität Berlin, Germany
[4]Institute of Space and Astronautical Science, Japan Aerospace Exploration Agency (ISAS/JAXA), Japan
[5]The university of Tokyo, Japan
[6]Department of Life Engineering, Maebashi Institute of Technology, Japan

Introduction: The surface temperature distribution of an asteroid is a proxy to the thermophysical state of the asteroid's surface. The larger the thermal inertia is, the lower the peak temperature becomes and the later the local time when the peak temperature is achieved becomes. Addition to this, the temperature distribution is a key when the asteroid's size is estimated from the ground-based visible and infrared observations.

The surface temperature of an asteroid is controlled by the balance between the solar radiation, the thermal radiation into the space, and the heat flux into subsurface. Previous studies (e.g., [1-3]) simulated the surface temperature distribution taking into account diurnal change of the solar radiation due to its spin rotation. They fixed the position of the asteroid in the inertial frame and simulate the thermal evolution due to its spin rotation to achieve the equilibrium state.

If the spin axis of an asteroid is not perpendicular to its orbital plane and/or if the eccentricity of its orbit around the sun is not zero, the asteroid would experience annual change of the solar radiation condition. The effect of annual change is in general much smaller than the diurnal effect. And it costs too high to simulate numerically the diurnal temperature evolution at the same time with the annual temperature history. Thus the annual effect is often omitted to simulate the surface temperature distribution numerically. However the condition to be satisfied to omit the annual effect in the numerical simulation is not clear so far.

In this study we compare the numerical results from diurnal thermal evolution (DTE) model and annual thermal evolution (ATE) model. The spin rotation period, the spin axis direction, and the orbit around the sun are assumed to be the same with asteroid Ryugu as reference value.

Results and Discussion: Fig.1 represents the temperature discrepancy between DTE and ATE models as a function of latitude when the local time is noon, dusk and midnight on 3rd Oct. 2018. This day is 2 month after the winter solstice on the northern hemisphere. The different colors represent the different thermal inertias. The temperature discrepancy is obvious if the thermal inertia is as high as 800 in MKSA unit. Even in this case the temperature discrepancy between DTE and ATE models is up to several degrees. On the other hand the temperature discrepancy becomes larger at the northern high latitude region. This came from the cold subsurface in the winter hemisphere.

The annual effect might seem to be minor because the discrepancy is obvious at high latitude region. However it is worth noting that the shape of Ryugu, Bennu, Didymos and probably also Phaethon are known as spinning top, which means almost all of their surface is covered by geometrically mid- to high-latitude region

References:

[1].Takita, J. et al. (2017) SSR 208, 287.
[2] Shimaki, Y. et al. (2020) Icarus 348, 113835.
[3] Senshu, H. et al. (2022) IJoT 43, 102.

Acknowledgments: This research is supported by Japan Society for the Promotion of Science (JSPS) KAKENHI (Grant No. JP21K03649) and JSPS summer program 2017.

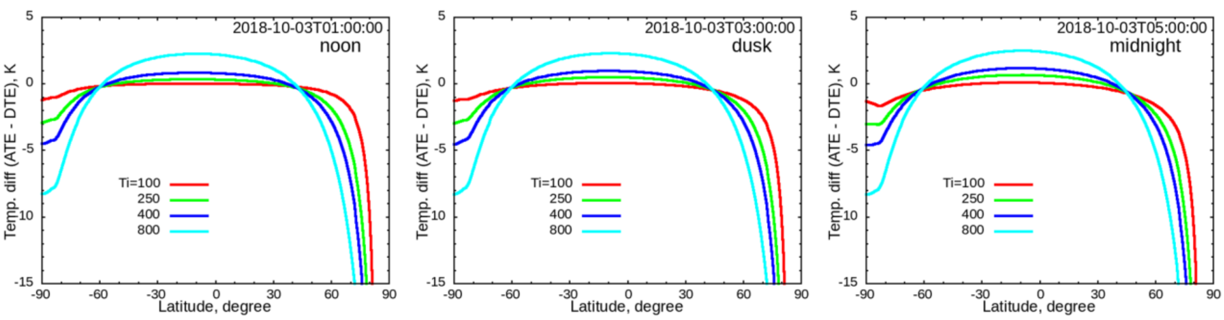

Figure 1: Temperature discrepancy between DTE and ATE model for various thermal inertia.

INVERSION OF THERMAL INFRARED DATA AND OPTICAL LIGHT CURVES OF ASTEROIDS – UNCERTAINTY OF THE DERIVED THERMOPHYSICAL PARAMETERS

Josef Ďurech[1] and Hanjie Tan[1]
[1]Charles University, Astronomical Institute (durech@sirrah.troja.mff.cuni.cz)

Introduction: Thermal infrared measurements of asteroids are used to unveil their physical properties. The observed disk-integrated thermal flux depends on the parameters we want to reconstruct (size, albedo, thermal inertia, roughness) and on the asteroid's shape that is usually assumed to be known. By modeling the relevant (thermo)physical parameters, their best-fit values are found, and their uncertainties are estimated. However, using a fixed shape of an asteroid usually leads to an underestimation of the derived parameter uncertainties.

Thermophysical models with fixed shape: Currently, the largest source of thermal infrared data of asteroids are the observations of WISE/NEOWISE mission [1]. The analysis of WISE measurements utilizing a Near-Earth Asteroid Thermal Model has led to sizes and albedos of tens of thousands of asteroids [2,3].

WISE data were also combined with asteroid shape models derived from photometry [4,5]. This way, thermal inertia – crucial physical characteristics of the surface – and surface roughness can be determined. However, using a fixed shape often leads to an insufficient thermal data fit and underestimating errors [6].

Convex inversion thermophysical modeling: The simultaneous inversion of optical and thermal data enables us to find models that correctly fit both data types and realistically estimate uncertainties [7]. In general, when an asteroid's shape and spin state are optimized, the model is more flexible than in the case of a fixed shape, and uncertainty intervals of parameters of interest (thermal inertia in the first place) are larger.

We will show examples of how fixed vs. optimized shapes provide different fits to thermal data and how the parameter errors differ. The results of applying the convex inversion thermophysical model to hundreds of asteroids will be presented in a separate talk [8].

Conclusion: The number of convex asteroid models reconstructed from light curves and sparse-in-time photometry has continuously increased, with about 10,000 shape models available now [9]. The number of models is expected to increase significantly further, mainly due to ongoing and future surveys (Gaia, ATLAS, ZTF, LSST). Thus there will soon be tens of thousands of asteroids for which a shape model is available, and data from WISE exist.

When applying any thermophysical modeling on asteroid disk-integrated thermal data and interpreting its results, one has to consider not only the uncertainties of thermal fluxes but also uncertainty in the shape model and model assumptions (emissivity, for example).

References:

[1] *Wright E. L., Eisenhardt P. R. M., Mainzer A. K., et al. 2010, AJ 140, 1868*
[2] *Masiero J. R., Mainzer A. K., Grav T., Bauer J. M., Cutri R. M., Dailey J., Eisenhardt P. R. M., et al., 2011, ApJ 741, 68*
[3] *Myhrvold N., Pinchuk P., Margot J.-L., 2022, PSJ 3, 30*
[4] *Hanuš J., Delbo M., Ďurech J., Alí-Lagoa V., 2018, Icarus 309, 297*
[5] *Hung D., Hanuš J., Masiero J. R., Tholen D. J., 2022, PSJ 3, 56*
[6] *Hanuš J., Delbo M., Ďurech J., Alí-Lagoa V., 2015, Icarus 256, 101*
[7] *Ďurech J., Delbo M., Carry B., Hanuš J., Alí-Lagoa V., 2017, A&A 604, A27*
[8] *Tan H. and Ďurech J., 2023, TherMoPS IV*
[9] *Ďurech J. and Hanuš J., 2023, A&A, submitted*

Acknowledgments: This work has been supported by the Czech Science Foundation grant no. 23-04946S.

Determining the physical parameters of asteroids with combined optical photometry and thermal infrared data

Hanjie Tan[1] and Josef Durech[1]
[1]Astronomical Institute, Faculty of Mathematics and Physics, Charles University, Prague, Czech Republic (hanjie@sirrah.troja.mff.cuni.cz)

Introduction: By applying a thermophysical model (TPM) to asteroid thermal infrared observations, we can estimate the physical parameters of asteroids, including thermal inertia, surface roughness, diameter, and albedo. To obtain the physical parameters of a large population of asteroids and explore the relationships between these parameters, we constructed the TPM of 1900 asteroids by combining optical and infrared data. In previous studies, the asteroid's shape and rotation state were often used as preconditions for TPM. This inevitably affects the accuracy with which the TPM reproduces the measurements and the parameters' uncertainties. In this study, we used convex inversion thermophysical models (CITPM) [1], which enable simultaneous optimization of all relevant parameters of the asteroid while considering the errors in the asteroid model and rotation state. We combined the asteroid model obtained from the inversion of the light curve, which helps the TPM converge faster and effectively constrains the parameters with infrared data. Many of the asteroids in our sample had their thermal inertia and other parameters calculated for the first time, which will expand our understanding of asteroids. With more examples, we move closer to finding correlations between parameters.

Method: We used the CITPM to reconstruct the asteroid's model and parameters. We set initial values, such as spin state, size, and Hapke parameters, to facilitate fitting convergence based on asteroid shapes and their spectral classifications. We used all the initial models from the Database of Asteroid Models from Inversion Techniques (DAMIT) [2] . And spectral classifications were from NASA Jet Propulsion Laboratory (JPL) or Asteroid Lightcurve Database (LCDB) [3]. The TPM was run on ten different roughness combinations with thermal inertia values fixed between 2 and 1000 [J m^{-2} $s^{-0.5}$ K^{-1}]. We determined the best-fitting values and the errors in the parameters by comparing the reduced chi-squared curves for only thermal fluxes in each roughness profile.

In this study, we comprised the optical data of dense and sparse lightcurve. Not all asteroids have dense lightcurves, so accurate sparse lightcurves become essential. Our sparse data were obtained primarily from surveys such as Gaia, ASAS-SN, TESS, ATLAS, USNO, etc. We now have 1900 asteroids with WISE thermal data in our dataset, they were observed in the W3 (11.1μm) and W4 (22.6μm) bands. In our dataset, 906 asteroids were also observed by Akari in the 9μm and 18μm bands or by IRAS in the 12, 25, 60, and 100μm bands. Moreover, 134 asteroids were observed during two different oppositions by WISE.

Result: In our result, for some asteroids, the model constructed from optical and thermal data does not fit well. The reduced chi-squared value would be significantly higher than 1, which requires us to examine optical and infrared data. However, for the other asteroids, the reduced chi-squared value is close to or less than 1. Still, the reduced chi-squared curve is very flat, making it impossible to constrain thermal inertia or other parameters within a narrow range. These cases will be the focus of our future work. Despite this, we still obtained acceptable parameters and errors for hundreds of asteroids from the clear minimum in their reduced chi-squared curves. In future work, we will investigate the correlation between their surface thermal physical parameters and other parameters.

Conclusion: The purpose of our research on thermal inertia and thermal physical models of asteroids is twofold. On the one hand, our study aims to estimate the thermal inertia, diameter, albedo, and other relevant parameters for individual asteroids. This information is necessary for quantifying the influence of the Yarkovsky and YORP effects on the asteroid. On the other hand, we aim to study the correlations between various physical parameters of the asteroids. The large number of parameters obtained from our study can help to investigate the correlations between different parameters and different asteroid families, spectral classifications, and distributions in the main belt.

References:

[1] Ďurech, J., et al. (2017). Astronomy & Astrophysics 604: A27.
[2] Ďurech, J., Sidorin, V., & Kaasalainen, M. (2010). Astronomy & Astrophysics, 513, A46.
[3] Warner, B. D., Harris, A. W., & Pravec, P. (2009). Icarus, 202(1), 134-146.

Acknowledgments: This work has been supported by the Erasmus+ program of the European Union under grant number 2020-1-CZ01-KA203-078200.

One-dimensional thermal modelling of cometary surfaces – implications for a pressure-induced ejection mechanism

C. Schuckart[1], D. Bischoff[1], B. Gundlach[1], N. Attree[1], J. Blum[1]
[1]Institute of Geophysics and Extraterestrial Physics (c.schuckart@tu-braunschweig.de)

Introduction: The problem of cometary activity is still largely unsolved and requires thorough experimental and numerical investigations to further our understanding. We have developed a one-dimensional numerical model based on the work of Gundlach et al. [1] to investigate pressure-driven dust ejection assuming ultra-low tensile strength of cometary materials as the main activity mechanism.

The numerical approach: We employed a forward time, centered space explicit finite difference approximation to solve the one-dimensional heat-transfer-equation and appended it with source and sink terms to allow latent heat transfer of volatile species, which we have modelled using H_2O und CO_2 ice.

Furthermore, we applied the description of heat conductance through a porous pebble-medium, given by Gundlach and Blum [2] to account for the increased heat conductivity through thermal radiation at higher temperatures that is present when the material consists of macroscopic voids.

The sublimation of volatile molecules is calculated via the Hertz-Knudsen equation and the molecules are redistributed in a fixed pattern and allowed to resublimate in colder layers. This additional heat-transfer mechanism displays a signature dent in the resulting temperature profiles for which a typical example is shown in Figure 1.

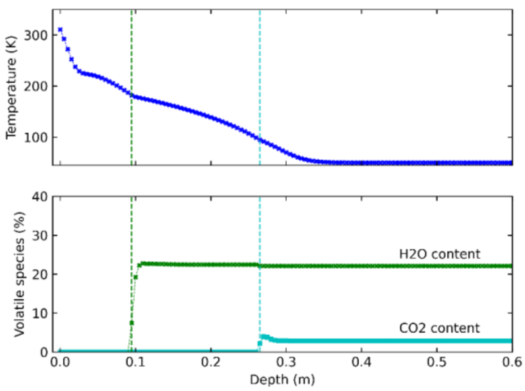

Figure 1: Temperature profile for a section of comet 67P's orbit between 5.68 and 1.32 au, taken at 1.32 au. The dent in the temperature, stemming from the water-ice sublimation, is clearly visible

Discussion of the ejection mechanism: While testing this model in different cases, including modelling an entire orbit, we encountered some caveats with the assumed ejection mechanism.

Firstly, dust activity tends to be completely governed by the most volatile species within the model, this being CO_2 in our case. While both volatile species show a largely similar, albeit low, peak pressure, the CO_2 sublimates faster and reaches its peak pressure faster, thus dominating the ejections.

Secondly, the pressures we have to assume to allow any dust activity are around one to two orders of magnitude lower than the ones usually assumed to be found on comets (typically in the range of 1 to 10 Pa [3]). If we assume higher tensile strengths, the volatile species recede too far into the comet to start ejections, even when approaching perihelion.

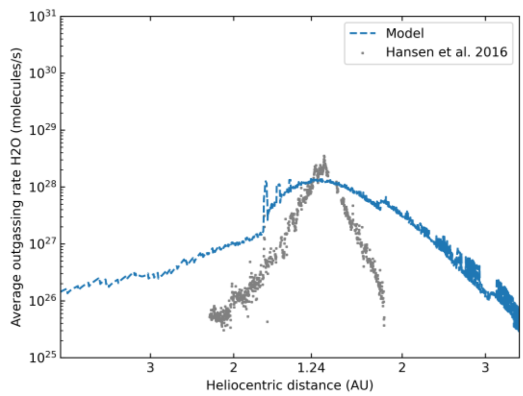

Figure 2: A comparison between the model prediction in H_2O outgassing and Rosetta data from [4]

Conclusion: Our simple one-dimensional thermophysical model tries to incorporate some of the most important aspects of cometary material and heat transport therein. While it is able to reproduce outgassing rates in the same order of magnitude as the observed data (see Figure 2), it struggles to reproduce the correct dust ejection and outgassing rates. Especially the connection between dust ejection and volatile recession needs to be understood to further improve the predictions of this type of model.

References:

[1] Gundlach et al. 2020
[2] Gundlach and Blum 2012
[3] Groussin et al 2019
[4] Hansen et al. 2016

How frequent are main-belt comets?

Yun Zhang[1] and Christine M. Hartzell[1]
[1]Department of Aerospace Engineering, University of Maryland, College Park, MD 20742, USA (yz917@umd.edu)

Introduction: Small bodies that contain volatile components hold valuable information about the evolution of the solar system and the origins of life on Earth, as well as being of interest for resource exploration. In recent decades, dust emission driven by sublimation has been detected on several asteroids located in the inner solar system, known as main-belt comets (MBC), which suggests the presence of buried ices in these bodies [1, 2]. Previous theoretical studies (e.g., [3–5]) have predicted that main-belt objects should be able to retain interior water ice throughout the lifetime of the solar system. A numerical simulation of the first discovered MBC, 133P/Elst-Pizarro [6], shows that, after 4.6 Gyr of evolution, while other volatiles would have been depleted, crystalline H2O ice can persist in the subsurface of this object at depths ranging from ~50 to 150 m. The depth to ice is shallower if the object was recently formed from the catastrophic disruption of its parent body, e.g., a few meters for a body with a 10-Myr lifetime [7]. These objects can exhibit comet-like activity when impacted by a small object that exposes their subsurface volatile ices [8].

However, some active main-belt asteroids, such as (596) Scheila [9], exhibit dust ejection related to impacts but without any signs of sublimation-driven activity, raising questions about the prevalence of subsurface ice in main-belt objects. In this study, we use thermophysical modeling to investigate the dust emission activities of a main-belt object and conduct a statistical analysis to determine the likelihood of an impact-induced sublimation activation event.

Method: We use the 3D thermophysical model, GTA3D (the Generalized finite difference method for modeling Thermal evolution of Active small bodies) [10], to simulate the heat and mass diffusion in a MBC. We consider an ellipsoidal shape for this object, i.e., 2.7 × 1.8 × 1.8 km for the three semi-major axes, resembling the shape of the first discovered MBC, 133P/Elst-Pizarro. To examine the gas and dust emission activity with varying dust-mantle thicknesses due to ejecta redepostion, the body is modeled as a heterogeneous structure comprised of a dust mantle and a homogenous interior of dust-ice mixture. The interior dust-to-ice mass ratio is set to ~3.6, lying within the range derived for Comet 67P/C-G [11]. The simulated body is placed in the orbit of 133P/Elst-Pizarro.

Results: A series of thermophysical evolution simulations were performed by varying the obliquity of the body's spin axis from 0º to 90º. As an example, Figure 1 displays the maximum dust mass loss rate over four consecutive orbital evolutions for a modeled MBC (top: obliquity = 0º; bottom: obliquity = 30º), with a dust mantle thickness of zero, as a function of latitude. The high-frequency fluctuations in mass loss rate at different orbital positions are caused by the geometry of the ellipsoidal shape and varying data-point sampling locations. The surface along the longest semi-axis is cooler than the surface along the shortest semi-axis at the same solar angle, resulting in different gas and dust emission strength. The results show that the strength of dust ejection activities is sensitive to the location of the impact crater and the obliquity. The outcomes for the models with different dust mantle thicknesses show similar trends, except that the mass loss rate magnitude is smaller for a thicker dust mantle.

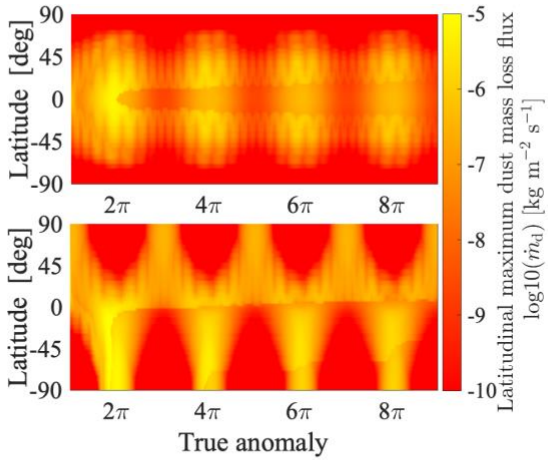

Figure 1: Latitudinal distribution of dust mass loss flux for a initially uniform dust-ice-mixed body.

Conclusion: By simulating the thermal evolution of a MBC, we found that the strength of gas and dust emission activities strongly depends on the body's obliquity, solstice, and the thickness of surface dust mantle and varies with the location. Consequently, an impact on an ice-rich object in the main belt might not always lead to detectable sublimation-driven activities. The main-belt comet candidate population may be substantially larger than the number currently detected.

References: [1] Jewitt et al., Asteroid IV 221–241 (2015). [2] Snodgrass et al., Astron. Astronphys. Rev. 25, 1–59 (2017). [3] Fanale & Salvail, Icarus 82, 97–110 (1989). [4] Schörghofer, ApJ 682, 697–705 (2008). [5] Schörghofer & Hsieh, JGR: Planets 123, 2322–2335 (2018). [6] Prialnik & Rosenberg, MNRAS 399, L79–L83 (2009). [7] Schörghofer, Icarus 276, 88–95 (2016). [8] Heish et al., AJ 155, 96 (2018). [9] (20). [10] Zhang & Hartzell, AAS/DPS 54, 114.03 (2010). [11] Patzold et al., MNRAS 483, 2337–2346 (2019).

Thermal and Optical Observations of Near-Earth Objects with the NASA-IRTF MIRSI Camera

Andy López-Oquendo[1], David E. Trilling[1], Joseph L. Hora[2], Howard A. Smith[2], John Rayner[3], Schelte J. Bus[3], Charles Lockhart[3], Mike Connelley[3]; [1]Department of Astronomy and Planetary Science, Northern Arizona University, Flagstaff, AZ 86011, USA (al2987@nau.edu); [2] Center for Astrophysics | Harvard & Smithsonian, 60 Garden St., MS-65, Cambridge, MA 02138, US; [3]Institute for Astronomy, University of Hawaii, Hawaii, USA

Introduction: Since the early '70s ground-based thermal observations began to play an important role in studying airless bodies [1]. Ever since, the development of more sensitive instruments and both ground-based and space-based facilities have converted the mid-infrared (MIR) range into a powerful tool for airless body characterization [2,3], especially the Near-Earth Objects (NEOs) population. With the close approach of NEOs orbits to the earth, human civilization's safety is under threat. Thus, with the beginning of the thermal surveys era (see [3]), primarily motivated by planetary defense efforts from entities such as NASA, tremendous improvements have been achieved with the broad understanding of the main belt and near-Earth asteroid populations [3].

Cryogenically cooled thermal instruments are challenging and increasingly expensive to maintaim them at operating temperature for long periods of time. This has led to the decommissioning of many thermal instruments at ground-based telescopes. Here we present a summary of our ongoing NEO observational campaign using the newly refurbished Mid-Infrared Spectrometer and Imager (MIRSI, [4], [5]) at the 3-meter NASA Infrared Telescope Facility (IRTF).

Methodology: The MIRSI data are obtained using the telescope nod and offsets to obtain images of the NEO at different locations on the array. The MIRSI Optical Camera (MOC) is used for telescope guiding on the NEO during the exposure sequence, while simultaneously acquiring R-band photometry. The images are first differenced in pairs to remove the sky background and array readout pattern. The frames are corrected for pixel-to-pixel gain variations. The final mosaic is then calculated by aligning the individual frames based on the commanded offsets, and a sigma-clipped mean value is calculated at each position. The standard star data is obtained and reduced in the same way. The fluxes are corrected for the airmass of the observation, and the standard star photometry is used to determine the Jy/ADU conversion factor, which is then applied to the NEO photometry. The MOC data was reduced using SExtractor [6]. The absolute magnitude (H) at R-band is then calculated using [7].

Results: We have performed simultaneous optical and thermal observations of 15 NEOs, including the next Hayabusa2 and DART targets, and measured their colors, albedo, and diameter. We modeled the measured spectral energy distribution (SED) at the wavelength of interest using the Near-Earth Asteroid Thermal Model (NEATM, [8]), and using H obtained from the simultaneous MOC data. In Fig. 1 we present the albedo and diameter measurements of 15 NEOs observed with MIRSI. Our sample contains detections of 0.2 Jy sources at 10σ down to 0.07 Jy at 3σ.

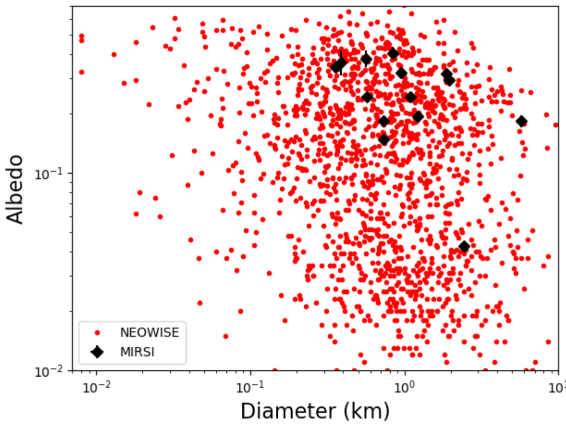

Figure 1: Albedo as a function of diameter for NEOs measured by NEOWISE and MIRSI in red circles and black diamonds, respectively.

Conclusion: MIRSI has shown to be a unique ground-based instrument to perform NEO characterization given its capability to acquire simultaneous optical photometry which allows blind stacking of very faint sources and color determination, and H measurements. We present the first MIRSI NEOs observations after its upgrade into a closed-cycle cooler. Our dataset includes NEOs from 6 km down to 300 m in effective diameter and albedos ranging from 4% to 50%. Approximately 90% of our dataset contains NEOs with albedos >15%, this clearly shows the fact that our objects are optically selected.

References: [1] Allen D. A. (1970), Nature, 227, 158. [2] Delbó M., et al., (2003), Icarus, 166, 116-130. [3] Mainzer A. et al., (2015), In Asteroids IV, 89. [4] Kassis M., et al., (2008), AJP, 120, 874, 1271. [5] Hora, J. L. et al. 2015, DPS, 47, 312.21 [6] Bertin, E., & Arnouts, S. (1996), A&AS, 117, 393. [7] Bowell et al., (1989), Ast. II, 524. [8] Harris, A. W. (1998), Icarus, 131, 291.

Acknowledgments: This material is in part supported by the NSF-GRFP grant No. 2021318193 and NASA Solar System Observations/NEOO program.

Unveiling the trans-Neptunian belt with the Square Kilometre Array

Pablo Santos-Sanz[1], Thomas G. Müller[2] and Emmanuel Lellouch[3]

[1]Instituto de Astrofísica de Andalucía-CSIC, Granada, Spain (psantos@iaa.es)
[2]MPE, Garching, Germany (tmueller@mpe.mpg.de)
[3]LESIA-Observatoire de Paris, CNRS, France (emmanuel.lellouch@obspm.fr)

Introduction: The Square Kilometre Array (SKA) will be particularly important for characterizing distant Solar System objects, such as trans-Neptunian objects (TNOs) and Centaurs. These objects, along with comets, are thought to be the most pristine remnants of the formation of the Solar System, and in this sense provide a link to the protoplanetary disks observed around other stars. The potential of the SKA to measure the thermal emission of these distant and cold Solar System objects will be presented in terms of the different wavelengths and expected sensitivities. These observations will be critical for the physical, thermal, and compositional characterization of individual TNOs/Centaurs and for understanding the alteration processes that take place on the (sub-)surface of these bodies.

TNOs and Centaurs thermal data: Previous studies of the thermal emission of TNOs and Centaurs have been based on the Spitzer Space Telescope (Stansberry et al., 2008), Herschel (Müller et al., 2009), WISE (Bauer et al., 2013), and more recently ALMA (Moullet et al., 2011; Gerdes et al., 2017; Brown & Butler, 2017, 2018; Lellouch et al., 2017). A summary of the results of these thermal studies has been presented by Müller et al. (2019). In the near to mid-term future, there will be no airborne or space-based option to directly measure these remote and cold objects at their thermal emission peak (about 50-100 microns). JWST's wavelength coverage will end at 28 microns (MIRI: Rieke et al., 2015), and it will not be efficient to measure radiometric diameters, albedos, or surface emission properties. From the ground, the thermal emission of TNOs is only accessible in the mm/cm wavelength range. ALMA measurements of 10 objects (Brown & Butler, 2017; Lellouch et al., 2017) show long-wavelength emissivity effects and spectral emissivity variations. Grain sizes certainly play a key role in explaining some of the results, but no clear correlations with physical or compositional properties have been found.

Thermal emission of TNOs and Centaurs with the SKA: The measure of the thermal emission of TNOs and Centaurs provides a unique way to obtain sizes, albedos and information on the thermal regime (e.g. thermal inertia Γ, surface roughness, etc) of the (sub-)surfaces of these objects via thermal and thermophysical models, as has been extensively demonstrated by the 'TNOs are Cool' Herschel Space Observatory key project (Müller et al., 2009; Lellouch et al., 2013; Santos-Sanz et al., 2017). We explore here if it would be possible to detect the thermal emission of TNOs/Centaurs with the SKA in order to derive their sizes, albedos and Γ's.

Conclusions: Thermal emission measurements of TNOs/Centaurs with the SKA are feasible and will allow us to study what happens to the relative spectral emissivity at long (centimeter) wavelengths and what this tells us about the subsurface of these bodies. In general, the spectral emissivity of TNOs decreases from ∼ 200 microns out to at least the mm range (Fornasier et al., 2013; Lellouch et al., 2017), sometimes in a strongly chromatic fashion (Brown & Butler, 2017). Obtaining multi-wavelength continuum fluxes with the SKA, and combining the results with other facilities such as ALMA, would allow constraints to be placed on the thermal/physical properties of the subsurface. These emissivity studies can be performed for TNOs/Centaurs for which we already have size and thermal inertia estimates, this would provide a benchmark study of the emissivity behavior. These emissivity results can be used to obtain sizes and thermal properties for many more TNOs/Centaurs for which we don't have thermal data. These SKA results will allow us to (i) improve the number of objects with determined size, albedo and thermal properties, (ii) obtain mass densities for multiple/binary systems for which the masses are known, (iii) refine the knowledge of the size distribution of these bodies related to the collisional history of the outer Solar System.

References:

[1] Bauer et al., 2013, ApJ, 773, 22
[2] Brown & Butler, 2017, AJ, 154, 19
[3] Brown & Butler, 2018, AJ, 156, 164
[4] Fornasier et al., 2013, A&A, 555, A15
[5] Gerdes et al., 2017, ApJL, 839, L15
[6] Lellouch et al., 2013, A&A, 557, A60
[7] Lellouch et al., 2017, A&A, 608, A45
[8] Müller et al., 2009, EM&P, 105, 209
[9] Müller et al., 2019, The TN Solar System, 153
[10] Moullet et al., 2011, Icarus, 213, 382
[11] Rieke et al., 2015, PASP, 127, 584
[12] Santos-Sanz et al., 2017, A&A, 604, A95
[13] Stansberry et al., 2008, The Solar System Beyond Neptune, 161

APPLICATIONS OF THERMOPHYSICAL MODELS TO THE OSIRIS-REX SAMPLE RETURN MISSION. B. Rozitis[1], A. J. Ryan[2], J. P. Emery[3], D. S. Lauretta[2], and The OSIRIS-REx Thermal Analysis Working Group. [1]The Open University, Milton Keynes, UK (benjamin.rozitis@open.ac.uk); [2]University of Arizona, Tucson, AZ, USA; [3]Northern Arizona University, Flagstaff, AZ, USA.

Introduction: NASA's OSIRIS-REx mission sampled asteroid (101955) Bennu in October 2020 and will return the collected samples to Earth in September 2023 [1]. Thermophysical models [2], aided by mid-IR (OTES [3]) and near-IR (OVIRS [4]) observations, were employed by the mission to support several aspects of scientific characterization and spacecraft operations. Here, we review these varied applications of thermophysical models and their outcomes.

Thermal Inertia Mapping: Disk-integrated [5], global-resolved [6], and local-resolved [7] thermal inertia maps were produced to aid sample site selection and to provide scientific context for the returned samples. These maps revealed that thermal inertia on Bennu is dictated by rock porosity [6,8], and identified a strong trend of increasing thermal inertia with increasing albedo [6,9]. This implied that Bennu has two or more types of porous rock with weak tensile strength.

Interpretation of Thermal Roughness: Thermal roughness was found to depend on the number density and shape of rocks not resolved in the topography used in the thermophysical model [6]. It correlated with geologic units [10] and other physical and photometric measures of surface roughness [9,11]. Attempts to directly model roughness at the skin-depth scale found that sub-skin-depth roughness still makes a contribution to the infrared beaming effect [7].

Yarkovsky Effect and Impact Hazard: The Yarkovsky effect of Bennu was precisely measured by ground- and spacecraft-based astrometry [12]. A model constructed from the thermal maps [6] produced a Yarkovsky-based bulk density estimate that was within 0.1% of that measured directly by gravity science [12,13]. Statistical forward propagations of Bennu's orbit, including the modelled Yarkovsky effect, estimated a 1 in 1750 chance of impacting the Earth in the late 22nd century [12].

Origin of Particle Ejection Events: Bennu was discovered to be an active asteroid shortly after OSIRIS-REx arrival [14]. It was hypothesized that the observed particle ejection events could be temperature-driven through ice sublimation and/or rock thermal fracturing. High-resolution thermophysical modelling found that buried ice was only stable at Bennu's poles, but in contrast, rock thermal fracturing was possible at any latitude due to Bennu's rugged shape [15].

Particle Trajectory and Gravity Field Determination: Bennu's ejected particles provided natural tracers for probing its gravitational field [13], but the trajectories of the particles were influenced by the thermal radiation pressure from Bennu. A model of thermal radiation pressure, derived from the disk-integrated observation [5], was interfaced with particle dynamical integration software to infer the gravitational field of Bennu [16]. A Bouger gravity anomaly map was constructed from which internal density inhomogeneities of Bennu were also inferred [13].

Spacecraft Operations: Like the ejected particles, the trajectory of the OSIRIS-REx spacecraft was influenced by thermal radiation pressure in close proximity to Bennu [17]. Therefore, a similar thermal radiation pressure model was delivered to Lockheed Martin for integration with their spacecraft navigation software. Additionally, assessments were performed before sample collection to identify any areas on Bennu with temperatures >350 K that could be hazardous to the sample and/or spacecraft. Our high-resolution thermophysical models [7] also helped to refine the reconstructed spacecraft pointing after low altitude sorties.

Spectral Interpretation: Simple pipelines based on single/multiple temperatures were implemented to extract spectral emissivity and reflectance data from OTES and OVIRS observations. The results of these pipelines were verified against extractions performed by the thermophysical model [18]. These spectral datasets found Bennu to contain carbon-bearing [19] and hydrated [18] minerals. Finally, the thermophysical model was used to estimate suitable instrument integration times at different phases of the mission.

References: [1] Lauretta *et al.* (2022) *Science*, 377, 285. [2] Rozitis & Green (2011) *MNRAS*, 415, 2042. [3] Christensen *et al.* (2018) *Space Sci Rev*, 215, 87. [4] Reuter *et al.* (2018) *Space Sci Rev*, 215, 54. [5] DellaGiustina *et al.* (2019) *Nat Astron*, 3, 341. [6] Rozitis *et al*. (2020) *Sci Adv*, 6, eabc3699. [7] Rozitis *et al*. (2022) *JGR Planets*, 127, e2021JE007153. [8] Cambioni *et al*. (2021) *Nature*, 598, 49. [9] Li *et al.* (2021) *PSJ*, 2, 117. [10] Jawin *et al*. (2022) *Icarus*, 381, 114992. [11] Daly *et al*. (2020) *Sci Adv*, 6, eabd3649. [12] Farnocchia *et al*. (2021) *Icarus*, 369, 114594. [13] Scheeres *et al.* (2020) *Sci Adv*, 6, eabc3350. [14] Lauretta *et al.* (2019) *Science*, 366, eaay3544. [15] Rozitis *et al*. (2020) *JGR Planets*, 125, e2019JE006323. [16] Chesley *et al*. (2020) *JGR Planets*, 125, e2019JE006363. [17] Hesar *et al*. (2017) *J Guid Control Dyn*, 40, 2432. [18] Hamilton *et al.* (2019) *Nat Astron*, 3, 332. [19] Simon *et al*. (2020) *Science*, 370, eabc3522.

Acknowledgments: This material is based on work supported by NASA under contract NNM10AA11C issued through the New Frontiers Program, and by the UK Science and Technology Facilities Council.

THERMAL MODELING OF NEAR-EARTH ASTEROID, 2100 RA-SHALOM

Kiana D. McFadden [1], Ellen S. Howell[1], Ronald J. Vervack Jr.[2], Yanga R. Fernandez[3], Christopher Magri[4], Lynn M. Carter[1], Samuel A. Myers[1], Sean Marshall[5]

[1]LPL /UArizona (kmcfadden@arizona.edu), [2] JHU/APL, [3] UCF , [4] University of Maine Farmington, [5] Arecibo Observatory/ UCF

Introduction: Near-Earth asteroid 2100 Ra-Shalom is one of the largest known Aten asteroids. Although it has been extensively observed at various wavelengths, its surface is still poorly understood. We have utilized the shape-based thermophysical model, SHERMAN, to simulate its thermal emission at multiple viewing geometries to investigate the thermal properties of its surface. SHERMAN has been proven to be successful in contraining albedo, surface roughness, and thermal inertia of other near-Earth asteroids [1,2], and we apply it here in a new anlaysis of this unusual NEA. Spectra in the near- and mid-infrared allow us to better characterize Ra-Shalom's regolith.

Methods: For our initial thermal models, we used the shape model of [3] which has a retrograde spin pole direction and agrees with all lightcurve observations. Previously, a prograde spin solution was determined by [4] using only radar data, and those authors also provided initial thermal properties. We used the lightcurve only model from [3] to determine if our thermal parameters as applied to new data (below) would be consistent with the thermal perperties reported by [4]. To constrain our initial thermal models, we obtained new spectra (0.7 – 5.1 μm) over five nights in August and September 2019 at NASA's Infrared Telescope Facility (IRTF) in Mauna Kea, Hawaii. SHERMAN fits to these data yielded thermal parameters that were not consistent with those reported by [4]. We then conducted a new study where we combined delay-Doppler images and continuous wave (CW) spectra from Arecibo Observatory along with the lightcurve model of [3] to create a new shape model. This model was then used in SHERMAN to find that a thermal inertia range of 500-800 J m^{-2} $s^{-0.5}$ K^{-1}, an albedo range of 0.13 ± 0.03, and a crater fraction (a proxy for surface roughness) of 0.30 provided good agreement between the models and our 2019 data.

We want to make further comparisons with mid-infrared spectra from [5] and NEOWISE photometry for Ra-Shalom. We will use our new combined lightcurve + radar shape model to simulate both sets of data to determine if the same thermal range that agreed with all five nights of IRTF data will also agree with these other observations. Examples of the lightcurve + radar shape model as well as the simulated spectra are included in Figures 1 and 2. Figure 1 highlights one of the spectra obtained by us from the IRTF, and Figure 2 shows a preliminary analysis of the mid-infrared spectra for Ra-Shalom.

Conclusion: In this presentation, we will show our work to find global thermal properties of 2100 Ra-Shalom with SHERMAN that will adequately reproduce near-IR spectra, mid-IR spectra, and mid-IR photometry.

Figure 1

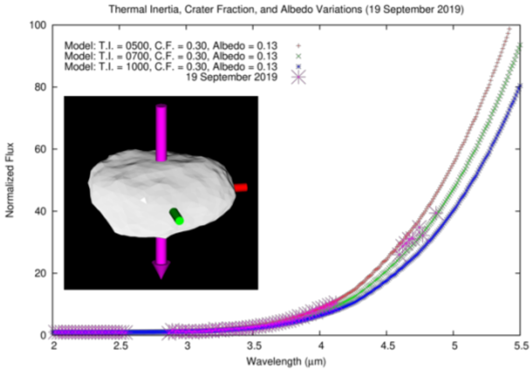

This graphic shows a plane-of-sky image of Ra-Shalom on 19 September 2019. The image demonstrates our use of the lightcurve + radar shape model. The pink stars represent the IRTF data. The three solid lines denote the thermal models with varying values of thermal inertia ("T.I.") while keeping crater fraction ("C.F.") and albedo constant.

Figure 2

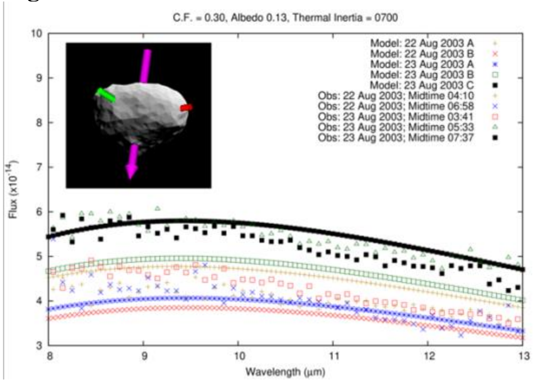

This graphic is a plane-of-sky image of Ra-Shalom on 22 August 2003. We are using the same shape model noted in Figure 1, but we are modeling the mid-infrared spectra from [5].

References:

[1] Magri C. et al. (2018) *Icarus, 303,* 203-219.
[2] Howell E. S. et al. (2018) *Icarus, 303*, 220-233.
[3] Durech J. et al. (2018) *Astronomy and Astrophysics,* 609, 1-10.
[4] Shepard M. K. et al. (2008) Icaurs, 193, 20-38
[5] Lim, L. F., et al. 2005. *AAS/Division for Planetary Sciences Meeting Abstracts* #37,37,07.10
[6] Mainzer A. et al. (2014) *The Astrophysics Journal, 792,* 30.

THERMOPHYSICAL MODELING OF (3200) PHAETHON TO CONSTRAIN REGOLITH PROPERTIES

R. J. Vervack, Jr.[1], E. S. Howell[2], Y. R. Fernández[3], C. Magri[4], S. E. Marshall[3,5], M. L. Hinkle[3], A. S. Rivkin[1], D. Takir[6], L. McGraw[7], and J. P. Emery[7]
[1]Johns Hopkins Applied Physics Laboratory (ron.vervack@jhuapl.edu), [2]U. Arizona/LPL, [3]U. Central Florida, [4]U. Maine-Farmington, [5]Arecibo Observatory, [6]Jacobs/ARES, NASA JSC, [7]N. Arizona U.

Introduction: Given widespread interest in near-Earth object (3200) Phaethon, we conducted a number of observations during the favorable December 2017 apparition and have carried out a series of thermophysical models to constrain the regolith thermal properties.

Observations: We observed Phaethon on four nights in December 2017 using the SpeX instrument on at NASA's IRTF [1]. Spectra covered 0.7-4.1 μm on all dates (0.7-5.1 μm on one date), which spans the range of wavelengths where the spectrum transitions from fully reflected to thermal. These observations covered a range of latitudes (decreasing from high northern latitudes to more equatorial with increasing date) and the full rotational phase of Phaethon.

Modeling: We used the Sherman thermophysical model [2] to carry out a detailed study of Phaethon's thermal emission, varying the geometic albedo, thermal inertia, and surface roughness (via the common proxy of hemispherical craters spread over a fraction of the surface [e.g., 3]). Sample results are shown in Figure 1.

Conclusion: We find that no single homogeneous set of thermal parameters across the surface of Phaethon can match all the spectral observations. As illustrated in Figure 1, there is a trend towards higher thermal inertia, lower albedo, and a smoother surface (smaller crater fractions) as the observations progressed and northern latitude decreased, strongly suggesting surface heterogeneity in the regolith thermal properties. We will present the full set of models and implications.

References: [1] Rayner et al. (2003), PASP 115, 362, [2] Magri et al. (2018), Icarus 303, 203, [3] Lagerros (1998), A&A 332, 1123.

Acknowledgments: This work is supported by NSF grant AST-1856411 to the U. Arizona and NASA grant 80NSSC21K0658 to JHU/APL.

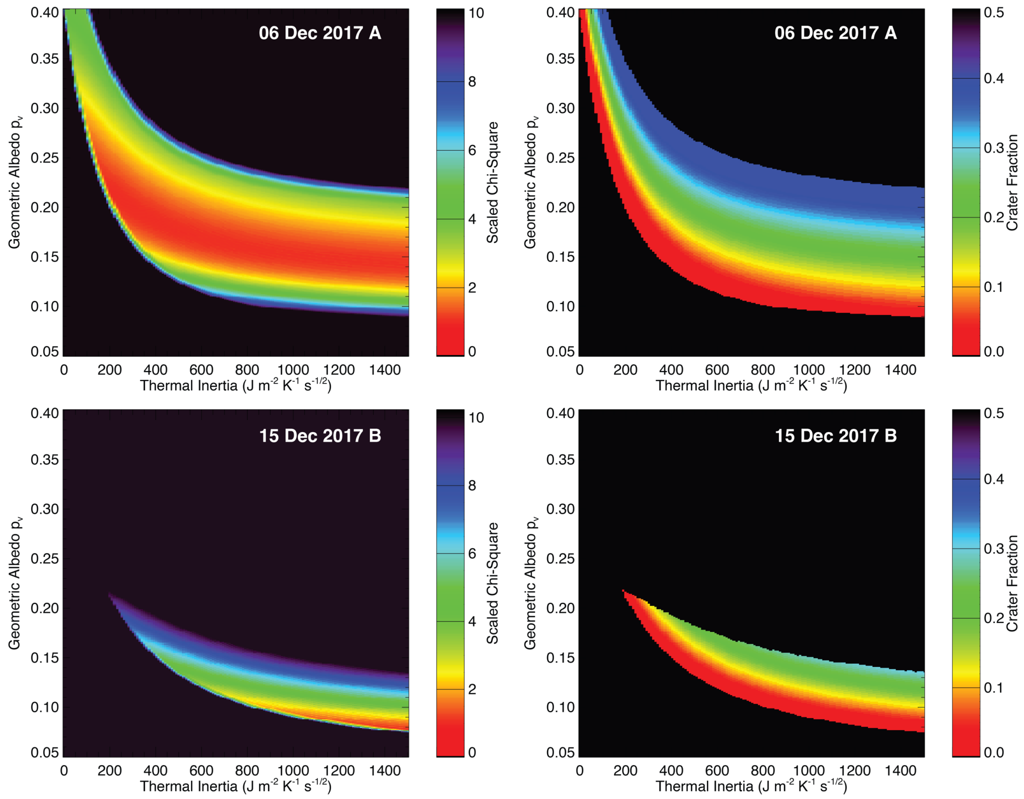

Figure 1. Thermophysical model results for two of our observations (top: 06 Dec 2017 A; bottom: 15 Dec 2017 B). The left panels show the chi-square of the model fits to the IRTF/SpeX data as a function of geometric albedo and thermal inertia. The right panels show the corresponding values of crater fraction. To provide a common basis for comparison, chi-square has been scaled such that the minimum value is 1 in both cases. These spectra bracket the observations, which exhibit a trend of chi-square space moving down and to the right with increasing date.

BOULDERS ON BENNU: USING THERMAL MODELING TO INVESTIGATE THE STRUCTURE OF LOW THERMAL INERTIA ROCK

C. M. Elder[1], [1]Jet Propulsion Laboratory, California Institute of Technology (celder@jpl.nasa.gov)

Introduction: Spitzer Space Telescope observations suggested that asteroid (101955) Bennu's surface has a low thermal inertia consistent with millimeter to centimeter scale regolith [1]. Infrared observations by OSIRIS-REx confirmed this low apparent thermal inertia [2, 3]. However, images revealed a surface covered in boulders with very little fine-grained material [2]. A similar boulder covered, low thermal inertia surface, was observed at asteroid (162173) Ryugu [4].

Porosity is the most likely cause for the low thermal inertia inferred for the boulders on Bennu and Ryugu [e.g. 3, 5]. [6], [3], and [5] used two different empirical fits to the thermal conductivity of meteorites to estimate boulder porosities on Bennu and Ryugu. However, the highest porosity of the meteorites used was ~20%, and the two empirical fits diverge at higher porosities [6]. [3] inferred porosities of 24-38% for high reflectance boulders on Bennu and 49-55% for low reflectance Bennu boulders. Some boulders on Ryugu have inferred porosities higher than 70% [5].

Here I conduct two-dimensional thermal modeling to investigate how the distribution of subsurface void space in boulders influences surface temperatures on Bennu.

Methods: I model the temperature of chondritic material on the surface of Bennu considering a range of subsurface void space configurations using COMSOL Multiphysics. I assume a density, heat capacity, and thermal conductivity consistent with the measured thermal inertia of Cold Bokkeveld, a CM chondrite. My preliminary work, presented here, considers one case with vertical fractures and several cases with horizontal fractures including cases with a 1 mm, 2 mm, 3 mm, or 4 mm thick fracture 1 mm below the surface and cases with a 1 mm thick fracture at a depth of 1 mm, 2 mm, 3 mm, or 4 mm below the surface. I also consider one case with two 1 mm thick horizontal fractures, one at 1 mm below the surface and the other at 3 mm below the surface. Additionally, I consider one scenario in which the rock has a density, heat capacity, and thermal conductivity consistent with the best-fit average Bennu thermal inertia (labeled "Bennu observed TI" in figure 1). In future work, I will compare my models to actual observations of the large boulders on Bennu that are fully resolved by OTES.

Results: A single horizontal fracture 1 mm below the surface has a significant effect on the surface temperature and could imply a lower thermal inertia than was inferred for Bennu (Figure 1). The thickness of the fracture has a negligible effect on the diurnal temperature curve, but the depth of the fracture controls how quickly the surface cools after sunset. A second deeper fracture, also parallel to the surface, has a negligible effect on the surface temperature. Preliminary results show that vertical fractures have a smaller effect on the surface temperature than horizontal fractures (Figure 1), but further modeling is needed to investigate the effects of fracture depth and width.

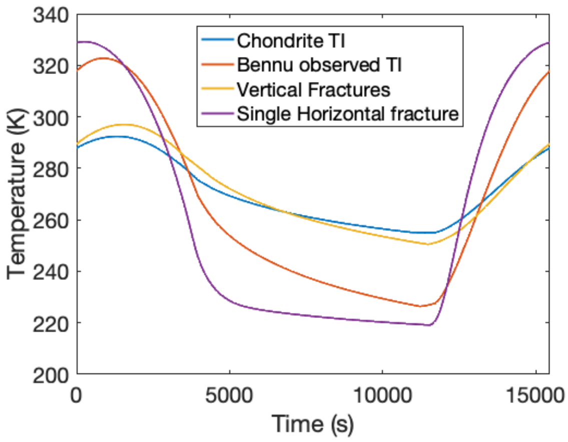

Figure 1: Model diurnal temperature curves for various materials and void space configurations in Bennu's shallow subsurface including the thermal inertia that best fits observations (red), solid chondritic material (blue), chondritic material with vertical subsurface fractures (yellow), and a 1 mm thick horizontal fracture 1 mm below the surface (purple).

Discussion and Preliminary Conclusions: High porosity may not be required to explain the observed surface temperatures of boulders on Bennu and Ryugu. A single thin subsurface fracture can have a significant effect on the surface temperature. Preliminary results suggest that surface temperature is not sensitive to the thickness of the fracture or the presence of additional deeper fractures but is sensitive to the depth of the fracture.

Fractures parallel to the boulder's surface are consistent with expectations for thermally driven exfoliation [7]. However, previous observations and modeling of exfoliation considered deeper fractures [7] than I have considered here. My future work will investigate the effects of deeper fractures on surface temperature.

References: [1] Emery J. P. et al. (2014) *Icarus 234*, 17-35. [2] DellaGiustina D. N., Emery J. P. et al. (2019) *Nat. Ast. 3,* 341-351. [3] Rozitis B. et al. (2020) *Sci. Adv. 6,* eabc3699. [4] Sugita S. et al. (2019) *Science 364*, eaaw0422. [5] Sakatani N. et al. (2021) *Nat Ast. 5*, 766-774. [6] Grott M. et al. (2019) *Nat Ast. 3*, 971-976. [7] Molaro J. L. et al. (2020) *Nat Com 11:* 2913.

Modelling of Ryugu's remote and in-situ thermal measurements

T. Müller (1), T. Okada (2), N. Sakatani (3), Y. Shimaki (2), T. Sekiguchi (4), V. Ali-Lagoa (1), J. Lagerros (5)

(1) Max-Planck-Institut für extraterrestrische Physik, Garching, Germany; (2) ISAS, JAXA, Sagamihara, Japan; (3) Department of Physics, Rikkyo University, Toshima, Japan; (4) Hokkaido University of Education, Asahika-wa, Japan; (5) Uppsala, Sweden

The near-Earth object and Hayabusa2 mission target 162173 Ryugu is a textbook case for testing and validating thermal models.

Ryugu was observed at thermal IR wavelength from ground (Subaru-COMICS) and space (Spitzer-IRS, Spitzer-IRAC, AKARI-IRC, Herschel-PACS, WISE-W1/W2) remotely [1], and by Hayabusa2-TIR in-situ [2]. At the same time, Ryugu's size, albedo, shape and spin properties are known with high precision [3,4,5,6,7]. This allows to apply different simple and more sophisticated thermal models, and to look into model-intrinsic parameters.

The thermophysical properties derived from remote (disk-integrated) observations can be compared to results obtained by in-situ measurements. It is also possible to look into surface heat conduction concepts, including shadowing and self-heating effects, into model roughness implementations (hemispherical craters, Gaussian random surfaces), or the influence of the hemispherical (spectral) emissivity assumptions. Also the Hayabusa2-TIR measured temperature patterns on the surface of Ryugu challenge the simplified techniques to calculate roughness effects.

The goal of this project is to find a single thermophysical model solution for Ryugu which explains remote thermal measurements (global object properties) and Hayabusa2-TIR obtained temperature maps (local object properties) at the same time.

What are the possibilities, limitations, and problems of different model implementations? How well do the Hayabusa2-TIR derived thermal properties agree with the ones derived from remote observations? Can we improve our knowledge of Ryugu's properties by combining all available remote and close-proximity data? Are there any indications of temperature-dependent thermal properties? What can we learn from this exercise for thermal model applications to other targets?

We present results from almost one decade of intense studies of Ryugu's thermal emission, a truly multi-scale approach to asteroid thermophysical modelling.

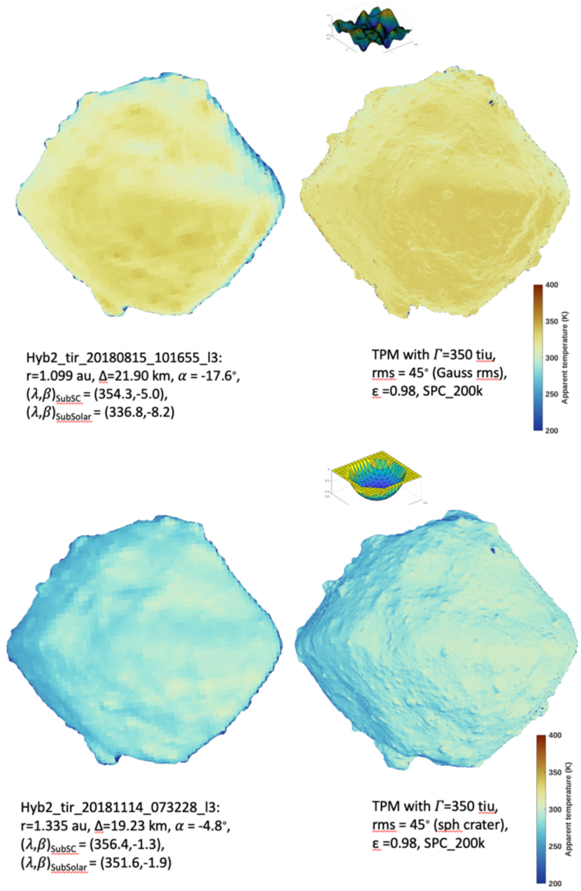

Fig 1: TIR temperature image of Ryugu and TPM temperature prediction for two epochs. On the left are the calibrated temperature maps of Ryugu as obtained by Hayabusa2-TIR in its 10-micron band. The right images show a thermophysical model prediction for the surface temperature using Ryugu's spin and shape properties, together with the simulated insolation and as seen by Hayabusa2. Top: using random Gaussian surface for roughness, bottom: using hemispherical segment craters. One of the surprising TIR findings is the very flat and almost homogeneous temperature distribution on the surface.

References:

[1] Müller et al. (2017), A&A, A103; [2] Okada et al. (2020), Nature 579, 518; [3] Sugita et al. (2019), Science 364, 252; [4] Watanabe et al. (2019), Science 364, 268; [5] Shimaki et al. (2020), Icarus 348, 113835; [6] Okada et al. (2021), JSAST 19, 654; [7] Sakatani et al. (2021), Nature Astronomy 5, 766.

Thermal Spectroscopy of the Didymos binary asteroid system after the DART impact

E. S. Howell[1], R. J Vervack, Jr.[2], Y. R. Fernandez[3], M. L. Hinkle[3], K. D. McFadden[1], S. A. Myers[1], C. Magri[4], S. E. Marshall[3], C. A. Thomas[5], A. S. Rivkin[2]

[1]LPL/U. Arizona, AZ (ellenshowell@gmail.com) [2]JHU/APL MD, [3]UCF Orlando, FL, [4]U. Maine at Farmington, ME, [5]NAU Flagstaff, AZ

Introduction: The DART spacecraft impacted Dimorphos, the satellite of near-Earth asteroid (65803) Didymos on 26 September 2022. We observed the binary system using the NASA Infrared Telescope Facility (IRTF) on 3 and 17 October using the SpeX spectrometer (0.7-5.1 microns) to measure the reflected and thermal flux from the system (described below). Closer to the impact time, near-infrared and mid-infrared spectroscopy were also obtained at the VLT as well as other telescopes around the world. This unprecedented opportunity to study the aftermath of an impact into a rubble-pile structure at high velocity will constrain the internal structure of this NEA binary system. Understanding how the momentum is distributed and enhanced will aid planning for possible mitigation of an impactor to Earth in the future.

Formation scenarios of NEA binaries [1] strongly suggest that these are gravitationally bound rubble piles, although friction may also play a role in their structure and response to stress. The DART impact produced a large amount of ejecta. Our thermal observations provide constraints on the thermal properties of the ejecta cloud in the weeks following the impact.

Observations: We observed the Didymos system on 3 and 17 October, 2022 at the NASA IRTF using SpeX [2]. We also saved images from the guider using the K filter (2.2 microns) for context of the coma morphology and orientation of the slit (Figure 1). The LXD spectra were obtained over 75 min and taken in pairs separated by 10 arcseconds, nodded along the slit. The total integration time is 12 minutes. The slit was oriented along the parallactic angle to minimize the losses due to differential refraction. The wavelength coverage (0,7-5.1 microns) includes the fully reflected to thermally dominated region for the asteroid when it was at 1.03-1.01au from the sun.

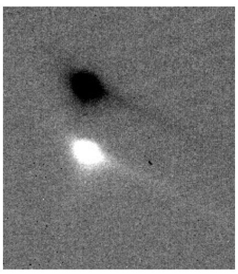

Figure 1: The K-band image (subtracted A-B pairs) taken of the Didymos system on 3 Oct 14:10 UT. The ejecta material is clearly still leaving the system one week after the impact. The slit is vertical at the left edge of the image.

Spectral Analysis: The spectra are shown in Figure 2 along with a NEATM-like model fit to the data. This preliminary analysis suggests that the best-fit model parameters for the 3 Oct observations also fit on 17 Oct, allowing for the changing viewing geometry. A simple NEATM-like model requires a high albedo as well as a large beaming parameter to match the spectral shape. This albedo is not consistent with the size and H magnitude of the system, so the dust contribution is important. Effects of thermal inertia and surface roughness are not included in these models.

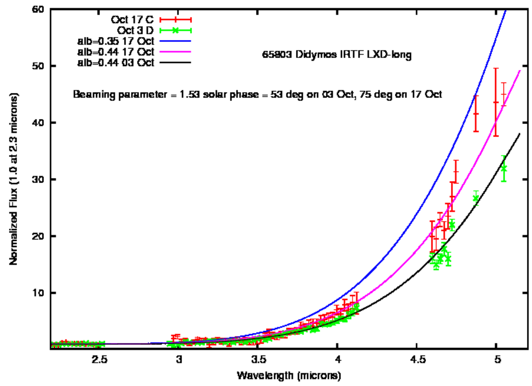

Figure 2: The observed thermal spectra in the 2-5 micron region along with the best-fit NEATM-like model. The unusually high albedo suggests that the dust effects are important.

We will apply our thermophysical model Sherman [3] which uses a shape model for Didymos [4] and incorporate thermal inertia, albedo, surface roughness and appropriate viewing geometry. We will allow for separate thermal distributions for the dust and solid body components to try to constrain these with the observed spectra.

Conclusions: Detailed thermal modeling of the asteroid system with ejecta 1-3 weeks after impact will constrain the significant dust component still present in the system. The results of the thermal models will be presented and placed into context with the myriad of other observations made at a wide range of times and wavelengths.

References:

[1] Pravec et al. (2015) in Asteroids IV and refs therein
[2] Rayner et al. (2003) PASP 115
[3] Magri et al., (2018) Icarus 303
[4] Barnouin, O. (pers. comm.)

Acknowledgments: The authors are visiting Astronomers at the Infrared Telescope Facility, which is operated by the University of Hawaii under contract 80HQTR19D0030 with the National Aeronautics and Space Administration.

THERMOPHYSICAL MODELING OF BINARY ASTEROIDS USING A SOPHISTICATED 3D RAY TRACING APPROACH

Kya C. Sorli[1] and Paul O. Hayne[1]
[1]Laboratory for Atmospheric and Space Physics, University of Colorado Boulder, CO, USA (kya.sorli@colorado.edu)

Introduction: Binary asteroids represent a significant (~16%) fraction of Near-Earth Asteroids [1] and demonstrate characteristic dynamical and evolutionary pathways. Some, like 1996 FG3, exist in stable end states with tidally locked secondaries [2] while others are dynamically evolving. The diverse nature of binaries made them the targets of several missions, notably DART [3] and Janus [4]. For asymmetric small bodies, differential thermal emission can induce torques that alter orbital evolution. The binary YORP (BYORP) effect [5] arises from net forcing in binary systems, and produces secular changes to the orbit of the secondary. BYORP is small but can alter binary evolution over time. It also depends on asteroid shape, making accurate models of surface temperatures and how they vary with time and shape critical to understanding the effect's magnitude.

We present a 3D thermophysical ray tracing model for binary asteroids. This model includes consideration of full-system properties like shadowing, radiation exchange and eclipses. We apply this model to the stable system 1996 FG3 to calculate surface temperatures. Existing models for binaries have been used to investigate temperatures and BYORP [6][7]. Our model offers several advancements: (1) topography through asteroid-specific shape models, (2) mutual reradiation from the primary to the secondary and vice versa, (3) consideration of the effects of thermal inertia, which affects temperature range and time-dependence, and (4) coupling to the 1D thermal model from [8], which includes temperature-dependent thermal conductivity and specific heat capacity.

Methods: Our 3D thermophysical model begins by coupling the 1D heat-conduction model from [8] to 3D triangulated shape models. This enables direct accounting of radiation scattering by topography. We apply an efficient ray tracing approach to calculate shadows and binary eclipses. Ray tracing also permits calculation of view factors, which are used to include the effects of reflection, scattering and infrared (IR) emission. The model calculates surface and subsurface temperatures by balancing IR emission, visible light reflection, scattered IR radiation and direct insolation at the surface as well as 1D heat conduction in the surface and near subsurface.

Results and Discussion: The model has previously been applied to individual bodies, including those in potential Janus mission target systems 1996 FG3 and 1991 VH [9]. Initial runs with the two-body model have successfully demonstrated binary properties such as eclipses (Figure 1). We apply this two-body model to the 1996 FG3 binary and calculate system wide diurnal temperature maps for the surface and near subsurface of the primary and secondary. This 3D thermophysical model has broad applicability to binaries and solitary asteroids, as well as to landscapes of interest if a digital elevation model is available. It can also be used to produce temperature estimates in support of missions to airless bodies. Future work will utilize these results to numerically estimate the magnitude of the BYORP effect and the sensitivity it has to thermal inertia.

References:

[1] Margot, J.L., et al. (2002) *Science* 296.5572: 1445-1448. [2] Scheirich, P., et al.(2015) Icarus 245 (2015): 56-63. [3] Cheng, A. F., et al. (2012) *EPSC: Vol. 7. 2012.* [4] Scheeres, D. J., et al. (2020) AGU Fall Meet. Abstracts. Vol. 2020. [5] Ćuk, M., & J. A. Burns (2005) *Icarus* 176.2, 418-431. [6] Pelivan, I., et al. (2017) *ASR* 59.7: 1936-1949.[7] McMahon, J., & D. J. Scheeres. (2010) *Icarus* 209.2: 494-509. [8] Hayne, P. O. et al. (2017) J. of Geophys. Res.: Planets, 122(12), 2371-2400. [9] Sorli, K. C., et al. (2022) LPSC. No. 2860.

Acknowledgments: This work was supported in part by the NASA Janus Mission and by NSF GRFP Grant No. DGE 2040434

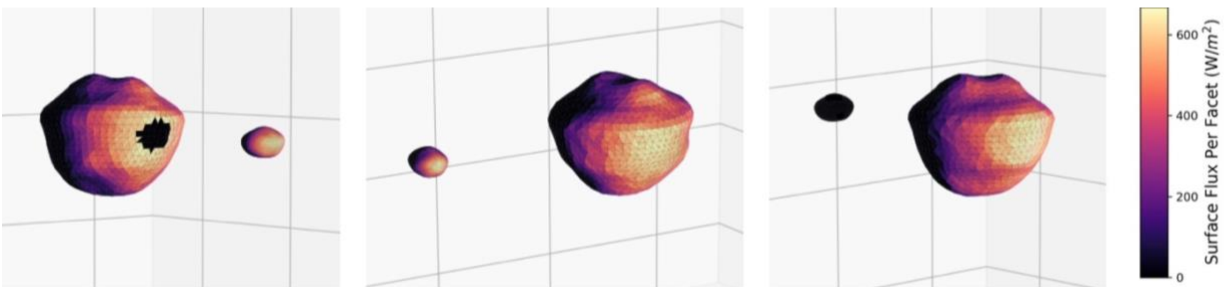

Figure 1: Demonstration of shadowing and ray tracing through the progression of eclipses as the 1996 FG3 secondary orbits the primary. The color gradient indicates the irradiance received by each surface facet.

Development of Thermophysical Model *Astroshaper* to Simulate Non-Gravitational Acceleration on Binary Asteroid.

M. Kanamaru[1] (E-mail: kanamaru@eps.s.u-tokyo.ac.jp), G. Tommei[2], T. Okada[3], N. Sakatani[3], Y. Shimaki[3], S. Tanaka[3], T. Ishizaki[3], H. Senshu[4], T. Arai[5], T. Sekiguchi[6], N. Hirata[7], H. Demura[7].
[1]The University of Tokyo (Japan), [2]The University of Pisa (Italy), [3]ISAS/JAXA (Japan), [4]Chiba Institute of Technology (Japan), [5]Maebashi Institute of Technology (Japan), [6]Hokkaido University of Education (Japan), [7]The University of Aizu (Japan).

Introduction: A thermophysical model (TPM) for an asteroid is useful to simulate the temperature distribution over the surface of the asteroid. In a spacecraft mission to an asteroid, TPM analyses can contribute to safety assessment, comparison with thermal observation, and prediction of non-gravitational acceleration such as Yarkovsky, YORP, and binary YORP effects.

Software Development – *Astroshaper*: We have been developing a dynamical simulator for an asteroid, *Astroshaper*, including an implementation of TPM. This numerical library is developed as an open-source code at GitHub [1]. Some sample code also will be released soon. Astroshaper was originally developed for predicting the thermally-induced torque (i.e., the YORP effect) on asteroid Ryugu, a target body of the Hayabusa2 mission [2]. We recently expanded the TPM code to apply to a binary asteroid for the Hera mission.

Astroshaper is a thermophysical model based on a 3D shape model of an asteroid. It is capable of calculating temperature on every facet of the shape model. The following basic thermophysical processes are implemented: 1-dimensional heat conductions in the depth direction, shadowing by the local horizon (self-shadowing), and reabsorption of scattered light and thermal radiation from interfacing facets (self-heating). For a binary asteroid, eclipse events by the mutual shadows also can be simulated. The mutual heating effect, in which the interfacing surfaces of the binary asteroid warm each other, has not yet been implemented. The thermal infrared beaming by microscopic surface roughness is also an issue for the future.

Results: We performed a thermophysical simulation of the binary asteroid Didymos and Dimorphos using the SPICE kernels provided by the Hera mission. In this study, shape models based on ground-based radar observation were used. Figure 1 shows the surface temperature distribution of Didymos (left) and Dimorphos (right). Each panel shows a snapshot of TPM when a mutual event occurs. One can see the shadow of Dimorphos projected on Didymos in the left panel. On the other hand, Dimorphos is about to enter the shadow of Didymos.

These dramatic changes in temperature may have a significant effect on the dynamics of the asteroid. We calculated the thermal recoil force on every facet of the shape model and integrated it over the whole surface. The thermally induced torque on the asteroid pair was obtained by averaging over several rotation cycles. The torques correspond to $\tau_1 = 0.19$ N·m for Didymos and $\tau_2 = -1.1 \times 10^{-4}$ N·m for Dimorphos. The negative acceleration of Dimorphos could decrease its spin velocity and expand the mutual orbit. It should be noted that this preliminary estimation can vary by updating the shape models.

References:

[1] M. Kanamaru, *Astroshaper: Asteroid Dynamical Simulator*. [Online]. Available: https://github.com/MasanoriKanamaru/Astroshaper.jl

[2] M. Kanamaru *et al.*, “YORP effect on asteroid 162173 ryugu: Implications for the dynamical history,” *J. Geophys. Res. Planets*, vol. 126, no. 12, Dec. 2021, doi: 10.1029/2021je006863. [Online]. Available: https://onlinelibrary.wiley.com/doi/10.1029/2021JE006863

Acknowledgments: This work was supported by JSPS KAKENHI Grant Number JP22J00435 and MEXT Promotion of Distinctive Joint Research Center Program Grant Number JPMXP0622717003.

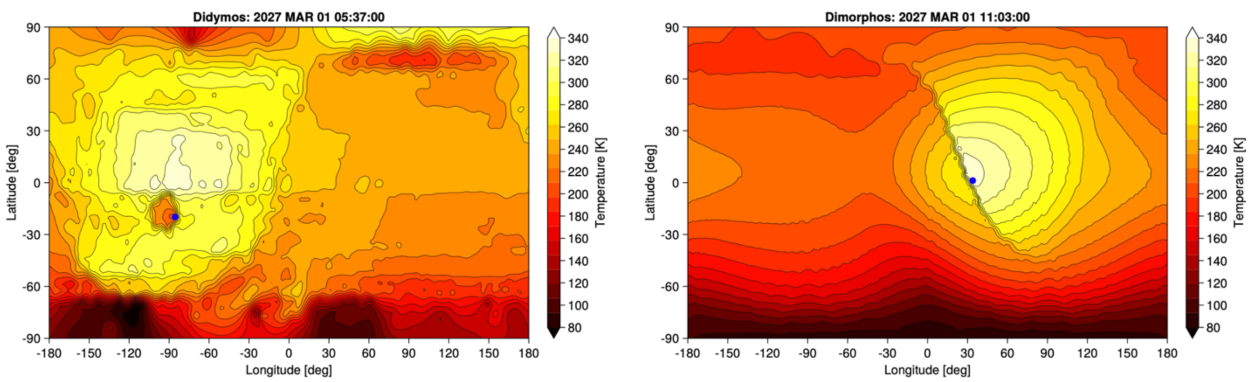

Figure 1: Surface temperature distribution on Didymos and Dimoprhos when the mutual events occur.

THERMOPHYSICAL MODELLING OF SMALL BODIES: APPLICATION TO BINARY ASTEROIDS

G. Henry[1,2], Ö. Karatekin[1], J. Blommaert[2,3] and C. B. Senel[1]
[1]Royal Observatory of Belgium (gregoire.henry@oma.be)
[2]Vrije Universiteit Brussel, [3]VITO

Introduction: Thermophysical models are widely used in combination with infrared observations to derive physical properties of asteroids [1]. The infrared observations can be obtained from Earth-based measurements or in-situ with a thermal camera on-board a spacecraft. The properties that can be derived from the combinations of these techniques are the shape of the asteroids, spin axis, density, emissivity, ground composition, surface roughness and more. These properties brings new clue for the comprehension of the composition and formation of these celestial bodies, and by extent the formation of the Solar System. Furthermore, binary asteroids are a recent topic of interest as they have been found to represent ± 15% of the population of asteroids, and undoubtedly their study will help to bring more understanding on the formation of the Earth and the Moon [2]. Individual body from the binary system may have different physical properties and their interaction can affect the overall thermophysical characteristics of the system. In this research, we present the thermophysical model for binary asteroid that we have developed.

Thermophysical Model: The thermophysical model developed at the Royal Observatory of Belgium supports the physics for binary asteroid system. Solar radiation is the principal source of heating at the surface. The mutual heating from bodies is implemented, both in term of solar flux reflection from one body to the other and as thermal re-radiation. The self heating is implemented with the same principle but considering one body with itself, and with additional checking of the distance and surface area between two regions interacting together. The surface is provided as an input file containing the shape model. The mutual and self heating fluxes depend on the calculation of shadows. Locally, the shape model can hide a surface region from an incoming heat flux. Globally, the primary body can be eclipsed by the secondary body (primary eclipse), or the secondary body can be eclipsed by the primary body (secondary eclipse). Generally a primary eclipse is partial and a secondary eclipse total, but this can change depending on the orbital geometry of the system and the respective size of the two bodies. The one-dimensional heat transfer equation is numerically solved with finite difference method for each surface element for the two asteroids. Ground fluxes are transferred until a certain depth where an adiabatic condition is assumed, based on the thermal and rotational properties of the asteroid.

Results: Application of the thermophysical model to the binary system Didymos over the period of Hera mission in 2027. Figure 1 bottom panel shows a drop of 80K in temperature resulting during secondary eclipse lasting for about 1 hour and 10 minutes. Change of surface temperature up to 100K during 2027 period.

Perspective: On-going work will concern the numerical solving of the heat transfer partial differential equation with finite element method with three spatial dimensions, and implementation of other effects such as the ground roughness.

References:

[1] M. Delbo et al. (2015) Asteroid IV
[2] I. Pelivan et al. (2017) Adv Space Res

Acknowledgments: ESA OSIP for funding the research.

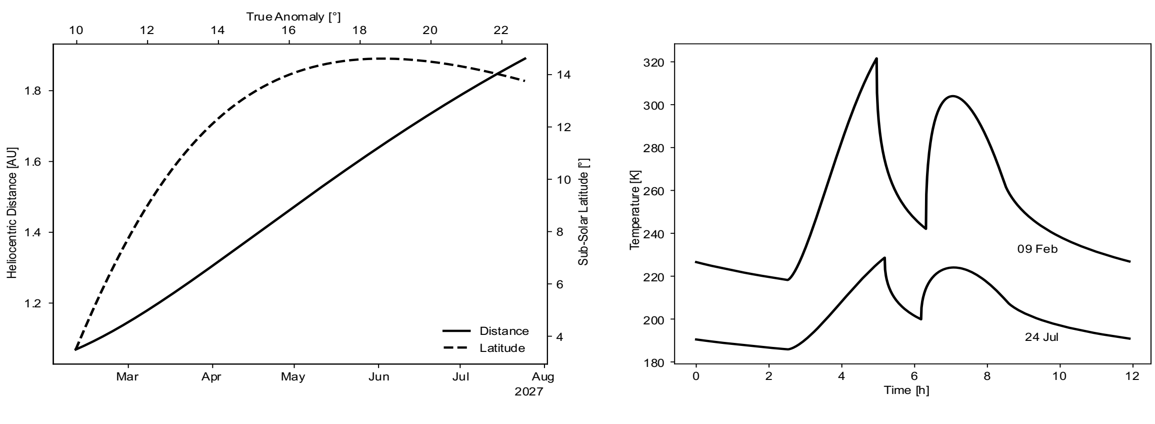

Figure 1: Left panel: Evolution of the heliocentric distance and sub-solar latitude of Dimorphos. Right panel:

MAPS OF THERMAL INERTIA AND DIELECTRIC CONSTANT OF ASTEROID (16) PSYCHE FROM SPATIALLY-RESOLVED ALMA DATA. Saverio Cambioni[1], Katherine de Kleer[2], Michael Shepard[3]. [1]MIT, Cambridge, MA, USA (cambioni@mit.edu); [2]Caltech, Pasadena, CA, USA; [3]Bloomsburg University, PA, USA.

Introduction: (16) Psyche is the largest M-type asteroid and the target of a NASA mission aimed at testing whether Psyche is the metal core of a differentiated planetesimal [1]. Variations in metal and silicate content on Psyche have been proposed based on rotational variations at visible, infrared and radar wavelengths [e.g., 2, 3, 4, 5]. While these variations cannot be spatially resolved at thermal infrared wavelengths using telescopes existing today, this can be done at millimeter wavelengths using the Atacama Large Millimeter Array (ALMA) [6]. Here we present our analysis [7] of ALMA data of Psyche at 30 km spatial resolution covering ~2/3 of its rotation.

ALMA data. The foundational theory of the analysis of mm-thermal emission data is rooted in lunar science [e.g., 8]. Building on this, in [7] we model the ALMA data from [6] as a function of dielectric constant ε (which controls the surface emissivity) and thermal inertia Γ and roughness (which control the surface temperature). Dielectric constant ε increases with metal content [6]. Consistently, the silicate-rich surface of asteroid Vesta has ε = 2.3–2.5, while the metal-rich surface of Psyche has $\varepsilon = 18.5 \pm 0.4$ [9, 6]. Thermal inertia is controlled not only by composition ($\Gamma_{Vesta} \sim 30\pm10$ J m^{-2} K^{-1} s$^{-1/2}$ versus $\Gamma_{Psyche} \sim 280\pm100$ tiu [10, 6]), but also grain size and rock porosity, as confirmed by recent asteroid missions [e.g., 11, 12].

Thermophysical model. We fit the thermal emission of Psyche area-by-area using a new approach that computes the time-varying thermal emission from the (sub)surface using the thermophysical model by [13] as a function of Γ and ε given the observation conditions and shape model by [5]. We assume a smooth surface as this was found to best fit both disk-integrated infrared and millimiter thermal data of Psyche [14, 15, 6]. A full description of our model, assumptions and related robustness tests is in [7].

Results. We find (Fig. 1) that Psyche has a heterogeneous surface in both thermal inertia and dielectric constant. The lowlands of a large depression in Psyche's shape (Fig. 1a) have statistically lower thermal inertia than the surrounding highlands. This can be explained by a thin mantle of fine regolith, a fractured bedrock, and/or implanted silicate-rich materials covering an otherwise metal-rich surface [7]. The dielectric-constant map (Fig. 1b) is indicative of variations in relative metal/silicate abundance.

Conclusion. We present evidence that Psyche is a metal-rich asteroid whose surface is heterogeneous, shows both metal and silicate materials, and appears to have evolved by impacts. The future NASA Psyche will allow for testing these predictions.

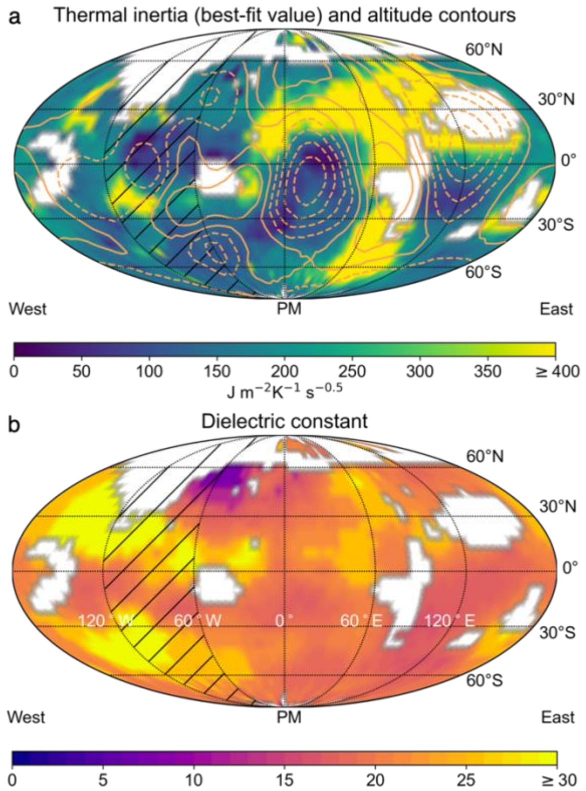

Figure 1. Asteroid (16) Psyche. (a) Thermal-inertia map with altitude contours computed using the shape model from [5]; (b) Dielectric-constant map. Results from [7] derived from the ALMA data from [6].

References. [1] Elkins-Tanton, L. T. et al. (2022) *SSR* 218.3:1-38; [2] Ferrais, M. et al. (2020) *A&A* 638: L15; [3] Sanchez, J.A. et al. (2016) *AJ* 153.1:29; [4] Takir, D. et al. (2017) *AJ* 153.1:31; [5] Shepard, M. K. et al. (2021) *PSJ*, 2(4), 125; [6] de Kleer, K. et al., (2021) *PSJ*, 2(4), 149; [7] Cambioni, S., et al. (2022). *JGR:Planets*, e2021JE007091; [8] Ulich, B.L. et al. (1974) *The moon* 10.2:163-174; [9] Palmer, E.M. et al. (2015) *Icarus* 262: 93-101; [10] Capria, M.T., et al. (2014) *JGRL* 41.5:1438-1443; [11] Cambioni, S. et al. (2021) *Nature* 598, 49-52; [12] Okada, T. et al. (2020) *Nature* 579 : 518-522; [13] Delbo et al. (2015) in *Asteroid thermophysical modeling*. UArizona Press; [14] Matter, A. et al. (2013) *Icarus* 226.1: 419-427; [15] Landsman, Z. et al. (2018) *Icarus* 304: 58-73.

Acknowledgments: This research was funded by Heising-Simons Foundation grant 2019-1611 and MIT EAPS Crosby Fellowship. We used the following ALMA data: ADS/JAO.ALMA \#2018.1.01271.S.

Shapes and Sizes of Jupiter Trojans

Josef Hanuš, Josef Ďurech and David Vokrouhlický
Charles University, Faculty of Mathematics and Physics, Institute of Astronomy, V Holešovičkách 2, CZ-18000, Prague 8, Czech Republic (josef.hanus@mff.cuni.cz)

Introduction: Jupiter Trojans (JTs) are minor bodies co-orbiting with Jupiter in the proximity of its Lagrangian points L4 and L5.

While a significant amount of data about the rotation rates of JTs have been collected, and analyzed, much less is presently known about the complete characterization of their spin state (i.e., rotation rate and pole direction). In our recent paper [1], we aim at filling this missing piece of information by deriving rotation state properties and convex shapes for many JTs. Particularly, we are interested in the direction of the rotation axis with respect to the orbital plane – the pole obliquity. This parameter reflects the object's dynamical history and could help constrain various theories aiming at explaining the population's origin.

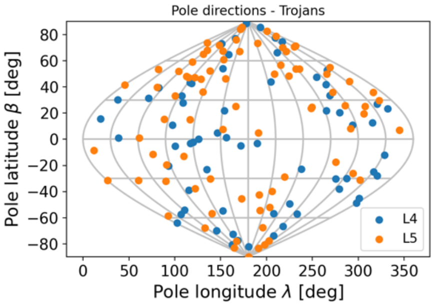

Figure 1: Spin vector distribution of JTs. L4 and L5 represent the two camps of JTs.

Shapes and sizes of JTs: We compiled photometric datasets for about 1000 JTs and apply the convex inversion technique in order to access their shapes and spin states in [1]. We obtained full solutions for 79 JTs (Fig. 1). The existence of shape models allows us to derive more accurate sizes than the radiometric ones based on thermal modeling with spherical shape model assumption [2]. The most accessible methods are scaling the shape models by stellar occultation observations [3] and thermophysical modeling (TPM) [4]. In this contribution, we present sizes of JTs derived by both methods and investigate the consistency of our results with those based on the simpler thermal model.

Stellar occultations: For eight JTs with shape models there were successfully observed stellar occultations with enough chords that enabled us to scale the shape models and, in some cases, also to reject one of the two possible pole solutions. The stellar occultations were assessed through the Occult software. For comparing the occultations with our shape models, we used the same approach as in [3].

For (1867) Deiphobus the agreement between the occultation and the shape projection was sub-optimal (Fig. 2). Therefore, we also reconstructed the shape model by the All-Data Asteroid Modelling (ADAM) inversion technique [5,6]. ADAM allows using the stellar occultation for the shape reconstruction contrary to the convex inversion where the shape is scaled in size only. The ADAM shape model of Deiphobus agrees better with the occultation and provides a more realistic size estimate. This highlights possible issues with the shape modeling of JTs where we usually have only low phase angle observations.

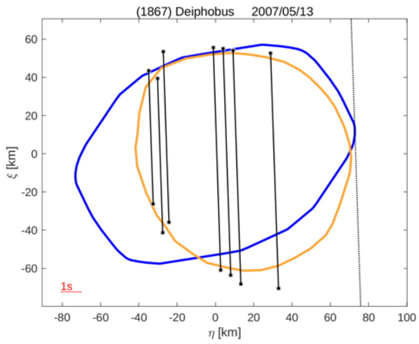

Figure 2: Projection of the shape model of (1867) Deiphobus. The convex shape model (blue) with the pole (338°, 79°) does not agree well with the observed chords. The nonconvex ADAM model (orange) provides a much better fit with the pole direction (329°, 67°) and an equivalent diameter of 108±4 km.

Thermophysical modeling: Shape models are necessary inputs for the thermophysical modeling. We apply the TPM to thermal IR data from the WISE satellite in bands W3 and W4 following the scheme of [7] and derive sizes and thermal inertias for several JTs.

Conclusion: We present size estimates of JTs based on two methods – scaling by stellar occultations and by thermophysical modeling. We discuss the accuracy and possible biases of the determinations and compare our values to radiometric sizes based on thermal modeling.

References:

[1] Hanuš et al. Shape models and spin states of Jupiter Trojans. Submitted to A&A. **[2]** Harris, A. W., Feb. 1998. A Thermal Model for Near-Earth Asteroids. Icarus131, 291–301. **[3]** Ďurech et al. 2011. Combining asteroid models derived by lightcurve inversion with asteroidal occultation silhouettes. Icarus 214, 652–670. **[4]** Lagerros, J. S. V., Jun. 1996. Thermal physics of asteroids. I. Effects of shape, heat conduction and beaming. Astronomy and Astrophysics 310, 1011–1020. **[5]** Viikinkoski et al. 2015. ADAM: a general method for using various data types in asteroid reconstruction. Astronomy and Astrophysics 576, A8. **[6]** Viikinkoski 2016. Shape Reconstruction from Generalized Projections. Ph.D. thesis, Tampere University of Technology. **[7]** Hanuš et al. 2018. Thermophysical modeling of main-belt asteroids from WISE thermal data. Icarus 309, 297–337.

Acknowledgments: This research has been supported by the Czech Science Foundation through grant 22-17783S.

Multi-Wavelength Characterization and Thermal Modeling of Comet 289P/Blanpain During the Historic Close Approach of its 2019-2020 Apparition

Schambeau, C. A.[1,4], Howell, E. S.[2], Mueller, B.[3], Samarasinha, N. H.[3], Fernandez, Y. R.[1,4], and Ye, Q.[5,6]
[1]Florida Space Institute, University of Central Florida, Orlando, FL, USA (charles.schambeau@ucf.edu).
[2]Lunar and Planetary Laboratory, University of Arizona, Tucson, AZ, USA.
[3]Planetary Science Institute, Tucson, AZ, USA.
[4]Department of Physics, University of Central Florida, Orlando, FL, USA.
[5]Department of Astronomy, University of Maryland, College Park, MD, USA.
[6]Center for Space Physics, Boston University, Boston, MA, USA.

Introduction: We present results from an observing campaign and data archive search focused on a multi-wavelength characterization of the low-activity comet 289P/Blanpain. Blanpain was discovered in Nov. 1819 and observed for ~ 2 months before it was lost only to be recovered in 2003 and classified as the asteroid 2003 WY_{25} [1, 2]. Its recovery while inactive in combination with its apparent lack of activity over the course of ~ two centuries afforded it the designation of a "dead" comet. This designation was short-lived after its recovery when a faint coma was detected [3] establishing Blanpain as a member of very-low activity, and highly-thermally evolved Jupiter-family comets (JFCs) population. In Dec. 2019 through Jan. 2020 Blanpain underwent a close passage of Earth, with a minimum distance of 0.0908 au on UT 2020 Jan. 11, providing a rare opportunity for its characterization.

During the historic close flyby of Earth we used the Arecibo Observatory 305-m telescope to make radar measurements of Blanpain from UT 2019 Dec. 27 through 2020 Jan. 3. These represent the last set of radar observations from this telescope of a comet prior to its unfortunate collapse [4]. We obtained S-band ($\lambda = 12.6$ cm) continuous wave (CW) spectra of the comet (Fig. 1) to determine nucleus properties and search for a large-grain (> 2 cm) dust coma. The radar echo was not strong enough for imaging of the nucleus through delay-Doppler techniques. The average radar bandwidth for all dates was 1.85 ± 0.4 Hz. To help interpret the bandwidth we independently measured the nucleus rotation period to be 8.83 ± 0.01 hr based on visible lightcurve data acquired in 2020 Jan. Using these data we estimate an extent of at least 600 ± 140 m in the line of sight at this time. Additional analysis is in progress to understand the observational biases.

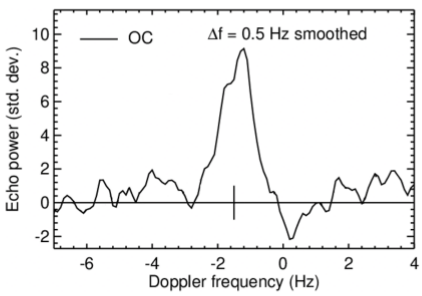

Figure 1: *The CW spectrum of Blanpain on UT 2020 Jan. 3 A coma skirt is not detected.*

We analyzed 13 epochs of WISE/NEOWISE W1 (3.368 μm) and W2 (4.618 μm) imaging data spanning UT 2019 Oct. 29 through 2020 Jan. 12 with sufficient S/N for thermal modeling (Fig. 2). Application of a NEATM [5] utilizing the radar-derived nucleus size enabled for the first time a measurement of Blanpain's visible geometric albedo and infrared beaming parameter. Preliminary analysis indicates both parameters to follow typical JFC ensemble values.

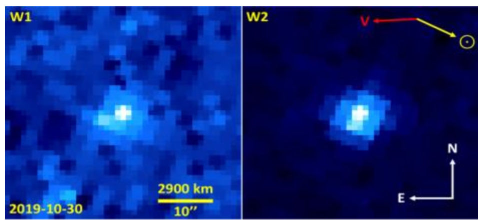

Figure 2: *Example of co-added NEOWISE thermal imaging data of Blanpain from 2019 Oct.*

Conclusion: The combination of radar, visible and thermal observations of Blanpain enabled a nucleus size estimate, that is slightly larger than previous estimates. We are working to contextualize our results in comparison to previously published estimates. Its surface reflectance in the visible and thermal emission properties were measured to be in line with typical values observed for the ensemble of JFCs.

References:
[1] Foglia, S. et al.: 2005, IAUC, 8485, 1. [2] Micheli, M.: 2005, *UAI*, 1, 47-53. [3] Jewitt, D.: 2006, *AJ*, **131**, 2327. [4] Clery, D.: 2021 *Science*, **371**, Issue 6526, pp. 225. [5] Harris, A. W.: 1998, *Icarus*, **131**, 291.

Acknowledgments: The Arecibo Observatory is a facility of the National Science Foundation operated under cooperative agreement by the University of Central Florida and in alliance with Universidad Ana G. Mendez, and Yang Enterprises, Inc. The Arecibo Observatory planetary radar program is funded through NASA's Near-Earth Object Observation (NEOO) program grant no. 80NSSC19K0523 awarded to the University of Central Florida.

SYNTHETIC INFRARED LIGHTCURVE GENERATION FOR BINARY ASTEROIDS

G. Henry[1,2], Ö. Karatekin[1] and J. Blommaert[2,3]
[1]Royal Observatory of Belgium (gregoire.henry@oma.be)
[2]Vrije Universiteit Brussel, [3]VITO

Introduction: Ground-based observations with infrared telescope are used in combination with thermophysical models to derive the properties of asteroids. Observations produce a ligthcurve of the asteroid, a periodic signal of the brightness of the asteroid over one rotation period around its spin axis. To either plan these observations or compare them with artificial customised parameters, we have developed a tool to generate a synthetic infrared lightcurve for binary asteroids.

Generating Synthetic Infrared Lightcurve: The thermophysical model for binary asteroids developed at the Royal Observatory of Belgium has been presented in a separate abstract. The simulation of synthetic infrared lightcurve is based on our thermophysical model. The major addition from the simulation framework of the thermophysical model, is the incorporation of Earth-centric reference as an observer point of view. The temperature at the surface of each element surface of the asteroids are computed nominally. The emitted flux from each surface element is computed. We envisioned two methods to generate lightcurve. 1) To render the scene of the asteroids viewed from the direction of the Earth and export the rendering as an image. The brightness of the scene can be computed for a given image, taking in consideration that the background is completely dark and using a sequential grayscale colormap with meaningful boundaries to represent the intensity of the emitted flux. In that way, the sum of the pixels is the brightness of the scene. Rendering the scene over one orbital period of the secondary around the primary body will produce a lightcurve. 2) To compute the quantity of emitted infrared flux from power law and geometry condition, for each facet, to produce the infrared lightness for one point in time.

Results: The synthetic lightcurve generation pipeline was run for the binary asteroid Didymos and Dimorphos for the 20th January 2021. Asteroids are positioned and oriented with respect to Earth viewpoint using SPICE and the emitted flux for each facet are computed from the thermophysical model. Using the first method described in the previous section, we produced the lightcurve visible in Figure 1. Shape models are taken from Hera kernels.

Acknowledgments: ESA OSIP for funding the research.

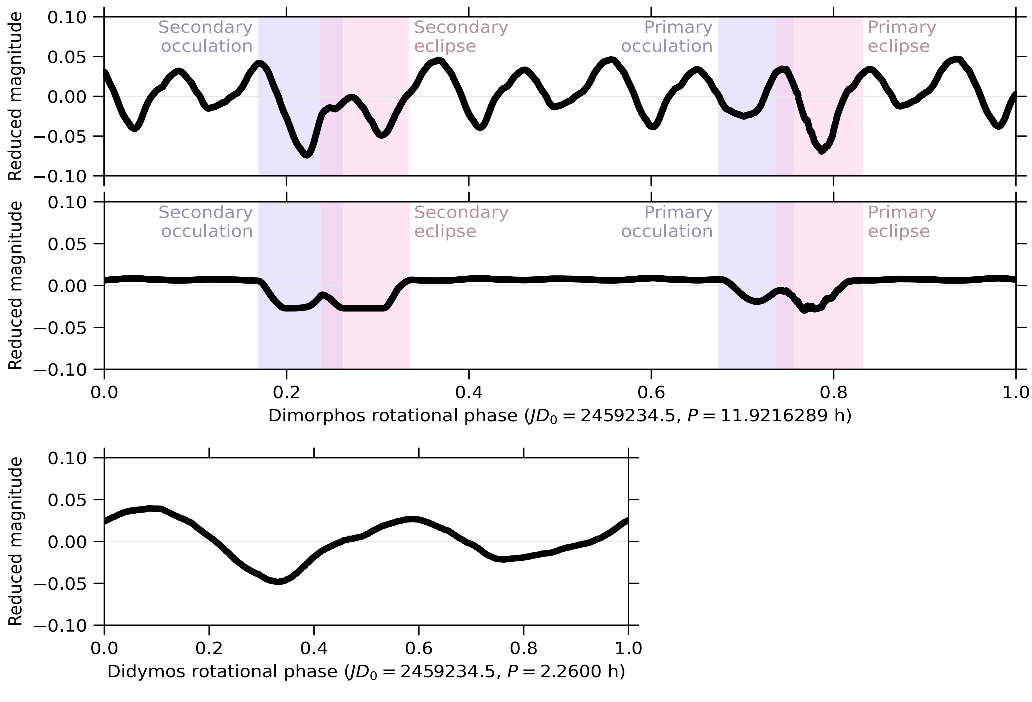

Figure 1: Ground-based synthetic lightcurve of the binary asteroid Didymos and Dirmophos.

SESSION 3

Thermal Modeling of the Moon and moons of the Solar System

ICY SATELLITE THERMAL MODELS IN SUPPORT OF THE EUROPA CLIPPER THERMAL EMISSION IMAGING SYSTEM (E-THEMIS)

Paul O. Hayne[1], John R. Spencer[2], Julie A. Rathbun[3], Oleg Abramov[3], Carly J. A. Howett[4], Michael T. Mellon[5], Francis Nimmo[6], Sylvain Piqueux[7], Samuel Aberbook[1], Philip R. Christensen[8]
[1]Laboratory for Atmospheric and Space Physics, University of Colorado, Boulder, CO, USA (Paul.Hayne@Colorado.edu) [2]Southwest Research Institute, [3]Planetary Science Institute, [4]University of Oxford, [5]Cornell University, [6]University of California, Santa Cruz, [7]NASA – Jet Propulsion Laboratory, [8]Arizona State University.

Introduction: Surface and subsurface temperatures on icy satellites are controlled by a range of geologic and geophysical processes affecting the interior heat flow and surface thermophysical properties. Thermal models of Europa have been developed previously in conjunction with the limited set of observational data available from spacecraft flybys and Earth-based telescopes [1,2,3]. In particular, the Voyager and Galileo missions provided multi-wavelength thermal IR and sub-mm measurements across a range of latitudes, longitudes, and local times on Europa's surface [4]. However, these data were limited, with spatial resolutions coarser than ~ 10 km, and generally only sampled one local time at each location. More recent Earth-based observations improve upon the radiometry of Europa's thermal emission, but also suffer from low spatial and temporal resolution.

In this study, we develop a suite of thermophysical models for Europa (applicable to other icy satellites), in preparation for the new dataset anticipated from Europa Clipper [5]. We focus primarily on the multi-spectral IR data to be acquired by the Europa Thermal Emission Imaging System (E-THEMIS) [6]. These and other datasets from Clipper are expected to revolutionize understanding of the geological and geophysical processes underlying icy satellite temperature variations.

Approach and Methods: Our goal is to develop a standard set of thermophysical models that are: 1) accurate, and 2) adaptable to a range of conditions and processes on icy satellites. A primary objective is to develop tools for simulating the E-THEMIS data using realistic observational and illumination geometry predicted for the Europa Clipper mission, expected to begin its science phase in early 2030.

1-d thermal model: The underlying 1-d thermal model is based on previously published code developed and validated for the Moon [6]. This model has previously been successfully applied to other planetary bodies, including Mars [7] and Ceres [8]. In this work, the 1-d model is adapted for the range of conditions on Europa, including the thermophysical properties of icy materials, effects of sublimation, and orbital/dynamical effects including Jupiter eclipses. The model is validated using data from Galileo PPR [2,4].

Roughness model: We adapt the surface roughness thermophysical model from [9], with observational constraints using Europa's thermal emission spectrum [1]. Briefly, the model generates a surface composed of individual surface facets chosen from a scale-dependent probability distribution. Craters are superimposed on this rough terrain with a specified area fraction at each spatial scale. The model generates surface temperatures and viewing-angle dependent emission spectra.

Heat flow model: Hot spots may be anticipated on Europa's surface due to variations in endogenic heat flow. For example, any plume sources would be associated with elevated heat flow, similar to those on Enceladus, which are responsible for ~10 GW of excess emission [10]. The model presented here accounts for both the background heat flow (primarily due to tidally driven dissipation in the ice shell) and local anomalies due to specific geologic features such as chaos, ridges, and lenticulae. Sublimation at the surface may also produce plumes, which decay as the hot spot cools over time.

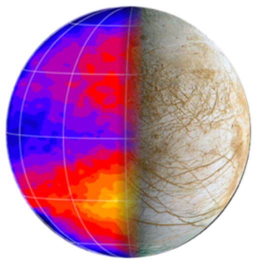

Figure 1: Map of Europa's thermal emission measured by the Galileo Photo-Polarimeter Radiometer (PPR). *(Adapted from [4].)*

Results and Discussion*:* We will present several applications of these models, including for example: 1) lifetimes and observable properties of hot spots and plumes; 2) thermal segregation of non-ice constituents; 3) thermal inertia variations inferred from global temperature patters (including the "equatorial cold band" – Fig. 1) on Europa. Finally, we will assess the capability of E-THEMIS and other future instruments to detect and map geophysically interesting features on Europa.

References: [1] Spencer (1987), thesis, *U. Arizona*. [2] Rathbun et al. (2010), *Icarus*, *210*. [3] Trumbo et al. (2017) *AJ*, *154*. [4] Spencer (1999), *Science*, *284*. [5] Christensen et al. (2017), *AGU Fall Meeting*. [6] Hayne 2017, [7] Wilcoski and Hayne (2020), *JGR*, *125*. [8] Hayne et al. (2015) *JGR*, *120* [9] Hayne et al. (2021) *Nat. Astron.*, *5*. [10] Howett (2011), *JGR*, 116.

Acknowledgments: This work was partially supported by the NASA Europa Clipper Project. Part of this work was performed at the Jet Propulsion Laboratory, California Institute of Technology, under contract with the National Aeronautics and Space Administration.

Modelling the Heat Flow from between Enceladus Tiger Stripes

C.J.A. Howett[1,2], J.R. Spencer[3], F. Nimmo[4], and G.M. Miles[3]
[1]University of Oxford (carly.howett@physics.ox.ac.uk)
[2]Planetary Science Institute (chowett@psi.edu)
[3]Southwest Research Institute
[4]University of California Santa Cruz

Introduction: There is abundant evidence that Enceladus' four south-polar fractures (dubbed tiger stripes) are a source of both material and heat. However, constraining the endogenic heat flow from this active region (often call South Polar Terrain, SPT) has proved challenging, and with estimates varying from 5.8 ± 1.9 GW [1] to 15.8 ± 3.1 GW [2]. Intriguingly the heat flow from only Enceladus' tiger stripes is estimated to be 4.2 GW [3], which means additional heat must be coming from somewhere else. The most logical place is from between the tiger stripes (known as interstitual or funiscular terrain).

This study is aimed at understanding what contribution (if any) these interstital regions provide to Enceladus' overall heat budget. To do this we analyse observations made by Cassini's Composite Infrared Spectrometer (CIRS) of these interstitual regions to estimate Enceladus' heat flow.

Observation: We focus on a single scan taken by CIRS focal plane 1 (FP1, 10 to 600 cm^{-1}) in December 2015. The scan, as shown in Figure 1a, crosses all four tiger stripes. It was taken during southern polar winter, when the passive surface emission is minimized.

Modelling: We first find the best-fitting blackbody temperature to each CIRS radiance. The results, given in Figure 1b, shows the surface temperatures increase significiantly over the tiger stripes.

We then use *thermprojrs*, a thermophysical surface model (c.f. [4]), to predict Enceladus' passive emission. The model works by setting the upper boundary of the surface so that the thermal radiation and incident solar radiation are balanced with the heat conducted to and from the surface and the change in the heat content of the surface layer. The lower boundary is set to a depth at which there is negligible temperature change with the temperature cycle.

We run the model tweleve times, to cover all combinations of three albedos (0.70, 0.75 and 0.80) and four thermal inertias (5, 27, 50, 100 MKS). These thermal inertia and albedo values were chosen because the span the range seen across Enceladus [5].

The results are given in Figure 1b. They show: 1) the temperatures of the interstitial regions aren't much lower than over the tiger stripes, 2) many models are able to fit the FP1 data outside the tiger stripes, implying the passive models are adequately predicting the observed passive emission close to (but, outside) the stripes, 3) none of the passive models can fit observations that lie either over or between the tiger stripes, inter-stripe temperatures are higher by 5 to 25 K.

These temperature difference are significant. Assuming they are representative of the entire interstitual regions, then its endogenic emission could be between 3.2±0.5 and 4.0±0.4 GW, which corresponds to heat flows between 279±48 and 380±36 mW m^{-2} using the known area of the interstitual regions (~3500 km^2 each). More work is required to confirm whether similar heat flows are indeed seen in other SPT interstitual regions.

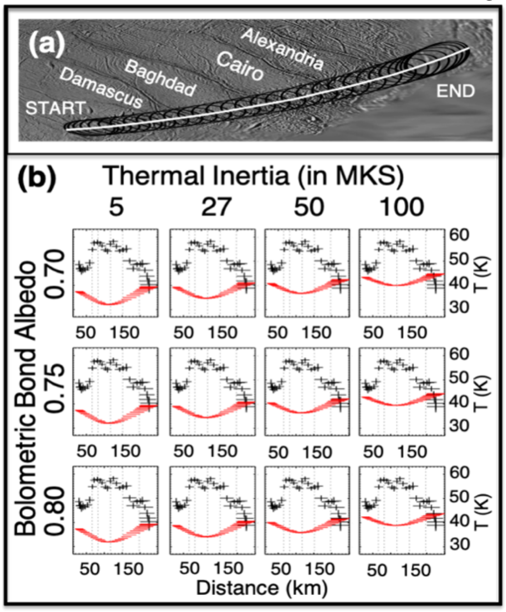

Figure 1: (a) FP1 footprints over Enceladus' SPT. (b) A comparison of passive modeled (red) and CIRS derived (black) surface temperatures. Tiger stripe locations given by dotted vertical lines.

Conclusion: Analysis of Cassini CIRS data has shown that the interstitual regions of Enceladus' tiger stripes are significiantly warmer than its expected passive temperatures. Depending on the thermophysical properties assumed, the endogenic emission from the interstitial regions alone could be between 3.2±0.5 GW and 4.0±0.4 GW (279±48 and 380±36 mW m^{-2}).

References: [1] Spencer et al., Science 311, 1401-1405, 2006; [2] Howett et al., JGR 116, E03003, 2011; [3] Spencer et al., in Enceladus and the Icy Moons of Saturn, 2018; [4] Spencer et al., Icarus 78, 337-354, 1989; [5] Howett et al., Icarus 206, 573-593, 2010.

Acknowledgements: We thank NASA's Cassini Data Analysis Program (CDAP) for their support of this work (Grant # 80NSSC19K0885).

THERMOPHYSICAL MODELS OF AIRLESS ICY SURFACES AND SPACE WEATHERING

C. Ferrari[1] and A. Lucas [1]
[1]Université Paris Cité, Institut de physique du globe de Paris, CNRS, F-75005 Paris, France (ferrari@ipgp.fr)

Introduction: We develop thermal models of icy saturnian moons (i.e., Mimas and Dione) to analyse Cassini CIRS spectrometer data and understand the properties of their regolith experiencing space weathering. These icy moons are submitted to such various aleration processes among which bombardment by meteorites, plasma, charged particles of the magnetosphere or E ring icy tiny particles. The effects of these competing processes are still uncertain. Thermal anomalies have been discovered on their surfaces by with the CIRS instrument during the Cassini mission [1]. This spectrometer observed the thermal emission of icy moons between 7 and 1000 µm with two focal planes of distinct spatial resolution, the focal plane FP1 (17-1000 µm) with an aperture of 3.9 mrad and the focal plane FP3 (9-17 µm) with a spatial resolution ten times as small. The thermal anomalies were found to be most prominent on Mimas and Tethys and consist of large temperature contrasts at similar local hour between a lens-shaped region centered on their leading hemisphere and the outside regions. Most of data were issued from the FP3, while FP1 was used to determine nighttime temperatures (1). The anomalies were interpreted as a change in thermal inertia, larger within the lens-shaped thermally anomalous region (hereafter the TAR) due to the bombardment of > MeV electrons which may yield sintering of icy grains and favor heat transport through the regolith [1, 2].

Effect of km-scale topography. We first aimed at constraining further the resulting effects of this bombardments on the regolith structural properties. Despite lower spatial resolution, the FP1 has the advantage of capturing the peak of thermal emission. Hence, both temperature and emissivity can be determined easily. We built a thermophysical model parametrized with regolith properties such as porosity, grain size or composition and including the local topography as a supplementary source of local variations in temperature and emissivity. In a first paper we show how these are impacted by both the topography and the regolith properties [3]. Heat transfer in the regolith may occur through conduction and radiation. Its bolometric albedo, A, and hemispherical emissivity, ε_h, are expressed as a function of grain properties. We have shown that the model roughly reproduces the observed variations of surface temperature, T_F, and apparent emissivity, ε_F, while assuming uniform regolith properties (Figure 1). The dispersion of temperatures within the large FP1 footprints due to the difference in local time of the surface elements explains most of the directionality of the apparent emissivity $\varepsilon_F(e)$ at emission angles $e \geq 30°$. Adding topography at the 8-km scale amplifies this effect by a few percent. Refining the scale to 1 km does not significantly change the result. This particular directionality $\varepsilon_F(e)$ cannot be explained by the directional emissivity ε_d of the regolith as defined in the Hapke model.

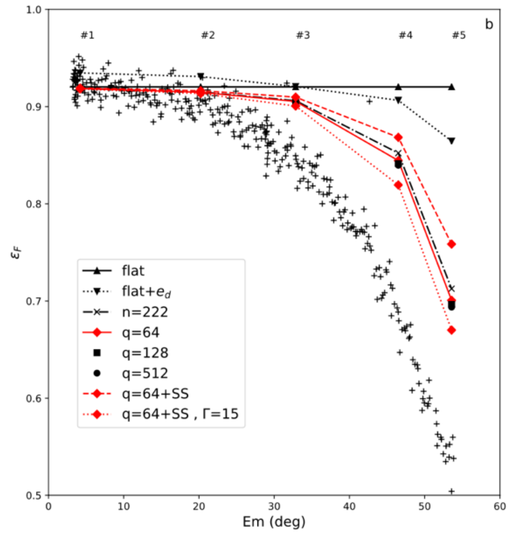

Figure 1: Apparent emissivity vs emission angle Em in a CIRS FP1 observation of Dione (+). Modelled emissivities considering either flat, ellispsoidal (n=220) or shape models with various spatial resolution (q) are also shown. SS stands for the Spatial Sensitivity of the focal plane. The regolith properties are A = 0.63, p = 0.5, R = 2 mm. The ice is amorphous. The thermal inertia Γ=0 or Γ=15 MKS).

The Mimas TAR. We applied this model to the analysis of Mimas TAR [4]. From CIRS FP1 low resolution observations, we retrieved the regolith properties such as grain size and composition at the regional scale, within and outside of the TAR, given the km-scale topography of Mimas. We will present how this study yield a new view on the regolith properties of the TAR. Sputtering by energetic electrons may be efficient at removing small superficial grains within the TAR. Sintering, does not yield significant changes in thermal inertia.

References:

[1] Howett et al. 2018 in Enceladus and the Icy Moons of Saturn, eds. Schenk, P. M., Clark, R. N., Howett, C. J. A., et al. (University of Arizona Press). [2] Schaible et al. (2017), Icarus, 285, 211. [3] Ferrari et al. A&A 655, A8 (2021). [4] Ferrari and Lucas (2023) A&A submitted.

Acknowledgments: We thank the Programme National de Planétologie for their support of the PISTE Project.

A CLOSED-FORM EXPRESSION FOR THE EQUILIBRIUM TEMPERATURES AND DIRECTIONAL EMISSIVITY OF SUNLIT AIRLESS PLANETARY SURFACES

Lior Rubanenko [1] and Norbert Schörghofer [2]
[1] Technion, Israel Institute of Technnology (liorr@technion.ac.il)
[2] Planetary Science Institute, USA (norbert@psi.edu)

Introduction: Insolation dominates the heat flux incident on sunlit airless surfaces compared to scattered and emitted radiation from topography and subsurface heat diffusion [1]. Surface slopes affect the temperature distribution by decreasing the downward component of the flux vector which in turn affects the directional emissivity. To account for these effects, thermal models often include an illumination component that calculates the radiation incident on each slope, typically using computationally extensive techniques [2, 3, 4]. Here we derive generalized closed-form expressions for the temperature distribution of illuminated rough airless surfaces, assuming a Gaussian slope distribution and Lambert scattering. Additionally, for the case of the Sun in zenith, we provide a closed-form solution to the integral equation of Smith (1967) [5, 6] which describes the directional emissivity of rough surfaces, and use it to investigate the topographic roughness of airless surfaces at the thermal separation scale.

Temperature Model: The topographic roughness of a surface can be described statistically by assuming the heights and slopes are normally distributed. In this *Gasussian Rough Surface* model, the probability density function (PDF) of the surface slope angles α is given by,

$$f_\alpha(\alpha) = \frac{\tan\alpha}{\omega^2\cos^2\alpha}\exp\left[-\frac{\tan^2\alpha}{2\omega^2}\right] \quad \text{(Eq. 1)}$$

where ω is the istropic RMS slope across a topographic transect. The PDF of the slope aspects (azimuths) is $\theta \sim \mathrm{U}(0,2\pi)$. By change of variables, we use f_α, f_θ and the equations that relate α to the solar incidence angle Θ, the solar flux F and the equilibrium temperature T [see 6], to derive their respective PDFs. For the case of the Sun in zenith (solar zenith angle $z = 0$), we find the temperature PDF,

$$f_{T(z=0)}(T) = \frac{4}{\omega^2\rho^2 T^9}\exp\left[-\frac{1}{2\omega^2}\frac{1-\rho^2T^8}{\rho^2T^8}\right] \quad \text{(Eq. 2)}$$

In the general case, the PDF-generating integral likely has no closed-form solution, and we obtain an asymptotic expansion for small ω,

$$f_T(T) = \frac{4\omega\rho T^3}{\sqrt{2\pi}}\frac{\sqrt{1+\tau_2}}{\tau_1}\left(1+\frac{1}{\omega^2\tau_3}\right)\exp\left[\frac{1}{2\omega^2}\left(1-\frac{1}{\tau_3}\right)\right] \text{ (Eq. 3)}$$

where $\tau_1 = \sqrt{1-\rho^2T^8}$, $\tau_2 = \frac{\rho T^4 \cot z}{\tau_1}$, $\tau_3 = \tau_1^2(1+\tau_2)^2\sin^2 z$, $\rho = \sigma\varepsilon(r/1\,\mathrm{AU})^2/S_0(1-A)$, $\sigma = 5.67\times10^{-8}\,\mathrm{W\,m^{-2}}\,T^{-4}$, $S_0 = 1367\,\mathrm{W\,m^{-2}}$ is the Solar Constant, A the albedo and r the distance from the Sun. The complete derivation and equations can be found in [6]. We validate our model by comparing the derived PDFs with those obtained by numerical illumination model [4].

Directional Emissivity: for the case of $z = 0$, we provide a closed-form solution for the surface directional emissivity (the surface brightness at some observation angle ψ normalized by the surface brightness when viewed from nadir), expressed as the mean brightness that would be measured by a remote sensing instrument.

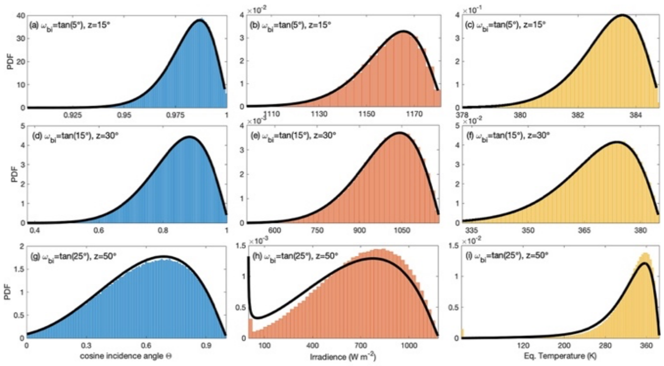

Figure 1: Solar incidence (a,d,g), incident flux (b,e,h), and equilibrium temperature (c, f, i) PDFs of a sunlit rough Gaussian surface based on theory (black lines) and a numerical thermal model (bars). Our analytic solution employs asymptotic expansion of the integral, which becomes less accuarate for higher values $\boldsymbol{\omega}$.

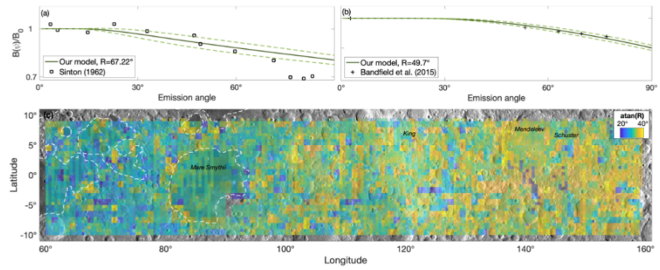

Figure 2: (a,b) by fitting the lunar surface brightness measured by telescopes [5] and LRO Diviner data [1] to our model we measure the surface RMS slope. (c) Using LRO Diviner high emission data, we find the roughness of the lunar maria is smoother than the highlands at the thermal separation scale.

$$\bar{B}(\psi,\omega) = \bar{B}(0) - \frac{\bar{B}(0,\omega) - \bar{B}\left(\frac{\pi}{2},\omega\right)}{\bar{B}\left(\frac{\pi}{2},\omega\right)}\tilde{B}(\psi,\omega) \quad \text{(Eq. 4)}$$

where the expressions for $\bar{B}(0,\omega)$, $\bar{B}\left(\frac{\pi}{2},\omega\right)$ and $\tilde{B}(\psi,\omega)$ are omitted for brevity, and can be found in [6]. In Figure 2 we show how we use our model to constrain the surface roughness of the Moon. At the conference, we will discuss applying our model to other airless planetary bodies.

References: [1] Bandfield et al., 2015. *Icarus.* [2] Paige et al., 2010. *Science* [3] Davidsson and Rickman, 2014. *Icarus.* [4] Rubanenko and Aharonson, 2017. *Icarus.* [5] Smith, 1967. *JGR.* [6] Rubanenko et al., 2020. *JGR: Planets.*

A MICROPHYSICAL THERMAL MODEL FOR THE LUNAR REGOLITH

J. Bürger[1], J. Blum[1], B. Gundlach[1], P. O. Hayne[2], M. Läuter[3] and T. Kramer[4]
[1]Institute of Geophysics and Extraterrestrial Physics, TU Braunschweig, Germany (j.buerger@tu-bs.de)
[2]Laboratory for Atmospheric and Space Physics, University of Colorado Boulder, CO, USA
[3]Zuse Institute Berlin, Germany
[4]Institute for Theoretical Physics, Johannes Kepler Universität Linz, Austria

Introduction: Existing thermal models for the lunar regolith differ in the models used to describe the regolith properties, with the models having a critical influence on the modeled temperatures. The current thermal model for the lunar regolith was developed by [1] and uses an empirical description with the *H*-parameter for the variation of bulk density and thermal conductivity with depth. We expand upon this work by developing a microphysical model that more directly simulates regolith properties such as grain size or bulk density.

Lunar Regolith Thermophysical Model: The developed thermophysical model solves the one-dimensional heat transfer equation and returns the temperature as a function of depth. The regolith bulk density profile is described by the stratification model of [2] and is a function of grain radius and depth. The steepness of the transistion from the loose packing at the surface to the maximum bulk density in the deeper layers is described by the parameter Δ. Figure 1 illustrates the influence of the grain radius and the transistion width Δ on the modeled bulk density profiles. The thermal conductivity is modeled as a function of temperature, grain radius and volume filling factor according to [3], who developed a thermal conductivity model for a granular packing of equally sized spheres in vacuum. The heat capacity is temperature-dependent [1].

The lunar highlands and maria are modeled separately, taking into account their difference in albedo [4]

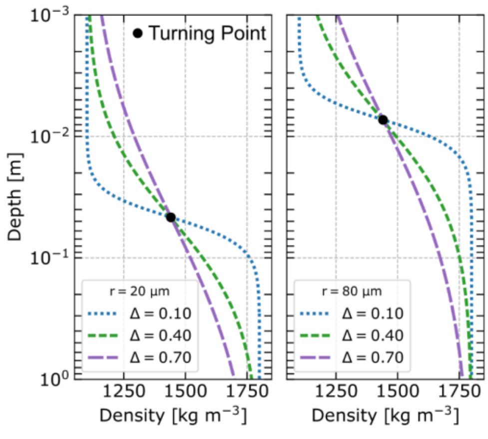

Figure 1: Illustration of the regolith bulk density profiles derived from the empirical model for the stratification of planetary regolith by [2]. The influence of the grain radius r and transition width Δ is shown.

and mass density [5]. In addition, the thermal conductivity model is fitted to measurements on returned samples from the maria [6] and the highlands [7]. For the model fits, a temperature-dependent thermal conductivity of the solid material was added, derived from [8], which approaches zero with decreasing temperature.

Derivation of Lunar Regolith Properties: The simulated regolith temperatures are compared with brightness temperature measurements from the Diviner Lunar Radiometer Experiment [9] on board the Lunar Reconnaissance Orbiter. Three model parameters are varied, namely the grain radius, the deep layer density, and the transition width Δ, and the best fitting parameter set is determined. Figure 2 shows the best model fit to Diviner nighttime regolith temperatures measured in the maria at the lunar equator.

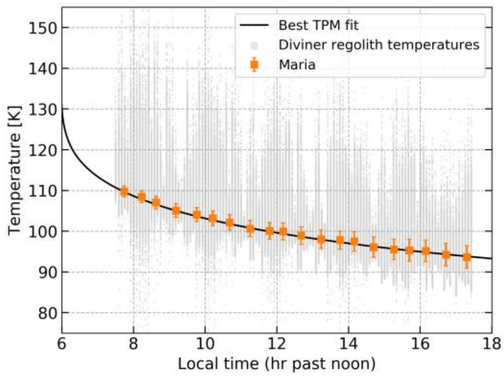

Figure 2: Comparison of modeled and measured regolith temperatures for the maria at the lunar equator.

Future Work: The overall goal for the future is to produce maps of the derived regolith properties (grain radius and stratification properties) that can be used for future mission planning and for understanding the geological history of the of the Moon.

References: [1] Hayne, P.O. et al. (2017) *JGR, 122*, 2371-2400. [2] Schräpler, R. et al. (2015) *Icarus, 257*, 33-46. [3] Gundlach, B. and Blum, J. (2012), *Icarus, 219,* 618-629. [4] Feng, J. et al. (2020) *JGR, 125,* E06130. [5] Kiefer, W. S. et al. (2012) *Geophys. Res. Lett., 39,* L07201. [6] Cremers, C. J. and Birkebak, R. C. (1971) *Lunar Planet. Sci. Conf. Proc. 2*, 2311-2315. [7] Cremers, C. J. & Hsia, H. S. (1974) *Lunar Planet. Sci. Conf. Proc. 3,* 2703-2708. [8] Opeil, C. P. (2012) *Meteoritics & Plan. Sci. 47,* 319-329. [9] Paige, D. A. et al. (2010), *Space Sci. Rev., 150,* 125-160.

A NEW THERMAL ROUGHNESS MODEL FOR THE MOON AND MERCURY: IMPLICATIONS FOR THE DIURNAL LUNAR HYDROXYL CYCLE AND MINERALOGICAL MAPPING WITH MERTIS ONBOARD BEPICOLOMBO Kay Wohlfarth[1], Christian Wöhler[1], Harald Hiesinger[2], Jörn Helbert[3]

[1] Image Analysis Group, TU Dortmund University, Otto-Hahn-Str. 4, 44227 Dortmund, Germany (kay.wohlfarth @tu-dortmund.de), [2] Institut für Planetologie, Wilhelm-Klemm-Str.10, 48149, Germany [3] Institute for Planetary Research, DLR, Rutherfordstr. 2, 12489 Berlin, Germany

Introduction: We extend [1,2] and use fractal-rough surfaces, self-heating, self-scattering, and shadowing to compute the thermal emission of airless planetary bodies. Reflectance and emissivity are given by [3]. See also the companion paper [4] and the full article [5].

Validation: We validate our model with the Chinese weather satellite Gaofen-4 [6] (Fig. 1) and lunar off-nadir measurements of Diviner [7] (Fig. 2). The model results agree with the data for θ= 20°-30°.

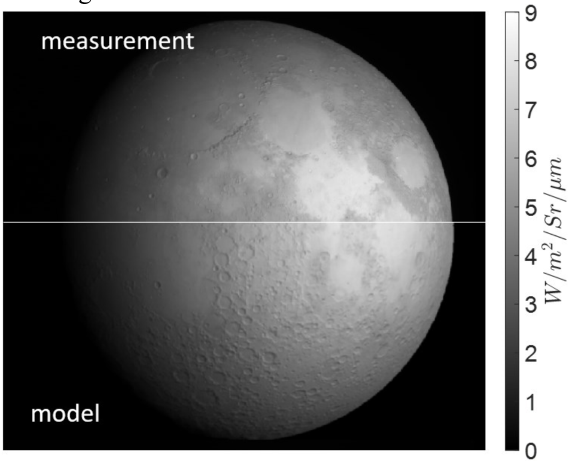

Figure 1: Top: Intensity measured by Gaofen-4 @ 3.77 µm on 25th July 2018 [6]. Bottom: Model results.

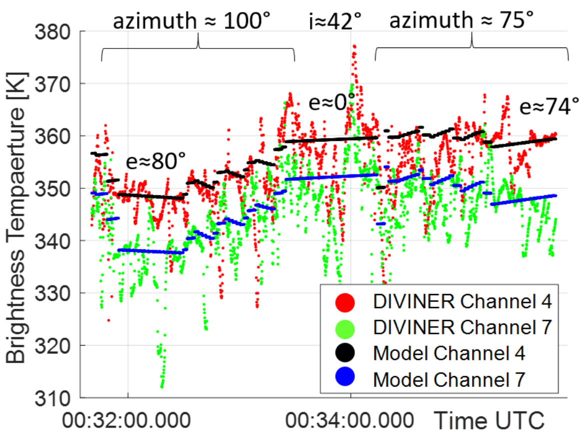

Figure 2: Off-nadir Diviner temperatures of channel 4 (8.25 µm) and 7 (13-23 µm) vs. our model. DIVINER covered emission angles between e≈80° and 0° at a constant incidence angle (i≈42°) and two azimuth ranges (az≈100° and 75°). See also [7].

Application 1 - Lunar Hydroxyl: We use the thermal model to reprocess the global lunar mosaic of the Moon Mineralogy Mapper (M³) [8] and derive new maps that show the diurnal lunar hydroxyl/water cycle (Fig. 3). These maps update the results from [9].

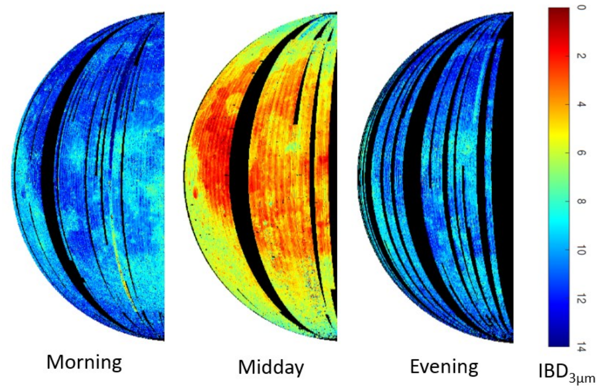

Figure 3: Integrated band-depth ($IBD_{3\mu m}$) of the 3-µm absorption band derived from M³ indicating surficial OH/H_2O. Note the temporal and spatial variations of $IBD_{3\mu m}$. Half of the lunar nearside is shown.

Application 2 - MERTIS lunar flyby: Our model reproduces the first data of the Mercury Radiometer and Thermal Infrared Spectrometer (MERTIS) [10] that scanned the Moon on 9th April 2020 [11].

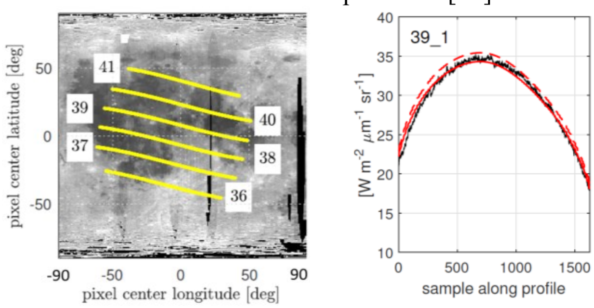

Figure 4: Left: footprint of 7 MERTIS pixels that scanned the Moon. Right: MERTIS data (black) and model for ε = 0.97 (solid red) and for ε = 1 (dashed red) of scan 39 @ 7.0-8.62 µm.

References: [1] Rozitis, B. and Green, S. F. (2011) MNRAS 415(3), 2042-2062. [2] Davidsson, B.J. et al. (2015) Icarus, 252,1-21. [3] Hapke (2012), Cambridge Univ. Press. [4] Wohlfarth et al. (2023), this conference. [5] Wohlfarth et al. (2023), A & A, under revision. [6] Wu, Y. et al. (2021) Geophysical Research Letters, 48, e2020GL088393 [7] Bandfield, J. L. et al. (2015) Icarus 248, 357-372. [8] Pieters, C. et al. (2009) Curr. Sci., 96(4), 500-505. [9] Wöhler C. et al. (2017) *Sci. Adv.*, 3(9). [10] Hiesinger et al. (2020) Space Sci. Rev. 2016, 110. [11] Hiesinger et al. (2021) LPSC LII, abstract # 1494.

A SEMI-ANALYTICAL MODEL FOR THE LUNAR THERMAL EMISSION PHASE FUNCTION

E. Jhoti, T. M. Powell and D. A. Paige[1]
[1]University of California, Los Angeles (ejhoti@ucla.edu)

Introduction: The Diviner Lunar Radiometer onboard NASA's Lunar Reconnaissance Orbiter has recently begun an observing campaign to collect directional thermal data from the Moon [1]. Our study utilizes this dataset to construct a semi-analytical model describing the lunar emission phase function (EPF) using surface roughness. The model could be used to predict the amount of radiation re-emitted into permanently shadowed regions.

Methods: Diviner radiance mesurements are representative of the surface temperature within the ~250 m detector footprint. However, small-scale roughness causes sub-resolution temperature variations that result in different measured brightness temperatures depending on viewing angle [1,2,3,4,5]. Altering Diviner's viewing angle results in different portions of the surface occupying the field of view, and therefore different temperatures are observed. Consequently, apparent emissivity from Diviner depends on viewing geometry and illumination geometry [2,3,6,7]. This effect is stronger at higher latitudes where the illumination conditions are more extreme. Previous works have used simulated surface roughness to model the EPF for the Moon and asteroids [3,4,6,7,8,9,10,12]. This study uses the semi-analytical bowl-shaped crater model used by [6,9,10,11]. The temperature of a single bowl-shaped crater was calculated, taking into account incident radiation from the Sun, scattered solar and infrared radiation, and shadowing [10]. Different combinations of crater shapes and surface fractions were trialed to find the qualitative best fit to the data. This was found to be a mixture of two craters with different depth to diameter ratios (Δ), one with $\Delta = 0.2$ and surface fraction 0.4, the other with $\Delta = 0.5$ and surface fraction 0.3. The remaining surface fraction of 0.3 was set to a flat surface temperature.

Results: The total bolometric temperature produced by the model with these best-fit crater parameters for a range of observer incidence angles (angle between the surface normal and the observer) were plotted with Diviner apparent bolometric temperature data from three targets (Figure 1) [1]. The left plot shows the model plotted against Diviner principal plane data (where the detector has the same azimuthal angle as the Sun), and the right plot shows Diviner cross plane data (where the detector has an azimuthal angle at +/-90° to the Sun). Azimuthal angle is defined as the angle between the projection of the observer incidence vector onto the horizontal and the projection of the solar incidence vector onto the horizontal. The solar incidence vector is the vector joining the point of interest and the Sun. Both geometries of the model appear to fit the data well.

Conclusions: The preliminary results of the model indicate that the driving topography affecting the directional emissivity on the Moon at the meter-cm scale can be well approximated using multiple bowl-shaped craters. Future work will include modelling the full azimuthal range of Diviner data. We plan to use these results to formulate an empirical or semi-analytical function to describe the lunar EPF, as has been done for other airless bodies such as asteroids [12].

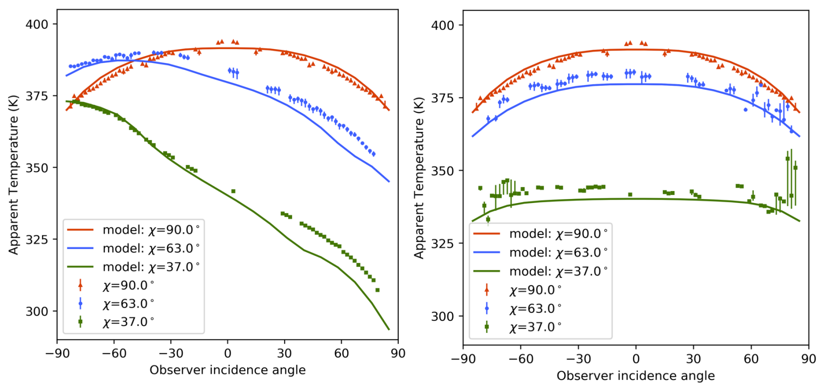

Figure 1: Triangle, circle, and square points are Diviner apparent bolometric temperature against observer incidence angle for three different targets on the Moon each with different solar elevation angles, χ, (where elevation angle is defined as 90°- incidence angle) [1]. Blue data are from an ejecta ray of Aristarchus crater, red data are from an equatorial highlands region and green data are from a high latitude mare region. The left plot shows Diviner principal plane data (Diviner has same azimuthal angle as the Sun), and the right plot shows Diviner cross-plane data (Diviner is oriented 90° in azimuth relative to the Sun). Solid colored lines are the model with best fit crater parameters described in the text.

References:

[1] Paige D. A. et al. (2010) *Space Sci Rev* (2010) 150: 125–160. [2] Paige D. A. et al. (2010b) *Science*, 330(6003), 479–482. [3] Bandfield J. L. et al. (2015) *Icarus*, 248, 357-372. [4] Rubanenko L. and Aharonson O. (2017) *Icarus*, 296, 99-109. [5] Hayne P. O. et al. (2021) *Nat Astron,* 5, 169–175. [6] Buhl D. et al. (1968a) *JGR*, 73, 5281. [7] Davidsson B. J. et al. (2015), *Icarus*, 252, 1-21. [8] Rubanenko L. et al. (2020) *JGR: Planets*, 125. [9] Buhl D. (1967) PhD Thesis, UC Berkeley. [10] Ingersoll A. P. et al. (1992) *Icarus*, 100(1), 40–47. [11] Winter D. F. and Krupp J. A. (1971) *The Moon* 2**,** 279–292. [12] Lagerros J. S. V. (1998) *Astron. Astrophys.* 332, 1123–1132.

THE THERMAL ENVIRONMENT OF DOUBLY SHADOWED MICRO COLD TRAPS ON THE MOON

P. O'Brien[1] and P. O. Hayne[1],
[1]Laboratory for Atmospheric and Space Physics, University of Colorado Boulder, CO, USA (patrick.o'brien@lasp.colorado.edu)

Introduction: Permanently shadowed regions (PSRs) experience a range of illumination conditions and, consequently, temperatures due to scattered sunlight and thermal emission from nearby sunlit surfaces [1]. Topographic depressions within PSRs, e.g., small embedded impact craters, can be fully or partially shielded from these secondary illumination sources and are therefore termed *double shadows*. Temperatures within lunar double shadows could be as low as 25 K [2], cold enough to sequester not only water ice but also "super-volatiles" like Ar [3], CO_2, and organics typically found in comets [4]. Shadow mapping with laser altimetry-derived topography found that permanent double shadows are rare (~0.04% of PSR area is doubly shadowed) and small (<1 km across) [5].

The footprint of the Diviner radiometer instrument is ~400 m x 140 m [6], rendering it challenging to directly measure surface temperatures within these often small, ultra-cold regions. Far-infrared emissivity features in Diviner data have, however, been attributed to anisothermality from unresolved ultra-cold traps [7]. Thermal modeling, in combination with high resolution topography data, can estimate temperatures at sub-Diviner scales. With upcoming in situ exploration from the VIPER rover [8] and Artemis III missions, it is crucial to understand the lunar thermal environments at the smallest spatial scales in order to predict the location and abundance of super-volatile compounds.

Micro cold traps: [9] demonstrated that water ice cold traps can exist down to spatial scales of ~1 cm and because small shadows are more abundant than large ones, micro cold traps constitute a substantial fraction of the total area where water ice could be stable at the lunar poles. Due to the similar scale dependence in double shadow abundance [5], micro cold traps likely also play an important role in super-volatile stability.

The amount of secondary illumination incident upon a PSR varies from point to point across the shadow and throughout the lunar year. Accurately modeling the effects of secondary illumination on double shadow temperatures thus requires detailed knowledge of small-scale lunar terrain and seasonal illumination.

Data and Methods: Digital elevation models (DEMs) from the Lunar Orbiter Laser Altimeter (LOLA) instrument exist at resolutions down to 5 m/pxl near the poles, sufficient to fully resolve doubly shadowed craters. We use a 1D thermal model [10] to calculate temperatures within PSRs using real lunar topography from high-resolution LOLA DEMs. Lateral heat conduction is negligible at scales >1 cm [9].

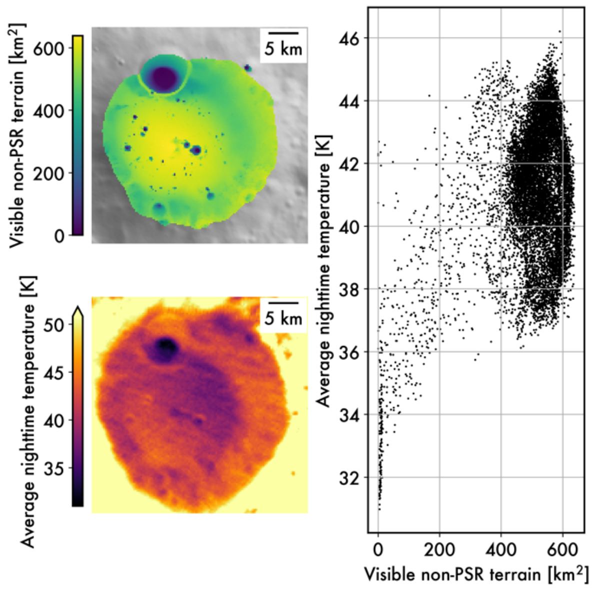

Figure 1. (left) Area of non-PSR terrain visible from Faustini crater and Diviner channel 9 average nighttime temperatures. (right) Scatter plot of temperature vs. secondary illumination proxy for permanently shadowed points within Faustini.

Secondary illumination: The main heating sources in double shadows are scattered sunlight and thermal emission. Therefore, the main task in modeling double shadow temperatures is computing the radiosity of all surface facets visible from a given point. As a proxy for the flux of secondary illumination, we first measured the total area of non-permanently shadowed facets visible from PSRs at the lunar south pole (Figure 1). There is good correlation between this proxy and Diviner temperatures, demonstrating that variation in secondary illumination drives a wide range of PSR temperatures.

Conclusions and Future Work: Using a seasonal illumination model, we will evaluate how the instantaneous double shadow area fraction varies throughout the year and we will present preliminary results of micro cold trap thermal modeling. Finally, we will discuss the implications of these results for interpreting unresolved Diviner surface temperature measurements.

References: [1] Kloos, J.L. et al. (2021) *AA*, 178. [2] Carruba, V. & Coradini, A. (1999) *Icarus*, 142. [3] Hodges, R.R. (1980) *LPSC*, 11. [4] Landis, M.E. et al. (2022) *PSJ*, 3. [5] O'Brien, P. & Byrne, S. (2022) *PSJ*, 3. [6] Williams J.-P. et al. (2019) *JGRP*, 124. [7] Sefton-Nash, E. et al. (2019) *Icarus*, 332. [8] Colaprete, A. et al. (2019) *AGU*, P34B-03. [9] Hayne, P.O. et al. (2021) *NatAstr*, 5. [10] Hayne, P.O. et al. (2017) *JGRP*, 120.

Acknowledgments: This work is supported by the LRO Diviner instrument project.

3D THERMAL AND VOLATILE TRANSPORT MODELING OF LUNAR PITS AND CAVES

A. X. Wilcoski[1], P. O. Hayne[1], and C. M. Elder[2] [1]University of Colorado, Boulder, CO, [2]Jet Propulsion Laboratory, California Institute of Technology (andrew.wilcoski@colorado.edu)

Introduction: Lunar water ice deposits have been widely discussed as mission targets for both their scientific value and their potential as resources for future human missions. This has led to many ongoing efforts to determine where ice is most abundant and most accessible. Thermal modeling is a particularly useful tool in these efforts, since the stability of volatiles is directly dependent on an environment's thermal conditions.

Lunar collapse pits (Fig. 1), particularly those that could be connected to subsurface caves, have been suggested as environments that could host ice deposits accessible to exploration and protected from destructive surface processes [1, 2]. [3] identified 228 lunar pits between ±50° latitude, most of which formed in impact melts. These impact melt pits should be similarly abundant at high latitudes, though they are difficult to observe because shadowing makes them hard to distinguish from other terrain [1]. At high latitudes (>70°) pit interiors should form permanently shadowed regions (PSRs) which, if cold enough, might allow water ice to be stable over billions of years [4]. However, the thermal environments within lunar pits have yet to be characterized to determine if they would make effective cold traps for water ice.

In this study, we create and validate a 3D thermal model and use it to investigate the thermal environments within high latitude lunar pits and their possible caves. We use the results of the thermal model to explore water ice stability within pits and caves using a volatile transport model. We determine how pit/cave latitude and geometry control interior temperatures, and how pit/cave temperature and geometry affect water ice stability within these features.

Methods: Our 3D thermal model is initialized with a 3D triangular mesh of arbitrary shape. The model calculates surface temperatures for each facet of the triangular mesh by balancing direct insolation, multiple scattering of visible and infrared radiation from other facets, 1D subsurface heat conduction orthogonal to each facet, and infrared emission (Fig. 2). The model also includes the effects of terrain shadowing on each facet from other facets in the mesh. We generate several different input geometries of interest based on the survey of lunar pits by [3], and characterize each geometry's thermal environment as it varies with latitude and time (Fig. 3).

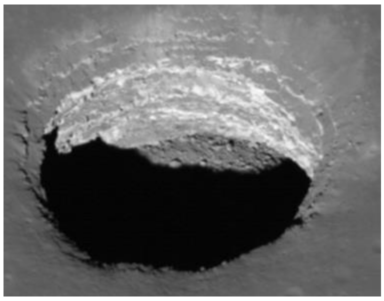

Figure 1 An oblique view of Tranquillitatis pit showing a view into the lunar subsurface. (LROC M175057326R, NASA/GSFC/ASU)

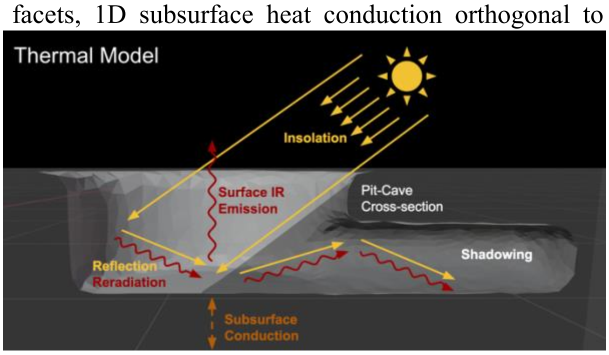

Figure 2 Schematic showing the energy balance of the 3D thermal model, within a cross-section of a pit with an attached cave.

Additionally, we develop a volatile transport model that calculates the loss rate of ice from each pit geometry using the thermal model results as inputs. Volatile loss from each facet is modeled by analogy with a radiative process, where particle fluxes between facets are treated the same as radiation fluxes.

Results and Conclusions: The model shows that lunar pits generally make poor cold traps for ice because their enclosed geometries cause efficient multiple scattering of infrared emission that raises pit temperatures. We find that ice loss rates are higher for pits/caves than for PSRs within craters at similar latitudes. However, there are some specific situations in which pits/caves can act as effective cold traps, such as when a pit opening is shadowed by exterior topography.

References:

[1] Avent W. and Lee P. (2021) *LPSC 52,* Abstract #2548. [2] Schörghofer, N. (2022) *Earth, Moon, and Planets* 126.2. [3] Wagner R. V. and Robinson M. S. (2014) *Icarus, 237,* 52-60. [4] Watson K. et al. (1961) *JGR, 66*, 1598.

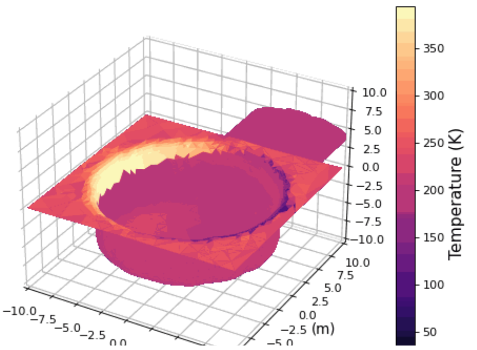

Figure 3 Modeled surface temperatures of a cylindrical pit with attached cave at 80° S latitude at local noon.

THE EFFECTS OF HEAT-PRODUCING ELEMENT ABUNDANCE AND DISTRIBUTION ON THE PRESENT-DAY LUNAR THERMAL PROFILE

Arkadeep Roy[1], Ananya Mallik[1], Paul M. Bremner[2], Heidi F. Haviland[2], Matthew R. Diamond[3], Tyler J. Goepfert[4], Richard L. Hervig[4]
[1]Department of Geosciences, University of Arizona, Tucson, AZ, USA (arkadeeproy@arizona.edu)
[2]NASA Marshall Space Flight Center, Huntsville, AL, USA
[3]Department of Physics, University of Illinois Chicago, Chicago, IL, USA
[4]School of Earth and Space Exploration, Arizona State University, Tempe, AZ, USA

Introduction: The lunar thermal profile (or selenotherm) is key to understanding lunar volcanism, mantle dynamics, and thermoelastic properties of the solid Moon. The range of selenotherms derived independently from geophysical inversions span up to 800 °C – too large to apply petrogenesis models or perform predictive geodynamic simulations [1]. The present-day selenotherm is primarily a function of the radiogenic heat generated through the lunar interior, which is canonically believed to be transported to the surface via conduction. The critical inputs in modeling a conductive selenotherm are the total abundances and distributions of the major heat-producing elements (HPEs: U, Th, and K) and the thermal conductivities and thicknesses of the major stratigraphic layers. As the lunar magma ocean (LMO) crystallized, the incompatible HPEs accumulated in the last dregs of the LMO. These HPE-laden dregs crystallized as shallow high heat-producing density gravitationally unstable ilmenite-bearing cumulates (IBCs), which may get overturned [2].

A lack of consensus over the HPE inventory in the lunar mantle poses a roadblock for constraining the selenotherm. We used a range of partition coefficients (K_D) for HPEs relevant for the minerals crystallizing from the LMO to constrain their stratigraphic distribution throughout the mantle and applied the HPE abundances obtained to a 1-D thermal conduction equation to predict heat transport in a spherical shell model. Step-by-step fractional crystallization modeling of a 600-km deep LMO using a stratified mantle sequence [3] was performed. The final 2.5% of the residual LMO by mass was designated as the IBCs. Since the Earth-Moon system shares a common origin [4], we considered the bulk silicate Moon's refractory element (U and Th) budget equivalent to that of the bulk silicate Earth (BSE), whereas the volatility of K has been accounted for by K/U ratios, derived from lunar materials [5]. Two different HPE concentrations for the BSM were explored in our models: (i) McDonough and Sun (1995) [6] and (ii) Faure et al. (2020) [7]. We explore selenotherms from various overturn scenarios where IBCs are relocated to the otherwise HPE-poor lower mantle.

Conclusions: The HPEs are concentrated within the thin IBCs and become a main contributor to the present-day heat production inside the Moon [8]. The key findings from this study are as follows: (i) The bulk Moon's HPE concentration dictates the HPE abundance of the IBC layer. (ii) The McDonough and Sun (1995) selenotherms far exceed the olivine solidus curves, while the HPE concentrations from Faure et al., (2020), which are lower by an order of magnitude, yield more reasonable, about half-as-hot values. (iii) Selenotherms using Faure's U and Th abundances support enstatite chondrites being the dominant building block of Earth [9]. (iv) Faure's half- and no-overturn curves closely follow the limits of geophysical inference (gray zone), suggesting that the present-day selenotherm falls within this region.

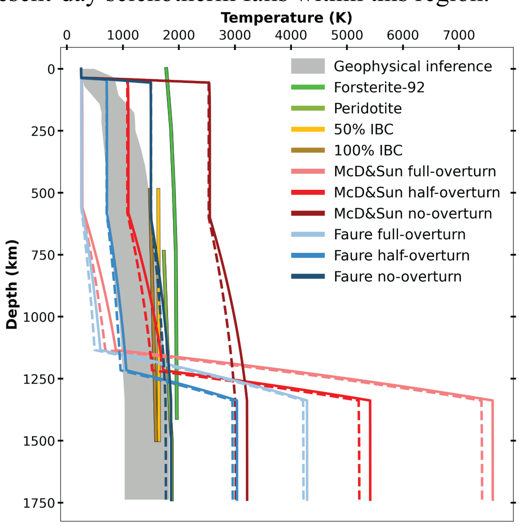

Fig. 1 Three selenotherm scenarios: no overturn, 50% IBCs overturn, and complete overturn for two HPE abundances [6, 7]; dashed lines - minimum K_D, solid lines - maximum K_D.

References: [1] Bremner P.M. et al. (2021) *LPI Contrib*, 2635, 5052. [2] Elkins-Tanton et al. (2002) *EPSL*, 196, 239-249. [3] Charlier B. et al. (2018a) *Geochim Cosmochim Acta*, 234, 50–69. [4] Canup R. (2012) *Science* 338, 1052-1055. [5] Korotev R.L. (1998) *JGR: Planets*, *103*, 1691–1701. [6] McDonough W.F. & Sun S.-s. (1995) *Chem. Geol*, 120, 223-253. [7] Faure P. et al. (2020) *Geochim Cosmochim Acta*, 275, 83-98. [8] Roy A. et al., (2023), LPI Contrib, 2696. [9] Dauphas (2017) *Nature*, 541, 521-524.

A THREE DIMENSIONAL FINITE ELEMENT APPROACH FOR A REALISTIC THERMOPHYSICAL BEHAVIOUR OF THE MOON AT LOCAL SCALES

K. Durga Prasad* and G. Ambily
Physical Research Laboratory, Ahmedabad, India (*E-mail: durgaprasad@prl.res.in)

Introduction: An understanding of the thermal environment of the Moon is an essential aspect of future missions and in-situ exploration[1,2]. Even though Moon provides advantages in terms of accessibility, resource potential and scientific importance, its complex thermophysical behaviour puzzles the scientific community. In addition, acquiring prior knowledge about the thermal environment of proposed landing site is necessary for any future mission. The effect of uppermost porous layer is significant since it inhibits the heatflux into the interior from the surface. This becomes more significant at local scales of few centimetres to metres, which is actually important for in situ exploration. Several models have been developed during the past 60 years to numerically estimate the lunar surface and subsurface temperatures[3,4]. Because of the lack of sufficient and systematic experimental observations, these model results have been widely accepted and used till now. However, most of these models were one-dimensional in nature and does not account for lateral heat transport within the subsurface. Towards this, we have developed a comprehensive three dimensional model using a finite element approach which provides more realistic thermophysical behavior even at the local scales.

Model description and Results: The present model can simulate the lunar surface as a multi-layered system with specific thermophysical parameters. The initial and boundary conditions needed for the model are obtained from earlier literature and in-situ measurements and other parameters are described in terms of analytic functions. The model is also capable of mimicking the actual topography, solar influx variation on the specific site, effect of uppermost fluffy layer etc[2]. The model has been validated using laboratory experiments and in-situ measurement.

Using this, simulations were carried out to estimate the thermophysical behaviour of two distinct high latitude sites - one of which is the proposed Chandrayaan – 2 (CH2) landing site and the other one is a similar site with relatively large relief. Since the proposed CH2 landing site was at high latitude, the influence of solar illumination and local topography would be more prominent which would not be manifested using a global one-dimensional model. Topography at all scales play a vital role in dictating the surface and subsurface thermophysical properties. In order to incorporate the same, topographic data from LOLA (Lunar Orbiter Laser Altimeter) instrument onboard LRO has been used in conjunction with the model and the surface and subsurface temperatures were derived. Thermophysical behavior of these two distinct sites are compared. Qualitative analysis of the results show that the surface and subsurface temperatures on these sites are quite different although the location and soil properties are quite similar. As the proposed CH2 landing site is characterized by a relatively flat terrain, significant temperature differences within the local vicinity has not been observed. However, a site within similar latitudes with a relief showed a significant temperature variability. Such a comparison was not feasible with a one dimensional models thus proving the credibility of our model.

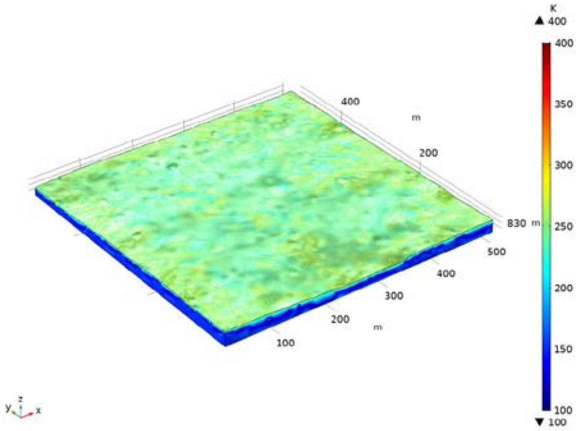

Figure 1: Surface temperatures derived form the model during dawn approach for the proposed Chandrayaan-2 landing site

Conclusion: A three-dimensional finite element model is developed to understand the thermophysical behavior of the lunar surface at local scales. It has lot of implications not only on understanding surface geophysics but also important for planning and operating future in situ experiments. Model details and some results will be discussed.

References: [1] Durga Prasad K, Kalyan Reddy. P, COSPAR abstract 2020. [2] Durga Prasad, K., Rai, V. K., & Murty, S. V. S. (2022) [3] Hayne, P. O., Bandfield, J. L., Siegler, M. A., Vasavada, A. R., Ghent, R. R., Williams, J. P., et al. (2017) [4] Ashwin R. Vasavada, David A. Paige, Stephen E. Wood, (1999)

ROUGH SURFACE THERMOPHYSICAL MODELS AND IR IMAGING FROM THE LUNAR SURFACE

Paul O. Hayne[1], Kerri Donaldson Hanna[2], Ben T. Greenhagen[3], Matthew A. Siegler[4], David A. Paige[5], Elisha Jhoti[5], Tyler Horvath[5], David Osterman[6], and the L-CIRiS and LV-CIRiS teams
[1]Laboratory for Atmospheric and Space Physics, University of Colorado, Boulder, CO, USA, [2]University of Central Florida, [3]APL, Johns Hopkins University, [4]Planetary Science Institute, [5]UCLA, [6]Ball Aerospace

Introduction: The Lunar Compact Infrared Imaging System (L-CIRiS; Fig. 1) is planned to acquire thermal infrared images from near the Moon's south pole as part of NASA's Commercial Lunar Payload Services (CLPS) program. Additionally, a successor instrument, LV-CIRiS, is planned to fly onboard the rover of the Lunar Vulkan Imaging and Spectroscopy Explorer (Lunar-VISE) mission, also part of the CLPS program [1]. In preparation for these new measurements, thermal models are needed that can accurately reproduce the complex temperature distribution and emission phase behavior of the lunar surface. Here, we discuss some of the thermophysical models in development by the L-CIRiS and LV-CIRiS teams, as well as their applications to these and other datasets.

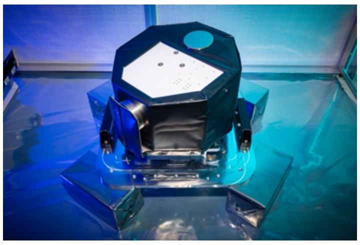

Figure 1: The L-CIRiS flight model, fully assembled at Ball Aerospace, Boulder, CO, USA.

Approach and Methods: We couple a 1-d lunar thermal model [2] to a 3-d surface [3], including a digital elevation model (DEM) and a statistical rough surface model, in order to accurately represent complex temperature distributions over a wide range of spatial scales. Thermal imaging data collected from the surface of an airless body will show a strong angular dependence of the emitted energy due to roughness [4,5]. Thus, measurements of the emitted infrared radiation field at multiple wavelengths can be used to derive the slope distribution. Slope distributions of natural surfaces can be characterized by the Hurst exponent, H: $s(L) = s_0 \left(\frac{L}{L_0}\right)^{H-1}$. Since H is typically in the range ~0.5 to 1, roughness increases with decreasing spatial scale [6].

Figure 2 shows a simulation at 84° latitude, where the surface temperature distribution is quite broad, with a mode of ~290 K and standard deviation $\sigma \approx 50$ K. L-CIRiS has sufficient accuracy and precision to measure the ~2-4 K brightness temperature differences among its four spectral bands (7 – 14 μm). The 16°-RMS slope used in this model is typical of spatial scales ~10 cm, near the length scale for maximal thermal gradients due to steep slopes and thermal insulation. Figure 2 also shows the dependence of apparent emissivity with azimuth angle, which must be taken into account.

Results: With knowledge of the Hurst exponent of the lunar surface [7], we can accurately model the contributions of rough surfaces at all relevant scales (meters to centimeters) to the IR emission phase function. Each surface facet of the DEM can be represented by a statistical rough surface unresolved by the detector. This forward model is then coupled to the instrument camera model, in order to simulate the L-CIRiS multispectral thermal infrared image data.

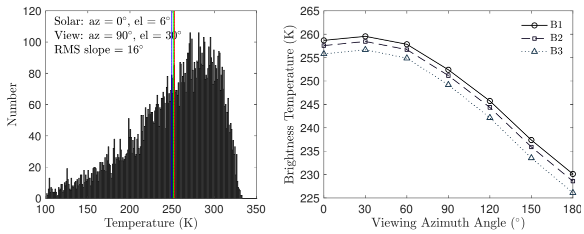

Figure 2: (Left) Temperature distribution of a surface with RMS slope of 16° at 84° latitude. The R, G, B vertical lines indicate brightness temperatures measured by L-CIRiS bands 3, 2, and 1. (Right) Apparent emissivity as viewed from different azimuth angles with respect to the subsolar point.

Discussion: Recent advances in surface roughness in thermal models [8,9,10] enable instruments like L-CIRiS to provide improved constraints on thermophysical properties of the lunar surface. Equivalently, direct measurement of small-scale temperature variations on the surface of the Moon will enable validation of these thermal models, which can in turn be applied to other airless bodies in the solar system.

References: [1] https://www.nasa.gov/press-release/nasa-selects-new-instruments-for-priority-artemis-science-on-moon [2] Hayne et al. (2017), *JGR*, *122*. [3] Hayne et al. (2021), *Nat. Astron.*, *5*. [4] Shimaki et al. (2020), *Icarus*, *348*. [5] Müller et al. (2021), *A&A*, *650*. [6] Helfenstein and Shepard (1999), *Icarus*, *141*. [7] Rosenburg et al. (2011), *JGR*, *116*. [8] Rubanenko and Aharonson (2017), *Icarus*, *296*. [9] Rozitis (2017), *MNRAS*, *464*. [10] Davidsson and Hosseini (2021), *MNRAS*, *506*.

Acknowledgments: This work was partially supported by the NASA Lunar Reconnaissance Orbiter project. Part of this work was performed at the Jet Propulsion Laboratory, California Institute of Technology, under contract with the National Aeronautics and Space Administration.

SESSION 4

Thermal Modeling of Rocky Planets.

Sixteen Years of Mars Surface Temperature Observations by the Mars Climate Sounder onboard the Mars Reconnaissance Orbiter

Sylvain Piqueux[1], David M. Kass[1], Armin Kleinböhl[1], Marek Slipski[1], Paul O. Hayne[2], Daniel J. McCleese[3,4], and John T. Schofield[1,4]

[1]Jet Propulsion Laboratory, California Institute of Technology, sylvain.piqueux@jpl.nasa.gov, [2]University of Colorado Boulder, paul.hayne@lasp.colorado.edu, [3]Muon Space, mccleese@gmail.com, [4]Retired.

Introduction: The Mars Climate Sounder (MCS [1]) onboard Mars Reconnaissance Orbiter (MRO) is a nine-channel visible and thermal infrared radiometer measuring atmospheric and surface radiances at approximately two local times (i.e., 3AM and 3PM). Millions of surface temperature observations have been acquired either through standard operation, or as part of dedicated campaigns. They have been analyzed for volatile cycle characterization and inventory at all latitudes, and to constrain the physical properties of the surface layer.

Volatile Cycles and Inventory: CO_2 ice is unambiguously identified on Mars from surface temperature observations (~150 K, depending on pressure). MCS has revealed the presence of large regions experiencing temperatures consistent with the presence of diurnal CO_2 frost [2], at all latitudes (Fig 1.), with important implications for the state of the surficial regolith [3].

At high latitudes, tracking the edges of the seasonal CO_2 caps with temperature data over 8 Mars years has shown a remarkable repeatability in an otherwise variable environment, with just modest changes after the occurrence of occasional global dust storms (GDS) [4].

Leveraging the unique thermophysical properties of H_2O ice, MCS observations have been used to map the depth to the water ice table [5] down to mid-latitudes. This information is important to constrain recent climates and plan for future crewed exploration.

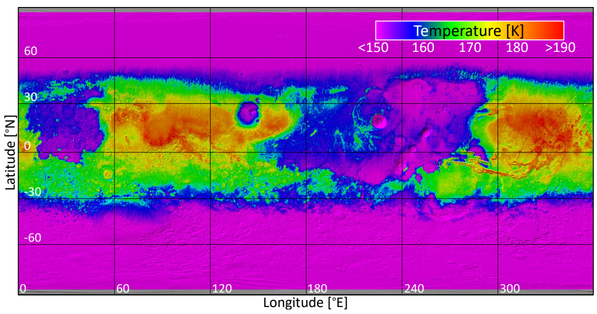

Figure 1: Minimum 3AM surface temperature over the course the MRO mission. Temperatures < 150 K correspond to CO_2 frosted terrains.

Regolith Physical Properties: Thanks to its global coverage and medium spatial resolution (~7 km), the MCS dataset is ideal to constrain the physical properties of the surficial regolith, and identify changes. At low and mid- latitudes, interannual temperature observations are used to identify changes in surface dust dis

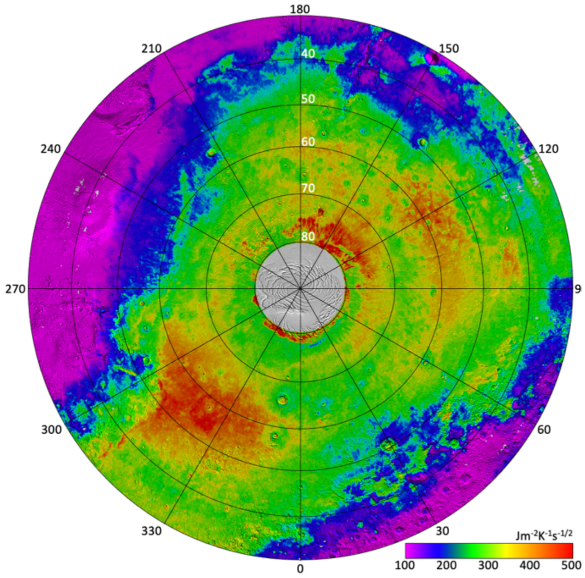

Figure 2: MCS-derived northern hemisphere thermal inertia map of the topmost dry regolith layer corrected for the apparent effect of the underlying water ice table.

-tribution, and map dust source/sink regions in relation to GDS [6]. Closer to the poles, MCS observations have been used to map the thermal inertia of the top regolith layer on top of the water ice, Fig. 2 [5]. Knowledge of the corresponding regolith properties is crucial to model the underlying ice stability, age, and prepare for future crews' engineering needs [7].

Conclusion: MCS is generating a rich open surface temperature dataset acquired at multiple wavelengths, local times and seasons. Its analysis has led to global scale processes characterization and discoveries, addressing important science questions and engineering needs in preparation of future exploration.

References: [1] McCleese *et al.*, JGR. **112** (2007); [2] Piqueux *et al.*, JGR. **121**, 1174 (2016); [3] Lange *et al.*, JGR. **127**, 25 (2022); [4] Piqueux *et al.*, Icarus **251**, 164 (2015); [5] Piqueux *et al.*, GRL **46**, 24 (2019); [6] Bapst *et al.*, **127** (2022); [7] Beaty *et al.*, in *Sixth Mars Pol. Sci. Conf.* (2016), # 6059.

Acknowledgments: This work was performed at the Jet Propulsion Laboratory, California Institute of Technology under a contract with NASA (80NM0018-D0004). US government support acknowledged.

Mars' polar paleoclimate as revealed through thermophysical modeling of trough migration.

K. L. Laferriere*[1], A. M. Bramson[1], K. Izquierdo[1], T. McClintock[2]
[1]Department of Earth, Atmospheric, and Planetary Sciences, Purdue University, West Lafayette, IN, [2]Cerebral Inc., San Francisco, CA, *(klaferri@purdue.edu)

Introduction: Mars' north polar region is covered by a kilometers thick water ice cap. A notable feature of this ice cap is a series ofdepressions that spiral outwards from the pole, referred to as the polar spiral troughs. Mars' north polar spiral troughs migrate poleward due to ablation from the trough wall and stratigraphically upwards due to deposition of water ice. This migration is recorded in the subsurface as unconformities detectable in radar sounding data, referred to as trough migration paths (TMPs) [1]. These TMPs provide information on local and cap-wide processes such as ablation and deposition rates [2], therefore providing a record of the past few million years of volatile mass balance, which can reveal new insights into Mars' paleoclimate.

We model the TMPs using a phenomenological model which considers horizontal retreat and vertical accumulation of ice [2]. Using a Markov chain Monte Carlo (McMC) approach, we can determine the best fit models that recreate the observed TMPs, exploring different scaling dependencies between volatile mass balance and parameters like solar insolation or Mars' obliquity [3]. The rate at which the trough wall retreats poleward is directly tied to sublimation, which can be interpreted using a 1D Crank-Nicholson thermal model to determine temperatures and sublimation rates, considering the affect of an insulating lag overlying the ice [2].

Methods: We use two modeling methods to understand the volatile mass state across time at the northern polar spiral troughs. Our phenomological model creates synthetic TMPs to determine the most likely accumulation and retreat rates given a mapped TMP. The thermal model provides insight into the conditions that lead to those retreat rates (including a lag deposit of variable thickness) at these locations. The mapped TMPs come from Mars Reconnaissance Orbiter (MRO) Shallow Radar (SHARAD) data [1–4].

We run an example McMC fit for 500,000 iterations using models for both accumulation and retreat that are quadratically dependent upon obliquity. For this initial run, we limit the maximum retreat rate to 20 mm/yr and the maximum accumulation to 10 mm/yr (~10x Levrard [6]). With our thermal model, we explore the conditions which would allow for the retreat rates from the McMC.

Our semi-implicit 1D thermal model [2] incorporates the effects of lag thickness, slope and orientation of the trough wall, Mars' axial and orbital parameters [5], and atmospheric characteristics. We consider re-radiation from surrounding flat icy terrains [7, 8]. We allow for the development of a seasonal CO_2 frost cover. This model is run across a Mars year, calculating surface and subsurface temperatures to determine the sublimation rate of the ice (Figure 1).

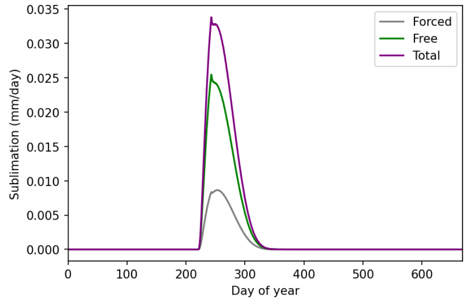

Figure 1: Sublimation rates across a Mars year from thermal model for lag-free surface.

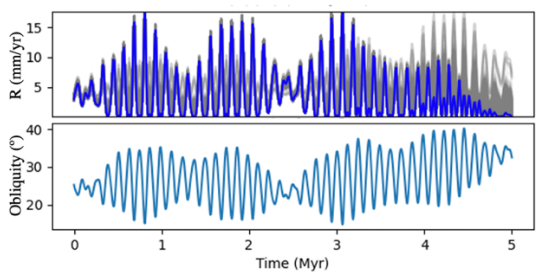

Figure 2: Preliminary run of a quadratic-quadratic model dependent on obliquity. Best fit retreat rate shown in dark blue, other iterations in gray.

Preliminary Results: We find that the retreat rates of the best fit McMC run (Figure 2) are very high and exceed the sublimation expected of a lag-free slope. These high retreat rates result in young troughs ~220 kyrs old and accumulation rates significantly above those of [6], suggesting periods of low-to-no sublimation are important in order to match ages and accumulatin rates currently proposed in the literature.

Conclusion: We will expand our model, explore other candidate dependencies, and apply this model to TMPs mapped in the 3D dataset, to explore variability in migration across individual troughs and regions [4].

References: [1] Smith, I. B. & Holt, J. W. (2015) JGR Planets, 120, 362-387. [2] Bramson A. M. et al. (2019) JGR Planets, 124,1020–1043. [3] Izquierdo, K. et al. (2023), *in prep*. [4] Laferriere, K. L et al. (2023), *in prep*. [5] Laskar, J. et al. (2004) Icarus, 170, 343-364. [6] Levrard, B. et al. (2007), JGR Planets, 112. [7] Kieffer, H. H. (1990), JGR, 95, 1481-1493. [8] Pathare A. V. & Paige D. A. (2005), Icarus, 174, 419-443.

Acknowledgments: This work is supported by a NASA MDAP under grant number 80NSSC20K0935. The 3D Planum Boreum dataset can be accessed at https://sharad.psi.edu/3D/. The authors thank SeisWare, Inc. for access to the interpretation software.

HOW DOES SMALL-SCALE ROUGHNESS INFLUENCE THERMAL INFRARED SPECTRA AROUND MERCURY's NORTH POLE? Kay Wohlfarth[1], Moritz Tenthoff[1], Christian Wöhler[1]
[1]Image Analysis Group, TU Dortmund University, Otto-Hahn-Str. 4, 44227 Dortmund

Introduction: Mercury is believed to host water ice in permanently shadowed regions around the North- and the South Pole [1, 2]. The polar thermal regime is crucial to understand the environment under which these ices form and sustain. Current thermal models such as [3] and [4] consider the equilibrium temperature and focus on self-heating effects and indirect illumination due to local topography. In this study, we focus not on the permanently shadowed regions but on the visible areas around them. We simulate the effect of surface roughness on the spectral shape in high-latitude regions on Mercury. We find that surface roughness leads to substantial deviations in the thermal infrared spectra compared to an equilibrium model. This effect has implications for the analysis of the polar thermal environment with infrared detectors and, ultimately, for the analysis of water ice stability. The simulation effects may be tested with MERTIS [5] and, similarly, with Diviner [6] on the Moon.

Simulation: We use our thermal roughness model [7,8] that extends [9,10]. We take the terrain model of [11] and place the subsolar point at 60°E and 0°N. A hypothetical detector observes the Northpole from above. The solar distance is fixed to the average solar distance of Mercury at 0.38 AU. We assume a surface roughness of Mercury of θ = 20°, similar to [12].

Results:. Figure 1 shows the simulated thermal radiance at 8 µm for latitudes >80° N at Mercury. We plot the spectrum of the rough thermal model (red) and the smooth thermal model (black) of Prokoviev's crater wall (Figure 2) and crater floor (Figure 3). In both cases, the rough model spectra deviate from the equilibrium model. In terms of brightness temperature, the rough model appears 10.9 K colder than the smooth model spectrum at the wall and 18.6 K hotter at the floor, computed at 8 µm. For other wavelengths, the effect is even stronger. Given these results, we recommend to include small-scale roughness in any thermal analysis of polar regions of Mercury (and the Moon).

References: [1] Harmon and Slade (1992), Science, 258,640-643. [2] Chabot et al. (2018), Chapter 13 in: Mercury - The View after Messenger, Cambridge, 2018. [3] Paige et al. (2013), Science, 339,300-303. [4] Potter et al. (2023), arXiv:2209.07632. [5] Hiesinger et al. (2020), Space Sci.Rev. 216, 110. [6] Paige et al. (2010), Space. Sci. Rev. 150,125-160. [7] Wohlfarth et al. (2023), A & A, under review. [8] Wohlfarth et al. (2023), this conference. [9] Rozitis, B. and Green, S. F. (2011) MNRAS 415(3), 2042-2062. [10] Davidsson, B.J. et al. (2015) Icarus, 252,1-21. [11] Bertone et al. (2023), Planetary Sci. J., 4:21. [12] Emery et al. (1998), Icarus, 136,104-123.

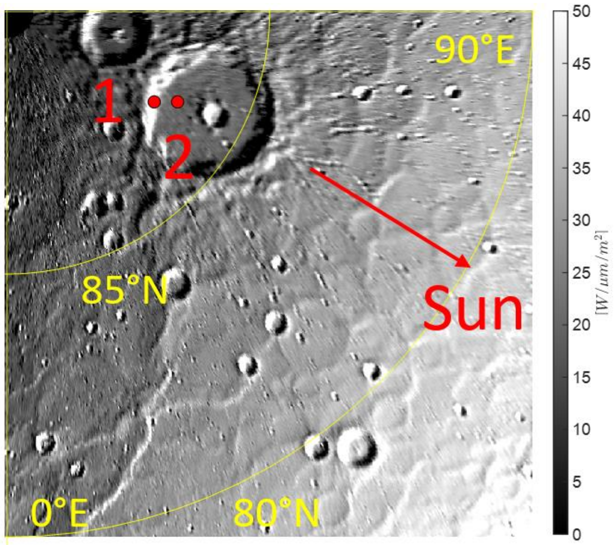

Figure 1: Thermally emitted radiance [W/µm/m²] at Mercury's north pole (latitude > 80°N). The Sun comes from 0°N, 60°E. We display the spectra at position 1 in Figure 2 and at position 2 in Figure 3.

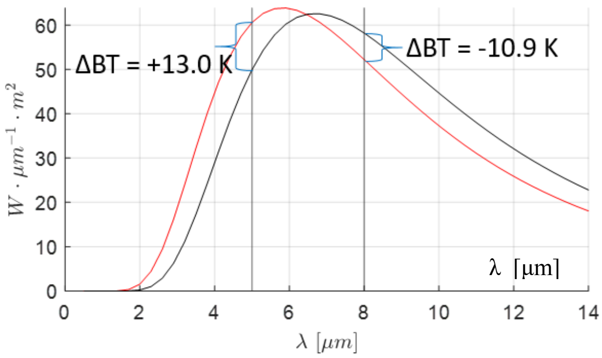

Figure 2: Spectral radiance [W/µm/m²] of the rough model (red) and the equilibrium model (black) at Prokofiev's crater wall (1). Note the strong deviation.

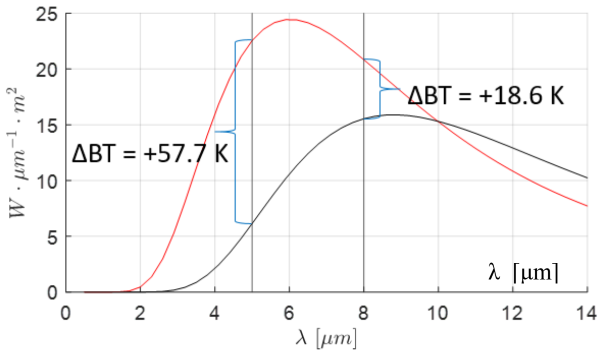

Figure 3: Spectral radiance [W/µm/m²] of the rough model (red) and the equilibrium model (black) at Prokofiev's crater floor (2). Note the strong deviation.

A NOVEL MODEL FOR THE INTERROGATION OF THERMAL INERTIA ON EARTH. A. Koeppel[1], C. S. Edwards[1], L.A. Edgar[2], A. Gullikson[2], K. Bennett[2], S. Piqueux[3], S. Nowicki[4], H. Eifert[1], A.D. Rogers[5], B. Carr[6]. [1]Northern Arizona University (akoeppel@nau.edu), [2]USGS Astrogeology Science Center, [3]Jet Propulsion Laboratory, [4]University of New Mexico, [5]Stony Brook University, [6]University of Arizona

Introduction: Surface thermal inertia derived from satellite imagery offers a uniquely valuable tool for remotely mapping the physical structure and volatile abundance of planetary soils, sediment, and regolith. Efforts to quantify thermal inertia using surface temperatures on Earth, however, have consistently yielded large uncertainties [1–4], and ground-truth observations are lacking. Unlike dry airless bodies, Earth's abundant water and dense atmosphere lead to dynamic thermal conditions that are a greater challenge to model than on a world like Mars [5].

In this work, we developed an approach using field experiments to inform and fine-tune a thermophysical model of terrestrial sediment and calculate thermal inertia on Earth with higher precision than has previously been achieved remotely. Ultimately, we aim to use data from analog sites to develop better interpretations of sediments on Mars, and an accurate thermal model for Earth is the key step to enable translation between the two worlds.

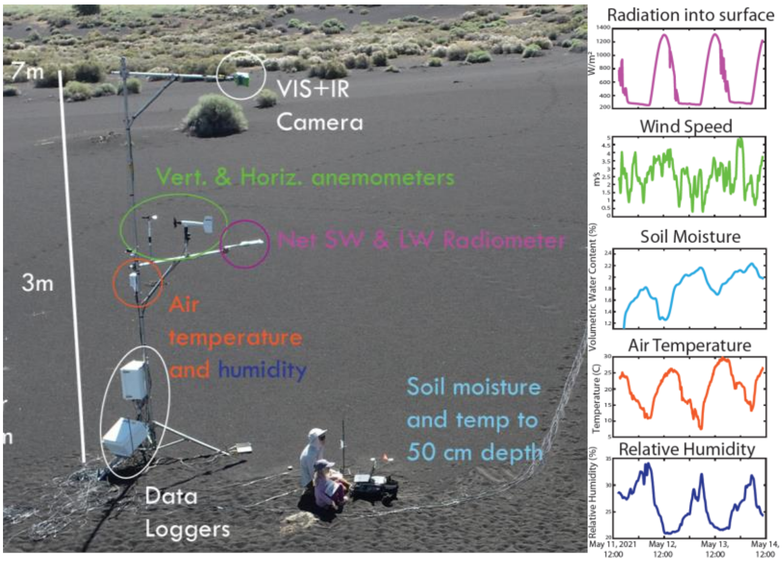

***Figure 1**. Weather station setup at eolian san sheet at Woodhouse Mesa, AZ and a subset of data collected over three days.*

Methods: We completed eight field campaigns to Mars-analog sites around the U.S. Southwest, Kīlauea, HI, and Breiðamerkurjökull, Iceland to study the controls on diurnal temperature curves in basaltic sedimentary deposits. At each site, we deployed a weather station (Fig. 1) designed to constrain the surface energy flux at one minute intervals.

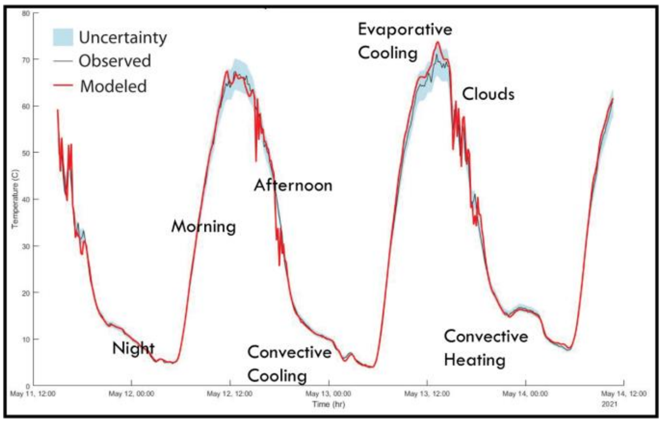

***Figure 2.** Example surface temperature fit and notable energy flux events from model.*

We selected a diverse suite environments (including fluviolacustrine, active eolian sand dune, glacial outwash plain, and volcanic terrains) to generate a robust dataset for model training. The model, in turn, fits thermal conductivity and other sediment physical properties from observed temperature data (Fig. 2).

Conclusions: We tested multiple mixing models [6–8] and modes of temperature-dependency [5,9,10] for the effect of water and pore geometries on thermal conductivity and evaporation. We found that consideration of nonlinear temperature controls on thermal conductivity and evaporation are key and influenced by porosity and grain shape. We validated the model by also capturing *in situ* thermophysical probe measurements and by revisiting and reproducing results at one of the field sites.

References: [1] Price, J. (1977) *JGR* [2] Scheidt, S. *et al.* (2010) *JGR* [3] Lu, S. *et al.* (2009) *AFM* [4] Wang, J. *et al.* (2010) *GRL* [5] Piqueux, S. & Christensen, P. (2009) *JGR* [6] Lu, N. & Dong, Y. (2015) *JGGE* [7] Zhang, N. *et al.* (2017) *Acta Geotech.* [8] Côté, J. & Konrad, J.M. (2005) *Can. Geotech. J.* [9] Lee, T.J. & Pielke, R.A. (1992) *JAM* [10] Tsilingiris, P.T. (2008) *ECM.*

Acknowledgements:

This work was supported by the NASA FINESST (19-PLANET20-0138) and PSTAR (17-PSTAR17_2-0044) programs.

THERMAL MODEL OF ROCKY PLANETS: ESTIMATION OF MAGNETIC DIFFUSION TIME SCALES

K. M. Hiremath[1]
[1] Indian Institute of Astrophysics, Bengaluru-560034, India; E-mail:hiremath@iiap.res.in

Abstract: From the information of hydrostatic equilibrium and with the estimated surface radius, mass and density, average central pressure at the core is estimated. With a simple equation of state and with composition of Iron and Nickel for the core masses > 1.0 Earth masses and Iron and Sulfur for the Earth masse < 1.0, core average temperature is estimated. For the Earth and Mercury, estimated core temperatures are almost similar to the temperatures as quoted in the literature. From the Wiedemann-Franz law and with the assumption of similar thermal conductivity as in the Earths core, magnetic diffusivity of the planetary cores are estimated.

SESSION 5

New Observations and New Instruments.

THERMAL IMAGING OF ASTEROIDS IN HAYABUSA2, HERA, AND FUTURE MISSIONS

Tatsuaki Okada[1,2], Satoshi Tanaka[1], Naoya Sakatani[1], Yuri Shimaki[1], Takehiko Arai[3], Hiroki Senshu[4], Hirohide Demura[5], Tomohiko Sekiguchi[6], Toru Kouyama[7], Masanori Kanamaru[2], Takuya Ishizaki[1],
[1]Institute of Space and Astronautical Science (ISAS), JAXA, Sagamihara, Japan (okada@planeta.sci.isas.jaxa.jp), [2]The University of Tokyo, Tokyo, Japan, [3]Maebashi Institute of Technology, Gunma, Japan, [4]Chiba Institute of Technology, Narashino, Japan, [5]The University of Aizu, Fukushima, Japan, [6]Hokkaido University of Education, Asahikawa, Japan, [7]National Institute of Advanced Industrial Science and Technology (AIST), Tokyo, Japan

Introduction: Thermal infrared imaging is a useful method to investigate thermophysical properties and composition of the surface of asteroids. Instruments and their science cases with the observation scenarios are briefly described.

Thermal Imager TIR on Hayabusa2: An infrared imager TIR is one of the remote sensing instruments onboard the JAXA Hayabusa2 mission, which was launched in 2014, rendezvoused with and observed the near-Earth C-type asteroid 162173 Ryugu during 2018 to 2019, and returned the surface materials to Earth in 2020. The mission is now extended (it is called as Hayabusa2#) to observe a rare type (L-type) near-Earth asteroid 2001CC21 during its flyby in 2026, and visit a very small (~30m diameter) asteroid 1998KY26 in 2031 [1]. TIR is a thermal infrared imager based on an uncooled bolometer array of 328 x 248 effective pixels, with a 16.7° x 12.7° field of view, covering the wavelength of 8-12 μm [2].

The single band thermographic imager has been proven to be useful for global mapping of the thermal inertia of the surface of Ryugu, when the spacecraft was kept at the home position, 20 km from Ryugu, to observe the asteroid for one rotation. It was the first time to take thermal images of an asteroid for one rotation, estimate the thermal inertia of its global average of Ryugu at 200-400 J kg^{-1} m^{-2} s$^{-0.5}$ (hereafter, tiu), and discover that the boulders have the almost the same thermal inertia as the surrounding, regolith and lower than that of typical carbonaceous chondrite meteorites [3]. The observed diurnal temperature profile indicated the existence of severe surface roughness, so that the surface microscopic roughness model is introduced [4] and applied for simultaneous determination of thermal inertia and roughness [5].

Therma imaging is also found useful to estimate thermal inertia of local crops like individual boulders during up-close imaging, for example, to find very cold boulders (Cold Spots) [3] as well as very hot boulders (Hot Spots) [6]. Shadows of the spacecraft where rapid cooling were observed are also used for the determination of thermal inertia of small rocks and boulders down to the scale of several centimeters. These thermal inertias could be compared with those of the laboratory measurements for meteorites and returned samples [7], and discussed about the internal textures of rocks (micro pores and cracks), considering their possible origin and evolution [8].

Therefore, even the flyby of the L-type asteroid 2001CC21 will bring us new insight, although it will be observed with the diameter of several pixels. It will be comparable with the data of Ryugu of similar pixel size, obtained during the approach to Ryugu. The small asteroid 1998KY26 will become the smallest asteroid ever visited by a spacecraft and investigated in detail whether such a small-sized asteroid is a monolithic or a rubble-pile body, and what is the average and variation of thermophysical properties, which is related to its origin and evolution process.

Thermal Imager on Hera and Future Missions: An infrared imager TIRI is now preparing for the ESA Hera mission to the near-Earth S-type asteroid binary 65803 Didymos and its moon Dimorphos, which will be launched in 2024 and rendezvous with the asteroid binary in 2027 for a half year observation [9], and the asteroid binary were imaged just before the kinetic impact to Dimorphos by the NASA DART spacecraft.

TIRI is based on an uncooled bolometer array of 1024 x 768 pixels, with 13.3° x 10.0° field of view, covering the wavelength of 8-14 μm for the wide band, as well as six narrow bands within 7-14 μm [10]. The observations will start at 20-30 km distance from the asteroid at large solar phase angles, and then, at nearer distances down to c.a. 1 km or so. The final sequence could be landing onto the surface of the asteroid. The shadow by the eclipse of Dimorphos will be observed. Therefore, the similar observations for global mapping and up-close imaging will be planned and the similar data sets will be expected to be obtained during the mission. Information on the surface composition will be additionally obtained in the Hera mission.

This instrument would be good to be used in the other future missions for asteroid flyby and rendezvous for the investigation of thermophysical properties and the constituent materials of the surface of asteroids.

References:

[1] Hirabayashi, M. et al. (2021) ASR 68, 1533.
[2] Okada, T. et al. (2017) SSR 208, 255.
[3] Okada, T. et al. (2020) Nature 579, 518.
[4] Senshu, H. et al. (2022) IJT 43, 102.
[5] Shimaki, Y. et al. (2020) Icarus 113835.
[6] Sakatani, N. et al. (2021) Nature Astron. 5, 766.
[7] Ishizaki, T. et al. (2023) IJT, accepted.
[8] Okada, T. et al. (2022) EPSC, #1187
[9] Michel, P. et al. (2022) PSJ 3, 160.
[10] Okada, T. et al. (2022) LPSC 2022, #1319.

MIRMIS – The Modular Infrared Molecules and Ices Sensor for ESA's Comet Interceptor.

N. Bowles[1], A. Näsilä[2], T. Kohout[3], G. L. Villanueva[4], C. Howe[5], K. L. Donaldson Hanna[6], B. T. Greenhagen[7], P. G. J. Irwin[1], S. B. Calcutt[1], R. Evans[1], K. Shirley[1], T. Warren[1], A. Akujärvi[2], A. Penttilä[3], A Kokka, S. Faggi [4,8],, S. Protopapa[9], K. Nowicki[1], D. Korda [3], H. Eshbaugh[1], R. Cole[2], A, Vitkova [1], M. Rashman[1] A. Guilbert-Lepoutre[9] and the Comet Interceptor team.

[1]Department of Physics, University of Oxford (neil.bowles@physics.ox.ac.uk), UK [2]VTT Finland [3]University of Helsinki, Finland [4]NASA Goddard Space Flight Center, [5]STFC RAL Space, UK,[6]Dept. Physics, Univ. Central Florida, USA, USA,[7]John Hopkins Applied Physics Laboratory, USA ,[8]American University Washington DC, [9]CNRS/University of Lyon, [9]South West Research Institute

Introduction: This presentation will describe the Modular Infrared Molecules and Ices Sensor currently being built at the University of Oxford, UK and VTT Finland for ESA's upcoming Comet interceptor mission.

The Comet Interceptor mission: The Comet Interceptor mission was selected by ESA as the first of its new "F" class of missions in June 2019 and adopted in June 2022. Comet Interceptor (CI) aims to be the first mission to visit a long period comet, preferably, a Dynamically New Comet (DNC), a subset of long-period comets that originate in the Oort cloud and may preserve some of the most primitive material from early in our Solar System's history. CI is scheduled to launch to the Earth-Sun L2 point with ESA's ARIEL [2] mission in ~2029 where it will wait for a suitable DNC target.

The CI mission is comprised of three spacecraft. Spacecraft A will pass by the target nucleus at a distance of ~1000 km to mitigate against hazards caused by dust due to the wide range of possible encounter velocities (e.g. 10 – 70 km/s). As well as acting as a science platform, Spacecraft A will deploy and provide a communications hub for two smaller spacecrafts, B1 (supplied by the Japanese space agency JAXA) and B2 that will perform closer approaches to the nucleus. Spacecrafts B1 and B2 will make higher risk/higher return measurements but with the increased probability that they will not survive the whole encounter.

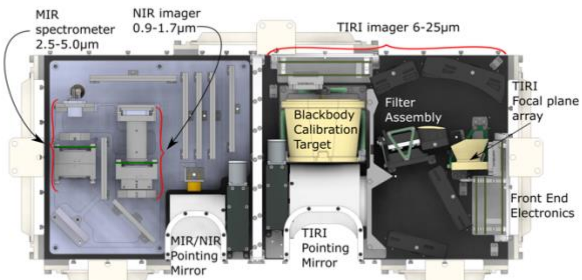

Figure 1: The MIRMIS instrument for ESA's Comet Interceptor mission.

The MIRMIS Instrument: The Modular InfraRed Molecules and Ices sensor (MIRMIS, Figure 1) instrument is part of the CI Spacecraft A scientific payload. The MIRMIS consortium includes hardware contributions from Finland (VTT Finland) and the UK (University of Oxford) with members of the instrument team from the Universities of Helsinki, Lyon, NASA's Goddard Space Flight Center, and South West Research Institute.

MIRMIS will map the spatial distribution of temperatures, ices, minerals and gases in the nucleus and coma of the comet using covering a spectral range of 0.9 to 25 microns. An imaging Fabry-Perot interferometer will provide maps of composition at a scale of ~180 m at closest approach from 0.9 to 1.7 microns. A Fabry-Perot point spectrometer will make observations of the coma and nucleus at wavelengths from 2.5 to 5 microns and finally a thermal imager will map the temperature and composition of the nucleus at a spatial resolution of 260 m using a series of multi-spectral filters from 6 to 25 microns.

The MIRMIS instrument is compact (548.5 x 282.0 x 126.8 mm) and low mass (<8.8 kg) and has single mechanical and electrical interface to the spacecraft, making the design also suitable for remote sensing mission from small satellites in LEO or other targets in the Solar System.

The Thermal Infrared Imager (TIRI). MIRMIS' multi-spectral thermal infrared imager has an integrated blackbody calibration target and pointing mirror. TIRI has eight narrow band filters for silicate and ice composition mapping (Figure 2) and a broad band (~7-25 μm) thermal imaging filter to map the temperature of the nucleus during closest approach.

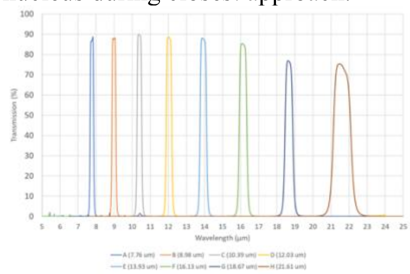

Figure 2: TIRI narrow band filters

References:

[1] Snodgrass and Jones, 2019, Nature Comms. 10, 5418. [2] Tinetti et al. 2018, Exp. Astron. 46, 135-209.

Acknowledgments: Thanks to ESA's Comet Interceptor mission team, the UK Space Agency for funding the UK contributions to the instrument.

LRAD – THE RADIOMETER FOR THE LUNAR SOUTH POLE HOPPER µNOVA.

M. Hamm[1,2], M. Grott[1], J. Knollenberg[1], M.S. Robinson[3], M. Atwell[4], K. Mabe[4], T. Martin[4], H. Rauer[1,2]
[1]German Aerospace Center (DLR) (Maximilian.Hamm@dlr.de), Berlin, Germany, [2]Free University Berlin, Germany. [3]School of Earth and Space Exploration, Arizona State University, Tempe, AZ, USA, [4]Intuitive Machines, 3700 Bay Area Blvd, Suite 600, Houston, TX 77058

Introduction: Permanently shadowed regions (PSRs) are present at the Lunar poles. The surface temperature inside a PSR can remain below 110K, low enough fow stable water ice to exist in vacuum. The presence of water ice at the Lunar Poles has been indicated by remote sensing observations, in particular by the Lunar Prospector, LCROSS, and LRO missions [1-5]. As part of the NASA Commerical Lunar Payload Service program, the Nova-C lander will be build and operated by the US-based company Intuitive Machines. Nova-C will land near the Lunar south pole for in-situ inverstigations of potential volatiles in the regolith [6]. Nova-C will carry the S.P. Hopper to the Moon which will in a sequence of short flights land within a PSR inside Marston crater (informal name) close to a potential landing site for the Artemis Astronauts [7]. The Hopper will map the lunar surface with two cameras and a themal infrared radiometer (LRAD).

The LRAD Instrument: The Lunar Radiometer (LRAD) uses thermopile sensors to measure net radiative flux in the thermal infrared wavelength range [8]. The LRAD sensor head carries six thermopile sensors, equipped with individual IR-filters to fulfill specific scientific measurement goals:

1. Determination of surface brightness temperature in the illuminated and shadowed terrain .
2. Derivation of thermal inertia
3. Derivation of the mm to cm-scale surface roughness.

The instrument design is based on the miniRAD radiometer of the Martian Moons Explorer's (MMX) rover [9].

Surface Brightness Temperature Determination: The primary goal of the LRAD instrument is the first in-situ measurement of the brightness temperatures within a PSR. The main challenge for a precise temperature measurement is the small flux emitted by the surface for the predicted temperatures which could be below 100 K [10]. To this end, the LRAD sensor head temperature is stabilized to the mK level, minimizing disturbances from instrument self-radiation. A closed sensor will help to estimate residual disturbances caused by self-radiation. Furthermore, the instrument is thermally decoupled from the environment as much as possible. A large field of view of 40° (FWHM) maximizes the collected signal. LRAD uses two longpass filters opening at a wavelength of 15µm and designed to measure low temperatures independently, allowing for a precise uncertainty estimate. A longpass filter opening at 10µm, will be used to measure the higher temperatures outside the PSR.

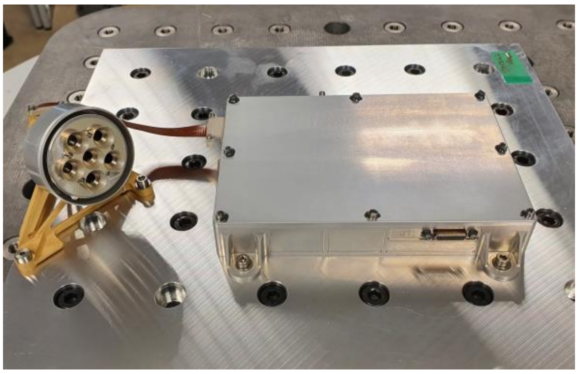

Figure 1: *The LRAD instrument undergoing vibrational testing with sensor head mounted on a thermally isolating bracket (left), and the avionics box (right.)*

Roughness and Thermal Inertia Derivation: LRAD carries two narrow band filters centered around 9 µm and 12 µm. Comparing fluxes observed in these filters to each other and the longpasses filters will allow for the determination of small-scale roughness in illuminated regolith outside the PSR. Observing the variation of temperature with varying insolation angle will allow for the determination of thermal inertia of the regolith.

Conclusion: LRAD will measure the brightness temperature of regolith at the Lunar southpole and within a PSR, providing in-situ measurements for understanding the regolith in a potential landing site for the Artemis Astronauts.

References:

[1] Feldman, W.C., et al. (1998) *Science*, 281, 5382, 1496-1500
[2] Colaprete, A., et al. (2010) *Science*, 330, 6003, 463-468
[3] Hayne, P.O., et al. (2015) *Icarus*, 255, 58-69
[4] Rubanenko, L. et al., (2019) *Nat. Geosci*,12, 597-601
[5] Hayne, P. O., et al. (2021). *Nat. Astr.*, 5, 169
[6] Voosen, P., et al., (2021). *Science,* 373, 6560, 1188-1192
[7] Martin, T., et al., (2022). *LPSC 2022*, 2007
[8] Grott, M., et al., (2017). *Space Sci Rev.*, 208, 413
[9] Ulamec, S., et al., (2021). *72nd IAC,* IAC-21-A3.4A.7
[10] Paige, D. et al. (2010b). *Science*, 330, 479

Acknowledgements: LRAD is supported by the German Federal Ministry for Economic Affairs and Climate Action on the basis of a decision by the German Bundestag.

A COLD OBJECT RADIOMETER (COBRA) TO EXPLORE THE URANIAN SYSTEM IN THE INFRARED

Elder, C.M.[1], M. Kenyon[1], A. Kleinböhl[1], D. Wenkert[1], W. R. Johnson[1], B. H. Eom[1]
[1]Jet Propulsion Laboratory, California Institute of Technology (celder@jpl.nasa.gov)

Introduction: The decadal survey by the United States' National Academies of Science [1] recently recommended that a mission to Uranus should be the highest priority for NASA's Planetary Science Division in the decade between 2023 and 2032. Here, we focus on infrared observations of the Uranus system which have the potential to answer high priority science questions about ice giant atmospheric structure, the radiative balance of Uranus, the thermophysical properties of satellite surfaces, and possibly the identification of endogenic geologic activity on the satellites.

Science Objectives: The Voyager 2 flyby of Uranus and subsequent ground- and space-based telescopic observations of the system raised many questions. Measurements of Uranus' albedo and thermal emission suggest that it may be in equilibrium with heating by the sun, unlike the other giant planets which emit a significant amount of endogenic heat [2]. However, Voyager instruments were designed for the warmer Jupiter and Saturn resulting in a low signal to noise ratio at Uranus. Voyager observations of clouds revealed zonal circulation in Uranus' atmosphere, but further observations are needed to constrain the overturning of these belt systems in the North-South direction. Infrared observations of icy satellites can be used to constrain thermal inertia which is modified by many processes including impacts of all sizes, bombardment by charged particles, and deposition of plume and ring material [3]. Currently there are no spatially resolved infrared observations of the uranian satellites at multiple times of day, which is required to estimate thermal inertia. Some studies have identified the possible presence of volatiles on the uranian satellites that should not be stable over geologic timescales, which could suggest cryovolcanism [e.g. 4] and endogenic thermal emission. Based on these open questions, we identified the following science objectives, which could be addressed by infrared observations in the Uranus system:

1. Determine the radiative balance of Uranus,
2. Characterize the thermal structure and understand the large-scale circulation in the upper troposphere/lower stratosphere of Uranus,
3. Quantify the thermal inertias and identify possible thermal anomalies on the Uranian satellites

To address these questions, we are developing the Cold Object Radiometer (COBRA), a next-generation radiometer optimized for cold temperatures.

COBRA: COBRA would use passive radiometry at wavelengths from 0.3 to >200 µm. It uses thermopile detector arrays, which provide high sensitivity at cold temperatures without requiring cooling. This technology has flown in Mars Climate Sounter (MCS) [5] on the Mars Reconnaissance Orbiter and the Diviner Lunar Radiometer Experiment (Diviner) [6] on the Lunar Reconnaissance Orbiter. COBRA also uses the state-of-the-art focal plane module from the Polar Radiant Energy in the Far-InfraRed Experiment (PREFIRE). Compared to MCS and Diviner, COBRA will have ~100x more pixels, with ~2x higher sensitivity per pixel, and the instrument will be ~50% less massive. A prototype instrument is being developed through the NASA Maturation of Instruments for Solar System Exploration (MatISSE) program and is expected to reach TRL 6 in 2023.

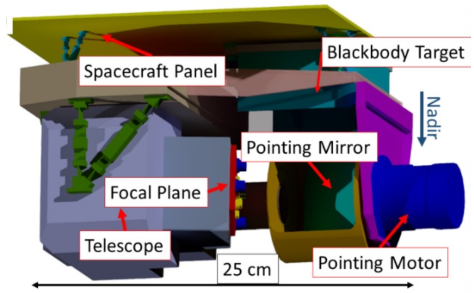

Figure 1: COBRA extends state-of-the-art thermal imaging radiometers' performance to very cold (<50 K) targets in a compact form.

Measurements: COBRA could address our science objectives through the following measurements. Objective 1: Constraining the radiative balance of Uranus requires measurements of both the thermal emission in the far infrared and also reflected sunlight in the UV, visible, and near-infrared wavelengths. Nadir and off-nadir observations using broadband channels would cover reflected sunlight over a wide range of emission and phase angles. Objective 2: Measurements of horizontal temperature contrasts would constrain vertical motions within the atmosphere. Measurements of the ortho- to para-hydrogen ratio and of C_2H_2 would further constrain vertical and lateral motions [7]. Objective 3: Observations of satellites at multiple times of day would allow the derivation of thermal inertia which is related to the physical structure of the shallow subsurface materials. Recently emplaced cryovolcanic materials would remain warm at all times of the day.

References: [1] "Origins, Worlds, and Life" (2022) National Academies Press. [2] Pearl et al. (1990) *Icarus 84,* 12-28. [3] Ferrari (2018) *SSR 214:111.* [4] Cartwright et al. (2020) *AJL 898:L22.* [5] McCleese et al. (2007) JGR 112, E05S06. [6] Paige et al. (2010) SSR 150, 125-160. [7] Roman et al. (2020) *AJ 159*, 45.

The Lunar Trailblazer mission: Understanding the Moon's water

Bowles, Neil[1]; Ehlmann, Bethany[2]; Klima, Rachel[4], Calcutt, Simon[1]; Evans, Rory[1]; Klesh, Andrew[3]; Howe, Chris[5]; Warren, Tristram[1], Shirley, Katherine[1]; Rashman Maisie[1]; Bennett, Lee[2]; Scire, Elena[2]; Fogg, Robert[3]; Furlan, Elise[2]; Llamas, Jake[2]; Seybold Calina[3]; Elkington, Nicholas[1]; Blaney, Diana[3]; Dickson, Jay[2]; Donaldson Hanna, Kerri[7]; Edwards, Christopher[9]; Green, Robert[3]; House, Martha[8]; Pieters, Carle[6]; Thompson, David[3]

[1]Department of Physics, University of Oxford, UK (neil.bowles@physics.ox.ac.uk), [2]California Institute of Technology, US, [3]Jet Propulsion Laboratory, California Institute of Technology, USA, [4]John Hopkins University Applied Physics Laboratory, USA, [5]STFC RAL Space, UK, [6]Brown University, Providence, RI USA, [7]Department of Physics, University of Central Florida, USA, [8]Pasadena City College, USA, [9]Northern Arizona University, USA

Introduction: Lunar Trailblazer is a pioneering NASA SIMPLEx mission to investigate the presence and form of water on the Moon. The mission was selected in June 2019 and will be ready for launch in 2023 as an ESPA Grande class ride-along. This presentation will describe Lunar Trailblazer's science and the status of the mission as the spacecraft and instruments are tested and integrated.

Lunar Trailblazer: Lunar Trailblazer (Figure 1, [1]) targets understanding of the Moon's water: its form (ice, H_2O, or OH), abundance, and distribution as well as the Moon's potential time-varying lunar water cycle. A Lockheed Martin integrated smallsat will carry the JPL High-resolution Volatiles and Minerals Moon Mapper (HVM3) shortwave infrared imaging spectrometer and the UK-contributed, University of Oxford-built Lunar Thermal Mapper (LTM) infrared multispectral imager (Figure 2), which simultaneously measure composition, temperature, and thermophysical properties. From ~100-km polar orbit, Lunar Trailblazer will detect and map water on the lunar surface at key targets with 4 science objectives: (1) determine its form (OH, H_2O or ice), abundance, and local distribution as a function of latitude, soil maturity, and lithology; (2) assess possible time- variation in lunar water on sunlit surfaces; (3) use terrain-scattered light to determine the form and abundance of exposed water in permanently shadowed regions; and (4) understand how local gradients in albedo and surface temperature affect ice and OH/H_2O concentration, including potential identification of new, small cold traps.

Figure 1: The Lunar Trailblazer spacecraft showing the LTM and HVM3 instruments in nadir pointing observation mode (credit Lockheed Martin Space).

This mission provides unprecedented sensitivity for direct detection of lunar water at key targets. HVM3 builds upon the demonstrated ability of M^3 [2] to detect lunar water even in permanently shadowed regions with enhanced spatial and spectral resolution, SNR, and spectral range. LTM has enhanced spectral (15 bands) and spatial resolution (~53 m at 100 km) relative to Diviner. Understanding the lunar water cycle and determining the abundance, local distribution and form of water will support exploration and utilization of the Moon and its resources. Identification and characterization of water and its forms is critical knowledge as lunar exploration moves forward. Reconnaissance of potential landing zones will also be possible.

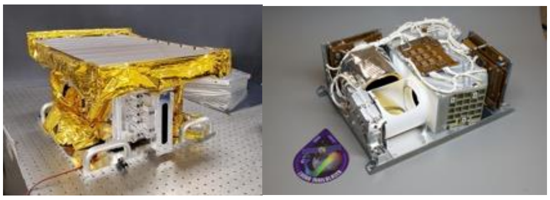

Figure 2: The HVM3 (left, NASA/JPL/Caltech) and LTM (right, Univ. Oxford) instruments prior to delivery to the spacecraft.

Currenthermot status: The HVM3 instrument has been calibrated, delivered and integrated with the Lunar Trailblazer spacecraft in December 2022. The LTM instrument is currently in testing for delivery and integration in February 2023.

References:

[1] B. L. Ehlmann et al., 2022 IEEE Aerospace Conference (AERO), Big Sky, MT, USA, 2022, pp. 1-14, doi: 10.1109/AERO53065.2022.9843663.

[2] C. M. Pieters et al., 2009, Science, Vol. 326, Iss. 5952, pp 568 – 572.

Acknowledgments: The LTM team thanks the UK Space Agency for the support of the instrument.

SMALL SCALE ROUGHNESS OF METEORITIC SAMPLES AND IMPLICATIONS FOR THERMAL RESPONSE OF ROCK RICH SURFACES. Rachael M. Marshal[1], Markus Patzek[1] and Ottaviano Rüsch[1]
[1]Precious Space Research Group, Institut für Planetologie, WWU Münster.

Introduction: The study and investigation of meter and sub-meter scale geological features, especially boulders and boulder fields, on the surface of airless bodies can provide insight into the evolution of the regolith and the contribution of various processes to its formation. Our understanding of the response of boulders to space weathering, micrometeorite abrasion, thermal fatigue, and consequently their evolution into regolith can be improved by characterizing the surface roughness of the uppermost layer of boulders. The lack of a fine-grained regolith cover on many small (<km) bodies further highlight the relevance of boulders [1-2]

In the first phase of our study [3] we characterized the surface roughness of boulder fields photometrically by using the phase ratio methodology applied to orbital image data of the Moon. In general, our results imply that the rock physical properties at the start of the surface exposure period are a function of petrology as well as the (shock) effects imparted upon ejecta rock formation and excavation. These findings warrant a detailed study on the microtexture of rock surfaces.

In the second phase of our study (in-progress) we focus on characterizing the sub-mm scale topography and roughness of naturally fresh surfaces of meteorite samples. The aim of the study is to characterize the surface roughness at the mm and sub mm scale, which is known to influence both the photometric as well as the thermal IR response of boulders [4-5]

Methods: The work-in progress deals with supplementing our aforementioned findings with detailed investigation of the sub-mm scale topography and roughness of meteorite and lunar samples. In order to study the sub-mm scale roughness of these samples we extract surface topography measurements thereby producing high resolution digital terrain models (DTMs) at the ~2 micro-meter scale using a non-contact optical profilometer. The DTMs are then detrended and slope maps are calculated at different downsample extents. An example of the high resolution DTM and slope map of Murchison is shown in figure 1

Results: From the high resolution DTMs we calculate the mean slope with decreasing resolution i.e., increasing spatial extent. This variation in mean slope of the sample surfaces, of different meteoritic types, is shown in figure 2. We find that, in general, carbonaceous chondrites are smoother on the ~2 μm scale when compared to achondrites, with the exception of the NWA 11050 and the Cumberland Falls aubrite. This is further illustrated by the rate of mean slope decrease from 2 μm-30 μm, which is much shallower for the carbonaceous chondrites when compared to achondrites and ordinary chondrites – indicating a decreased presence of large slopes at the smallest i.e., ~2 μm scale that quickly diminish with downsampling- resulting in a relatively constant mean slope in this range.

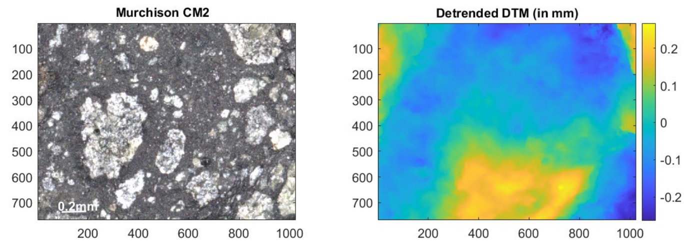

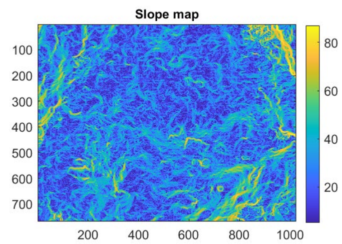

Figure 1:Optical image (a), detrended digital terrain model obtained from the non contact profilometer (b) and the associated slope map with slope in degrees for the Murchison CM2 sample. X and Y are μm steps.

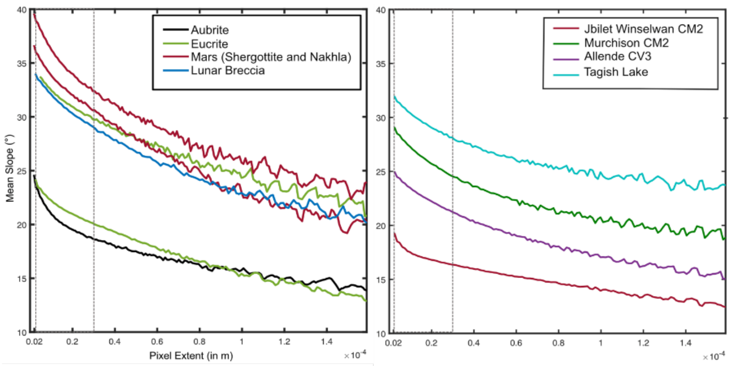

Figure 2: Left and right panels show the mean slope plotted against increasing pixel extent i.e., decreasing resolution of the DTM for achondrites an carbonaceous chondrites respectively.The range taken into account for the calculation of the rate of mean slope decrease is highlighted in dashed lines.

Next, we will further characterise the scale dependent rock micro-texture of various samples, and provide typical values of surface roughness that will in turn inform photometric and thermal modelling of rock surfaces. Aside from the surface roughness comparison between different rock groups, the intra sample heterogeneity will also be considered as well as between chondrite samples of different petrologic type

References: [1] Michikami T. et al.(2010).Icarus, 207(1),277-284. [2] DellaGiustina D. N. et al. (2019). Nat. Astron., 341-351. [3] Marshal, R. M.et al., (2022). Icarus, 115419 [4] Davidsson B.J.et al. (2015). Icarus, 252, 1-21. [5] Shepard M. and Campbell B. (1998). Icarus, 134(2), 279-291.

Acknowledgments: RMM, OR and MP are supported by the Sofja Kovalevskaja award of the Alexander von Humboldt foundation. R. Bartoschewitz is thanked for provided samples for this study.

GROUND-BASED CALIBRATION AND PERFOMANCE TEST OF THERMAL INFRARED MULTIBAND IMAGER (TIRI) ONBOARD HERA MISSION

N. Sakatani[1,*], T. Okada[1], H. Senshu[2], T. Arai[3], H. Demura[4], Y. Shimaki[1], T. Sekiguchi[5], T. Ishizaki[1], M. Kanamaru[6], T. Kouyama[7], and S. Tanaka[1]

[1]Institute of Space and Astronautical Science, Japan Aerospace, Exploration Agency, Japan. [2]Chiba Institute of Technology, Japan. [3]Maebashi Institute of Technology, Japan. [4]University of Aizu, Japan. [5]Hokkaido University of Education, Japan. [6]University of Tokyo, Japan. [7]National Institute of Advanced Industrial Science and Technology, Japan. (* sakatani.naoya@jaxa.jp)

ESA's Hera mission [1] will explore a binary S-type asteroid Didymos. JAXA develops a thermal infrared multi-band imager TIRI. Scientific goal of TIRI is to reveal the thermophysical properties and infrared spectral properties of the S-type asteroid, as well as an artificial crater on its moon Dimorphos formed by the spacecraft impact via DART mission. TIRI consists of an uncooled micro-bolometer array of 1024 x 768 pixels, optics with the field of view of 13.3 x 10.0 degrees, 7 filters including wide bandpass covering 8-14 μm wavelength and 6 narrow bands at 7.8, 8.6, 9.6 10.6, 11.6, and 13.0 μm.

At the moment of this abstract submission, we are under development of the engineering model (EM) of TIRI, and going to perform the calibration test of the EM. We will present the result of the calibration and multi-band performance test using rocks and meteorites.

Fig. 1 is the overview of the experimental apparatus. TIRI is placed on a 2-axis gimbal, which enables us to change the attitude of TIRI inside the vacuum chamber. Heat generation during the operation is designed to be escaped to the cooling plate from the radiator through flat copper braid cables. In front of the TIRI FoV, an IR-transparent Ge window is installed, through which IR targets outside the vacuum chamber can be imaged.

Below is the list of the IR targets we prepared.

- IR collimator
  - ✧ target viewing angle : 0.1 to 2.8 degree
  - ✧ temperature range : -20 to +150 degC
- Blackbody furnace
  - ✧ Area : 178mm x 178mm
  - ✧ Temperature range : 0 to +125 degC
- Low-temperature blackbody plate
  - ✧ Area : 200mm x 200mm
  - ✧ Temperature range : -120 to +20 degC

Only the low-temperature blackbody plate is installed in the vacuum chamber, and others are observed through the Ge window. Using these targets with different temperatures, sizes, and viewing angles, we will evaluate the items below:

- Radiometric calibration
  - ✧ conversion formula from output digital count to target radiance for each pixel
- Size-of-source effect (SSE) correction
  - ✧ The output varies with the target size in FoV even if the target temperature is the same [e.g., 2]
- Instrument temperature correction
- Distortion correction

Furthermore, we will have a plan to carry out the multi-band imaging of collimated radiation from some reference minerals such as rocks, and meteorites. This will allow us to evaluate the performance of TIRI EM.

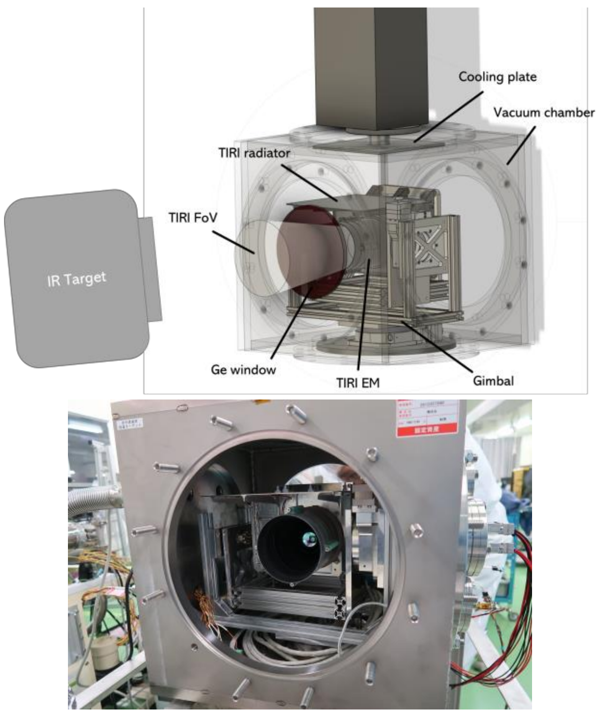

Fig. 1 : Overview of the experimental system.

References:

[1] Michel et al., PSJ 3:160, 2022.
[2] Budzier&Gerlach, J. Sens. Sens. Syst. 10, 179-184, 2021.

Acknowledgments: N.S. is supported by Japan Society for the Promotion of Science (JSPS) KAKENHI (grant nos. JP20K14547).

Deciphering Comets: A Mission Concept for a Cometary Characterization and Observation Apparatus Cubesat (CoCOA-Cube)

Gal Sarid[1], Yanga R. Fernandez[2]
[1]SETI Institute (galahead@gmail.com)
[2]University of Cenrtral Florida (yan@ucf.edu)

Introduction: Comets represent some of the most pristine, observable material remaining from the era of Solar System formation. Since today's comets were once part of the icy planetesimals, comets are vital to our understanding of the chemical and physical properties of our natal protoplanetary disk. However comets have also experienced 4.5 Gyr of various evolutionary processes that have changed their physical and compositional properties.

The census of known comets has greatly expanded in recent years, though their characterization lags behind. Typical data for a given comet is often limited to somewhat sparse photometric information about the dust production rate. Repeated measurements of gas production rates as a function of heliocentric distance – a more fundamental measurement since it is tied to the basic process driving cometary activity in the first place – happen for relatively few comets. This is not to diminish the significant results and insights from extensive surveys of daughter species production (e.g. [1][2][3][4][5]), of organic volatile components (e.g. [6][7]), and of cometary Ly α by Sun-observing facilities (e.g. [8]). Our mission concept envisions a broader observational campaign that could provide synoptic monitoring of parent species among a large number of comets. This would give us additional assessments of ensemble properties as well as provide further constraints that can be folded into mixed and layered thermal models of cometary interior evolution (e.g. [9][10]).

The issue at hand: We are specifically concerned here with addressing the relative lack of simultaneous production rate measurements of two of the most abundant volatile species, H_2O and CO_2. These relative abundances can give cosmogonical clues to comet origins [11], and recent assessments give tantalizing hints of the connectedness of these species (e.g. [12][13]). While water can be measured by proxy through its daughter product OH's fluorescence band near 309 nm, there can be significant atmospheric extinction. CO_2 is an even more challenging species to study since, e.g., the atmosphere is opaque at its asymmetric-stretch (ν_3) vibrational band near 4.26 microns. Thus it is difficult in practice to constrain the total volatile mass loss from comets.

What we propose: We propose a space-based imaging all-sky survey to measure both OH and CO_2 emissions simultaneously by using a 6U CubeSat platform configuration. The survey's science goals would be: (i) find the distribution of CO_2 production rates and abundances relative to water across the whole comet population and across its subgroups; (ii) assess the two species' dependences on each other and on heliocentric distance; (iii) use thermal modeling to interpret CO_2 ice and water ice layering in cometary interiors; (iv) tie modeling results to evolutionary processes.

Basic cubesat and survey properties: We would conduct observations in four narrow bands: a 309 nm band for OH emission, a 4.26 micron band for CO_2 emission, and two nearby bands each just off the main OH or CO_2 band respectively. We will thus be able to distinguish comets from other astronomical sources by their color. Our main instrumentation contribution would be in developing a 3U-length appropriate optical apparatus that can provide imaging in both the near-UV and the near-IR. A low-Earth polar orbit and a wide field of view (~tens of degrees) toward the antisolar direction will maximize the efficiency and feasibility of our planned survey. The telescope optics can be extremely fast, with scales of ~arcmin per pixel, since we are searching for gas comae that are extended sources.

The proposed approach represents an innovative and cost-effective way to greatly advance our knowledge of both the current state of cometary bodies and the relation to natal planetary disk conditions and evolution. We will perform measurements that traditionally require either major spacecrafts, dedicated satellites or combined ground-observing campaigns.

References: [1] A'Hearn, M. F. et al. (1995) Icatus, 118, 223–270. [2] Cochran, A. L. et al. (2012) Icarus, 218, 144–168. [3] Fink, U. (2009) Icarus, 201, 311–334. [4] Schleicher, D. G., Farnham, T. L. (2004) Comets II, 449. [5] Pierce, D. M., Cochran, A. L. (2021) PSJ, 2, 19. [6] Disanti, M. A., Mumma, M. J. (2008) SSRv, 138, 127–145. [7] Dello Russo, N. et al. (2016) Icarus, 278, 301–332. [8] Combi, M. R. (2021) Icarus, 365, 114509. [9] Prialnik, D. et al. (2008) SSRv, 138, 147–164. [10] Sarid, G. et al. (2005) PASP, 117, 796–809. [11] A'Hearn, M. F. (2012) ApJ, 758, 29. [12] Ootsubo, T. et al. (2012) ApJ, 752, 15. [13] Harrington Pinto, O. et al. (2022) PSJ, 3, 247.

Acknowledgments: G. S. acknowledges support by NASA grant 80NSSC18K0497.

SESSION 6

Planetesimal Thermal Evolution.

REVEALING PARENT BODY ACCRETION TIME SCALE FROM MODEL FITS TO METEORITE CHRONOLOGY: THE CASES OF CR-RELATED METEORITES AND NEA RYUGU

Wladimir Neumann[1,2], Audrey Bouvier[3], Mario Trieloff[4]
[1]Technical University Berlin, Institute of Geodesy and Geoinformation Science (wladimir.neumann@tu-berlin.de)
[2]German Aerospace Center (DLR) Berlin, Institute for Planetary Research (wladmir.neumann@dlr.de)
[3]University of Bayreuth, BGI (audrey.bouvier@uni-bayreuth.de)
[4]Heidelberg University, Institute of Earth Sciences (mario.trieloff@geow.uni-heidelberg.de)

Introduction: Accretion processes in protoplanetary disks produce a diversity of small bodies that play a crucial role in potentially multiple reshuffling events and in both early and late accretion of planets. Application of thermo-chronometers to meteorites provides precise dating of the formation or cooling ages of mineralogical components. Nucleosynthetic anomalies that indicate a dichotomy between non-carbonaceous (NC) and carbonaceous (C) meteorites (Fig. 1) and parent body (PB) chronology can be combined with planetesimal thermal evolution models to constrain the timescale of accretion and dynamical processes in the early solar system.[1-8]

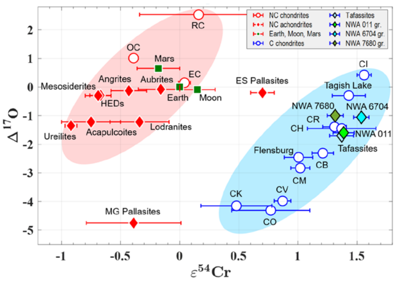

Figure 1: The $\Delta^{17}O$-$\varepsilon^{54}Cr$ systematics of C (blue) and NC (red) materials. Flensburg, CR, Tafassites, NWA 011, NWA 6704, and NWA 7680 plot close to each other, all within the same region of the C field, reflecting a similar accreting material within a confined region further out in the protoplanetary disk (from [9]).

Accretion timescale: Melting and differentiation requires heating that can be provided by ^{26}Al, but only early after the formation of Ca-Al-rich inclusions (CAI).[10,11] Thus, achondrite PBs are considered to have formed early (and mostly in the NC region). By contrast, late accretion in the C region is believed to have produced chondritic objects, such as the CR PB that could have formed as late as 4 Ma after CAIs.[12] However, presence of more evolved CR-like achondrites suggests earlier accretion also in the C reservoir. Observations of C-type NEAs and lab investigations of meteorites indicate a high porosity of C-type asteroids. Ryugu´s material porosity is much higher than for CI and CM groups, [13] indicating, potentially, distinct PB evolution paths. Aqueous alteration of Ryugu, CI, and CM samples suggests accretion times not very different from that of the altered CR PB. The meteorite record provides only weak accretion time estimates from chondrule or mineral phases formation ages, and no information about the PB size. However, thermal evolution and differentiation modeling provides a valuable tool for obtaining more precise constraints on the PB accretion time (and size, internal structure, and burial depths of meteorites) by fitting models to the sample thermo-chronological data or porosity.[5,14-15]

Accretion time from modeling: Previously, we constrained with a temperature and porosity evolution model that Ryugu PB was only a few km big and formed at 1-3 Ma after CAIs.[14] Our model fits to CI and CM carbonate formation ages indicate PB radii of 20-25 km and formation at 3.75 Ma. Here, we fitted Flensburg, CR, NWA 011, and NWA 6704 thermo-chronological data. We present modeling evidence for a temporally distributed accretion of parent bodies of CR-like meteorites that range from altered chondrites to equilibrated chondrites, and to achondrites. The PB formation times derived range from the formation of CAIs to ≈4 Ma after CAIs, with ≈3.7 Ma, ≈1.5-2.75 Ma, ≲0.6 Ma, and ≲0.7 Ma for CR1-3, Flensburg, NWA 6704, and NWA 011, resp.

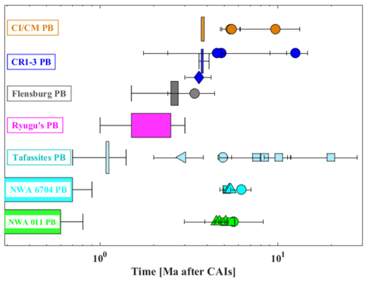

Figure 2: Parent body accretion timescale (big patches) derived from model fits to the data (small symbols) for objects in the C reservoir considered (from [9]).

Conclusions: Accretion processes in the C reservoir started as early as in the NC reservoir and produced differentiated PBs with carbonaceous compositions in addition to undifferentiated CC PBs. Accretion times correlate inversely with the meteorite alteration, metamorphism, or differentiation degree, and those for CI, CM, Ryugu, and Tafassites of 3.75 Ma, 3.75 Ma, 1-3 Ma, and 1.1 Ma, resp.,[14,15] fit well into this correlation (Fig. 2).

References: [1] Trieloff et al. (2003) Nature 422, 502. [2] Henke et al. (2012) A&A 537, A45. [3] Henke et al. (2013) Icarus 226, 212. [4] Henke et al. (2016) A&A 589, A41. [5] Neumann et al. (2018) Icarus 311, 146. [6] Gail and Trieloff (2019) A&A 628, A77. [7] Bischoff et al. (2021) GCA 293, 142. [8] Trieloff et al. (2022) Icarus 373, 114762. [9] Neumann et al. (2023) Temporally distributed parent body accretion in the C reservoir of the solar system. Submitted. [10] Neumann et al. (2012) A&A 543, A141. [11] Neumann et al. (2014) EPSL 395, 267. [12] Schrader et al. (2011) GCA 75, 308. [13] Grott et al. (2019) Nat.Astron., 3, 971. [14] Neumann et al. (2021) Icarus 358, 114166. [15] Ma et al. (2022) GPL 23, 33.

Acknowledgments: We thank Klaus Tschira Foundation, DFG (project number 434933764), and ISSI/ISSI-Beijing.

HOW DOES SURFACE ROUGHNESS AFFECT THE PHASE CURVE OF AIRLESS EXOPLANETS?

Moritz Tenthoff[1], Kay Wohlfarth[1], Sebastian Zieba[2,3], Laura Kreidberg[2], Christian Wöhler[1]
[1]Image Analysis Group, TU Dortmund University, Otto-Hahn-Str. 4, 44227 Dortmund, Germany (moritz.tenthoff @tu-dortmund.de), [2]Max-Planck-Institute for Astronomy, Königstuhl 17, 69117 Heidelberg, Germany. [3]Leiden Observatory, Leiden University, Niels Bohrweg 2, 2333CA Leiden, the Netherlands

Introduction: Rocky airless solar system bodies bear a rough surface that causes non-Lambertian thermal emission. At opposition, these bodies appear to emit more thermal radiation than a smooth thermal model predicts (thermal beaming). The thermal emission is smaller for large phase angles compared to a smooth model. The effects of thermal roughness might also occur in extrasolar planetary systems. The planet LHS3844b is the only known exoplanet that does not sustain an atmosphere and is believed to be rocky [1, 2]. In our recent study, we simulate the thermal emission of exoplanet LHS3844b with a thermal roughness model [3, 4] that extends established approaches such as [5, 6]. We find that phase curves predicted by the rough model deviate from those predicted by a smooth model and depend on the wavelength. We discuss how mechanisms such as thermal gradient formation might behave under the extreme conditions of LHS3844b and how phase curves of airless rocky worlds open a window to understanding their surface structure.

Thermal Limb-Brightening on LHS3844b: First, we simulate the disk-resolved thermal emission of LHS3844b for various phase angles. The planetary parameters are given by [7]. We assume a roughness of θ = 30° and find that the planet exhibits significant thermal limb brightening at opposition (φ = 0°) and reduced thermal emission near the limb for large phase angles (φ = 120°) compared to a smooth surface (Figure 2). Current technology only allows for disk-integrated measurements of the combined thermal emission from the planet and the star. Consequently, it may be possible to observe these effects with the help of thermal phase curves but not directly.

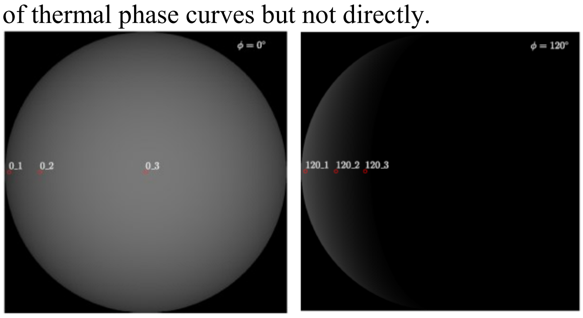

Figure 1: Left: Disk-resolved planet at opposition. The spectral thermal emission at point 0_1 is shown in Figure 2 (top). Right: Disk-resolved planet at (φ = 120°). The spectra at 120_1 are shown in Figure 2 (bottom).

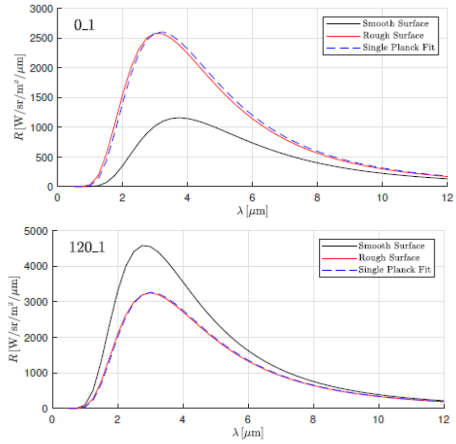

Figure 2: Emission spectra of a smooth (black) and a rough model (red) at the limb in opposition (top) and for φ = 120° (bottom) (emissivity ε = 1). See Fig. 1 for positions.

Phase curve of LHS3844b: We obtain the phase curve (Figure 3) via integration and find significant enhancement for φ < 60° and reduction for φ > 60°.

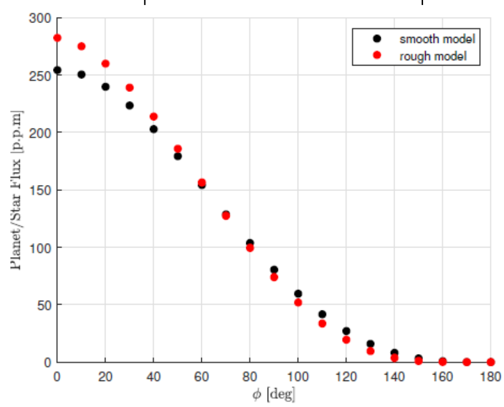

Figure 3: Phase curves of LHS3844b @ 4 μm.

Discussion: Our study assumes that the exoplanet has a surface structure similar to the Moon – a rough and thermally isolating silicate regolith. Currently, we explore how thermal gradients, thin atmospheres, topography, and various surface structures influence the phase curve to make this a tool for exoplanet analysis.

References: [1] Kreidberg et al. 2019 Nature, 573, 87. [2] Diamond-Lowe et al. 2020 AJ, 160, 188. [3] Wohlfarth et al. 2023, this conference. [4] Wohlfarth et al. 2023, A&A, under review. [5] Rozitis, B. and Green, S. F. (2011) MNRAS 415(3), 2042-2062. [6] Davidsson, B.J. et al. (2015) Icarus, 252,1-21. [7] Vanderspek et al. (2019) AJ Letters, 871, L24.

Early thermal evolution of Earth's embryos due to ^{26}Al and impact-generated steam atmosphere

Gurpreet Kaur Bhatia
Department of Physics, Maharishi Markandeshwar (Deemed to be University), Mullana, India 133207
(gurpreetkaur@pu.ac.in ; gurpreet.kaur@mmumullana.org)

Introduction: Earth and Enstatite chondrites are known to have same isotopic composition. Previous cosmochemical studies along with planet formation theories suggested that Earth primarily formed by accretion of Enstatite (dry) chondrite type material. However, new findings recommend that the Enstatite chondrite contain 0.08–0.54 wt% H_2O [1]. It implies to the formation of an impact-induced steam atmosphere on the surface of embryos during accretion [2-3]. Further, recent planet formation theories suggested rapid accretion and diiferentiation of proto-Earth during the initial ~5 Ma of the formation of solar system [4]. The early accretion suggests the active role played by the short-lived radionuclide ^{26}Al in large scale heating and meting of interior of Earth forming emryos. Based on these findings, we modelled the early thermal evolution and core-mantle differentiation of embryos of Earth ($0.4M_E$-$0.6M_E$, Earth masses) by considering the the SLR ^{26}Al and blanketing effect of impact-generated steam atmosphere.

Methodology: The heat conduction partial differential equation was solved numerically using the finite difference method [5]. The accretion time of embryos was considered to be in range $t_{acc.}$~1.3–1.5 Ma after the formation of CAIs. The embryos were assumed to accrete by the linear accretion of planetesimals. The onset of accretion was commenced at t_{onset} ~0.5 Ma after the formation of CAIs. The bulk composition of the embryos was considered to be of Enstatite type with initial water content (X_{wp}) ~0.1 – 0.54% by weight in accreting planetesimals [5]. Figure 1 shows the growth of the water-vapor steam atmosphere on the surface of $0.2M_E$ for different values of X_{wp}. The atmosphere was considered to be gray, radiative and plane- parallel. The pressure dependent liquidus and solidus temperature of iron and silicate were calculated at each spatial point inside embryos.

Result: Figure 2 shows the thermal evolution of $0.2M_E$ embryo with radius 4,006 km during the initial 5 Ma of the formation of soalr system. The simulation parameters were consisded to be t_{onset} = 0.5 Ma, $t_{acc.}$ = 1.5 Ma and X_{wp} = 0.1%. The interior of the embryo was heated effectively due to the episodic transport of heat by SLR ^{26}Al during the initial stages of accretion. In the final stages of accretion, the blanketing effect of the impact generated steam atmosphere raised the surface temperature sufficiently to initiate the melting of silicates. Complete core formation in this model was comlete during the initial 3.55 Ma of solar system's formation.

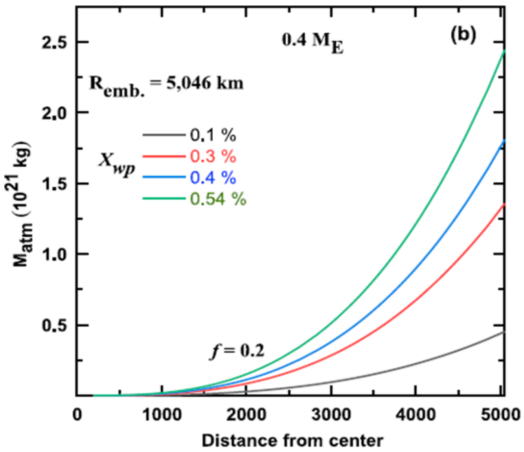

Figure 1: The increase in the mass of water-vapor atmosphere during the accretion of $0.2M_E$ embryo

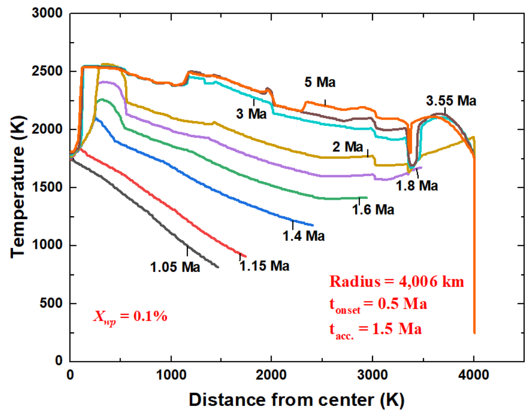

Figure 2. Thermal evolution of $0.2M_E$ embryo with X_{wp} = 0.1%

Conclusion: Magma oceans of several depths formed at surface of growing embryos due to significant blanketing by the impact-generated steam atmosphere. The results show that the embryos must accrete within the initial ~1.3-1.5 Ma for complete core formation. These results seem to be consistent with new finding for the rapid accretion and differentiation of main accretion phase of Earth within the initial ~5 Ma of the solar system [4].

References: [1] Piani, L., et al., 2020. Science 369, 1110-1113. [2] Abe, Y., Matsui, T., 1985. J. Geophys. Res: Solid Earth 90, C545-C559. [3] Abe, Y., Matsui, T., 1986. Proc. 17th Lunar Planet. Sci. Conf. Part 1, J. Geophys. Res. (Suppl.) 91, E291-E302. [4] Schiller, M. et al., 2020. Sci. Adv. 6(7), p.eaay7604. [5] Bhatia, G.K., 2021. Planet. Space Sci. 207, 105335.

SESSION 7

Laboratory Investigations and Validation of Thermal Models.

FRACTURING BUT NO FLAKING ON CM-LIKE ASTEROIDS DUE TO THERMAL FATIGUE

M. Patzek[1] and O. Rüsch[1],
[1]Institut für Planetologie, Westfälische Wilhelms-Universität Münster, Münster, Germany (markus.patzek[at]uni-muenster.de, ottaviano.ruesch[at]uni-muenster.de).

Introduction: Particle ejection from small asteroids has been recently reported for Bennu [1]. It is important to assess which process/es could be responsible for such activity in order to determine airless regolith evolution. The role of two processes for particle ejection from asteroid Bennu have been studied: meteoroid impacts and thermal fatigue [2,3]. Here we report ongoing experiments of thermal fatigue that show evidence for micro-flaking and particle removal/ejection or absence of these effects depending on the type of samples.

Setup and Samples: The experimental setup follows that used by [4] and consists of a thermal vacuum cycling chamber operated with liquid nitrogen. Temperatures are cycled between 175 K and 375 K at a rate of ~1.8 K/min. High vacuum ($1x10^{-6}$ mbar) avoids humidity and its effects on sample cracking. Samples are placed on a cold finger. Sample cubes of different ordinary and (aqueously-altered) carbonaceous chondrites have been selected and prepared to 5 mm width. These include El Hammami (H5), Chelyabinsk (LL5), Allende (CV3), Murchison (CM2), Jbilet Winselwan (CM2), and Tagish Lake ($C2_{ung}$).

Results and Implications: Formation and extension of cracking was only observed for Jbilet Winselwan (CM2), Murchison (CM2), Tagish Lake ($C2_{ung}$), and – in only one single occasion – in Chelyabinsk (LL5). El Hammami (H5) and Allende (CV3) do not show formation or extension of cracks on their surface. In CM chondrites, cracking is often associated with fine-grained rim material that surrounds chondrules and other coarse-grain constituents, but is not limited to this. In some cases, the cracks formed radially from the chondrules through the rim into the clastic matrix (Fig. 1c,d). Importantly, flaking or micro-flaking observed for achondrite samples (see [4]) has not been identified on any of the chondritic samples, which might be attributed to the dramatically different petrology having higher abundance of glass and plagioclase and the observation that micro-flaking happens statistically more often on these minerals and constituents [4]. The observed cracking pattern for Murchison (Fig. 1a,b) might be explained by the combination of the chondrule consisting of anhydrous silicates (olivine and pyroxene) surrounded by a hydrous fine-grained rim and the difference of their thermal expansion coefficients.

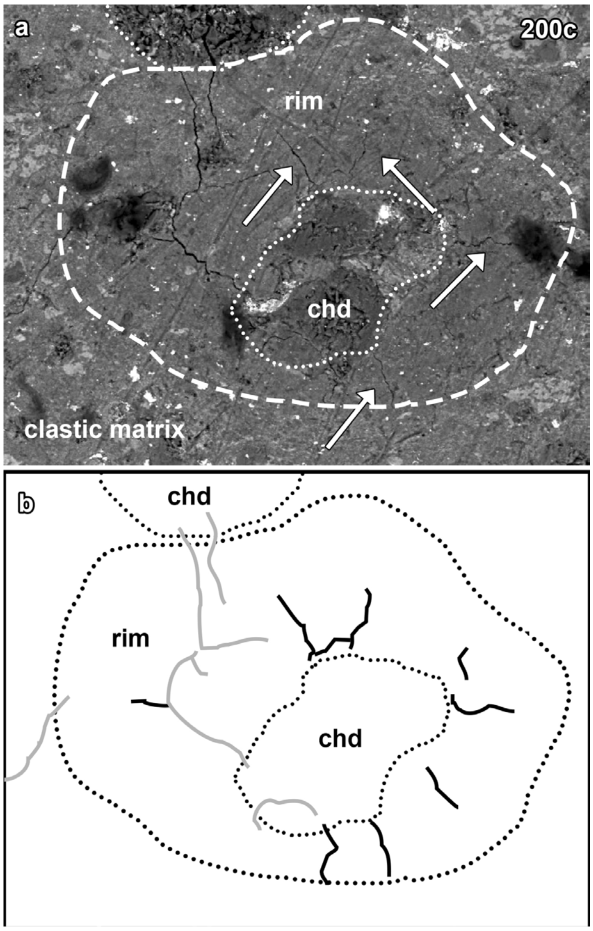

Fig. 1: (a) *SEM-BSE image of CM2 chondrite Murchison after 200c showing a chondrule (chd) surrounded by rim with adjacent clastic matrix. The dashed line is marking the border between rim and matrix. Arrows indicate the location of cracks diverging from the chondrule into the rim. Image width is ~400 µm.* (b) *drawing of the cracks that were already in the uncycled sample (grey) and those that formed in the course of 200 total cycles (black) showing the radial distribution around this chondrule.*

References:

[1] Lauretta D. S., et al. (2019) *Science*, 366.6470. [2] Bottke W. F. et al. (2000) *JGR: Planets*, 125.8. [3] Molaro J. L. et al. (2020) *Nature Comm.*, 11:2913. [4] Patzek M. and Rüsch O. (2022) *JGR: Planets* 127.10.

Acknowledgments: The authors are supported by a Sofja Kovalevskaja Award Project of the Alexander von Humboldt Foundation.

Using observations to constrain models of endogenic activity on Enceladus

G Miles[1], CJA Howett[2,3] and J Spencer[1]
[1]Southwest Research Institute (georgina.miles@boulder.swri.edu)
[2]University of Oxford
[3]Planetary Science Institute (chowett@psi.edu)

Introduction: We present preliminary results from a study to identify whether endogenic activity is detected outside of Enceladus' south polar terrain (SPT) using measurements from Cassini Composite InfraRed Spectrometer (CIRS) Focal Plane 1 (FP1) observations. This measurement is important because understanding the total energy budget for Enceladus will help constrain tidal heating models that predict the evolution of the satellite and the longevity of the sub-surface ocean. Using a 1D surface temperature seasonal model ([1],[2]) we establish expected passive emitting temperatures collocated with CIRS observations. We have reprocessed CIRS FP1 data with improved temperature error characterization and estimated model uncertainty by perturbation. Measurement-model differences exceeding uncertainty bounds indicate possible thermal anomalies.

Observations: We focus here on a north polar stare observation made in July 2005. Fitting a single temperature and assuming unit emissivity does not produce a good fit to the observation. It is better fit jointly with effective emissivity (38 ± 0.5 K and 0.58 ± 0.03 respectively) and is shown in Fig. 1. This very low emissivity initially seems lower than conventionally expected for water ice in far-infrared remote sensing. We can show that this results from its dependence on water ice grain size which can be significant at low temperatures/wavenumbers where the Planck function peak coincides with very low spectral emissivity. This becomes important for translating model temperatures to a forward model for observed radiance of very cold scenes (< 55 K).

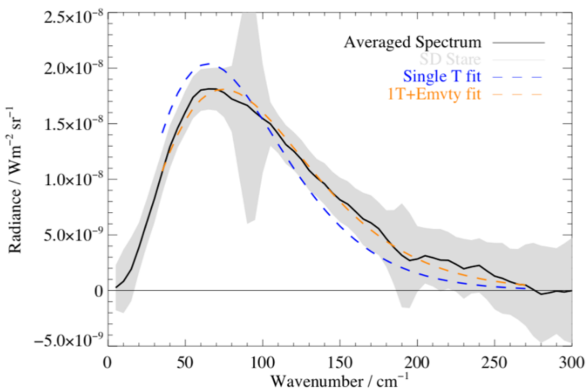

Figure 1: Fits to CIRS FP1 north pole stare observation in NH winter, July 2005.

Modelling: Our surface temperature model predicts passive temperatures that are considerably colder than the observation. We evaluate model uncertainties CIRS-derived thermal inertia and albedo error [2]. It is important to account for temperature variation with longitude within the CIRS field of view that arises due to the effects of Saturn-shine. We introduced endogenic heating to the base layer of the 1D surface temperature model. Optimum fits to the CIRS observations are found using basal heat flow of between 80 and 110 mWm^{-2} (Saturn-facing and anti-Saturn). The emitted energy at the surface is somewhat lower due to the low effective emissivity at these temperatures.

Conclusion: These values, if interpreted as conductive heat flow, are highly consistent with the model estimates proposed by [4] at high northern latitudes, which peak at circa 80 mWm^{-2} outside the SPT. The modelled conductive heat flow is strongly related to the ice shell thickness. It is notable that emissivity becomes an increasingly important consideration for constraining such models with observations and for interpreting overall energy lost by Enceladus. We hope to apply this methodology to further measurements with detailed forward modelling of the observation in order to provide more globally applicable upper constraints to the conductive heat flow.

References:

[1] Spencer, J. A Rough-Surface Thermophysical Model for Airless Planets, Icarus, Vol. 83, pp. 27-38, 1990. doi: 10.1016/0019-1035(90)90004

[2] Howett, C.J.A., Spencer, J. R., Pearl, T., Segura, M. Thermal inertia and bolometric Bond albedo values for Mimas, Enceladus, Tethys, Dione, Rhea and Iapetus as derived from Cassini/CIRS measurements. Icarus 206, 2, pp573-593. 2010, https://doi.org/10.1016/j.icarus.2009.07.016

[3] Čadek, O., Souček, O., Běhounková, M., Choblet, G., Tobie, G. and Hron, J., 2019. Long-term stability of Enceladus' uneven ice shell. Icarus, 319, pp.476-484.

[4] Hemingway, D.J. and Mittal, T., 2019. Enceladus's ice shell structure as a window on internal heat production. Icarus, 332, pp.111-131.

Acknowledgments: This work is funded by the NASA CDAP program 80NSSC20K0477.

THERMAL INERTIA OF RYUGU SAMPLES AFFECTED BY CRACKS INSIDE SAMPLE

Takuya Ishizaki[1], Hosei Nagano[2], Satoshi Tanaka[1], Tatsuaki Okada[1], Naoya Sakatani[1], Tomoki Nakamura[3], Masayuki Uesugi[4], Ryohei Fujita[2], Abdulkareem Alasli[2], Tomoyo Morita[3], Mizuha Kikuiri[3], Kana Amano[3], Eiichi Kagawa[3], Hisayoshi Yurimoto[4], Takaaki Noguchi[5], Ryuji Okazaki[6], Hikaru Yabuta[7], Hiroshi Naraoka[6], Kanako Sakamoto[1], Shogo Tachibana[8, 1], Sei-ichiro Watanabe[2], Yuichi Tsuda[1]
[1]Japan Aerospace Exploration Agency, 3-1-1 Yoshinodai, Sagamihara, Kanagawa 252-5210, Japan
[2]Nagoya University, Furo-cho, Chikusa-ku, Nagoya, Aichi, 464-8603, Japan
[3] Tohoku University, 2-1-1, Katahira, Aoba-ku, Sendai, Miyagi 980-8578, Japan
[4] Japan Synchrotron Radiation Research Institute, 1-1-1, Koto, Sayo-cho, Sayo, Hyogo 679-5198, Japan
[5] Hokkaido University, 5, Kitahachijonishi, Kita-ku, Sapporo, Hokkaido 060-0810, Japan
[6] Kyoto University, Yoshidahonmachi, Sakyo-ku, Kyoto, Kyoto 060-0810, Japan
[7] Kyushu University, 6-10-1 Hakozaki, Higashi-ku, Fukuoka, Fukuoka 812-8581, Japan
[8] Hiroshima University, 1-3-2 Kagamiyama, Higashihiroshima, Hiroshima 739-8526, Japan
[9] The University of Tokyo, 7-3-1 Hongo, Bunkyo-ku, Tokyo 113-0033, Japan

Introduction: 5.4 g of Ryugu samples were brought back in 2020 by Hayabusa2, and preliminary analyses for 15wt% of the returned samples were performed. In this study, we developed a lock-in thermography (LIT) periodic heating method that can measure the thermal diffusivity of small sample of several mm scale without contact [1]. Then we evaluated the anisotropic distribution of thermal inertia for six Ryugu samples. By using X-ray computed tomography (CT), the relationship between the thermal inertia and cracks inside sample was discussed.

Samples and Methodology: In this study, six samples of C0002-plate 3, C0002-plate 4, C0025, C0033, A0026 and A0064 were evaluated. C0002-plate 3 and C0002-plate 4 are flat plates cut out from C0002, and the others have granular shape. A spot on the sample is periodically heated using a laser and the temperature response is measured by LIT to obtain the phase lag distribution on the sample surface. The thermal diffusivity is analyzed from the gradient of the phase lag according to this equation; $D = \pi f / (d\theta/dr)^2$. Here, D is thermal diffusivity, f is heating frequency, θ is phase lag and r is distance from heating point. Thermal inertia, which is expressed as the product of the square root of thermal diffusivity, density, and specific heat, was evaluated based on the reported density and specific heat [2]. The heating frequency was selected according to the sample size to avoid the influence of reflected temperature waves at the sample edge, and then measurements were performed at 2, 1, 4, 4, 4, and 20 Hz for C0002-plate 3, C0002-plate 4, C0025, A0026, C0033, and A0064, respectively. Before the measurements, inner structure of the samples were investigated by using X-ray CT.

Results and Discussion: Figure 1 shows the phase lag map, the thermal inertia and a crack visualized X-ray CT image of C0002-plate 3 as a representative result. The CT image expresses a crack element as one black voxel of 3.3 μm cube. The maximum, minimum and average value of the thermal inertia was 1296, 227 and 748 J/(s$^{1/2}\cdot$m$^2\cdot$K). The thermal inertia distribution (Fig. 1 (b)) shows that there is thermal anisotropy inside the sample and that the thermal inertia decreases significantly in the direction of 120–180 degree, whereas the X-ray CT image (Fig. 1 (c)) shows that there are some cracks distributed parallel to the sample surface in corresponding region (highlighted by green circle). This region coincides with the region where the phase lag is large (Fig. 1 (a)), and the large phase lag means that the thermal diffusivity is small. It was, therefore, found that the decrease in thermal inertia is attributed to the decrease in thermal diffusivity due to cracks. The thermal inertia of the entire grain is determined by the sum of the thermal inertia weighted by the ratio of the cross-sectional area with and without the cracks along the heat transfer direction. If the two ends of the sample are structurally separated by cracks inside the sample, the minimum value of this measurement can be acceptable as the representative thermal inertia of one grain. However, since X-ray CT image analysis reveals that the crack region is not dominant over the entire sample, the representative value of the thermal inertia of a grain is possible to be close to the average value.

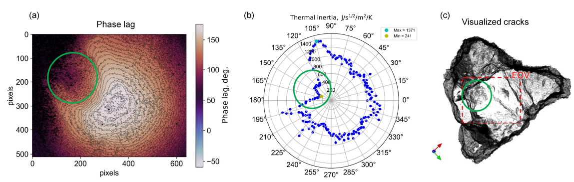

Figure 1 (a) Phase lag map, (b) thermal inertia distribution and visualized cracks by X-ray CT imaging of C0002-plate 3. Green circle corresponds to large phase lag, low thermal inertia and cracks respectively.

References:

[1] T. Ishizaki et al., Int J Thermophys. 43 (2022).
[2] T. Nakamura et al., Science abn8671 (2022).